Decay & Final–State Interaction Effects in Near–Threshold ω Production

Mahmoud Ismail Al Jaghoub

Department of Physics & Astronomy,
University College London.

A thesis submitted to University College London in accordance with the requirements for the degree of Doctor of Philosophy 1995.

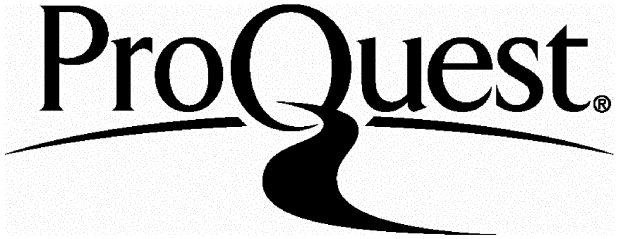

Abstract

The ω production amplitude in the $\pi^- p \to \omega n$ reaction seems to be sharply suppressed near threshold, despite remaining isotropic and consistent with S-wave production. Furthermore, the ratio of the $\pi^-\pi^+\pi^0$ and $\pi^0\gamma$ decay channels of the ω is constant. The threshold suppression is also seen in the $pd \to {}^3He\,\omega$ process. Theoretical models are studied which might lead to such abrupt behaviour.

The effect of final-state interactions between the ω decay products and the recoil neutron (nucleus) has been investigated in a simple semi-classical model and a more realistic quantum mechanical one. The results of the former reproduced well the near-threshold suppression, as well as the scale in energy of the effect. On the other hand, the quantum model, where only the radiative decay channel is considered, produced a 9% reduction, which is significantly smaller than the 70% observed experimentally.

An attractive ηn interaction, which leads to the formation of the $N^*(1535)$ S-wave resonance, enhances the η production in $\pi^- p \to \eta n$ near threshold. A similar $\omega - n$ resonance might also be possible if the ω and the neutron interacted *via* an attractive potential, but such a system may be destroyed due to the short lifetime of the ω. This is an alternative threshold suppression mechanism which is independent of the ω decay channel. This hypothesis was studied by deriving a dynamical ωn interaction amplitude which was fit using the scattering parameters of the elastic ηn channel, as the corresponding ωn ones are not known. The effect of a short lifetime was then investigated by assuming the η to have a width equals to that of the ω. Two different models, which could lead to an S-wave resonance production, were adopted. A two-term S-wave separable non-local potential was first considered. The Schrödinger equation was solved,

and a dynamical ωn interaction amplitude extracted, but this could not describe the data. A plausible description is obtained when the resonance is trapped as a virtual state in a multi-channel system. Three channels were considered, ηn, $\pi^- p$ and $K\Lambda$, and an ηn interaction amplitude derived. Introducing an η lifetime equal to that of the ω does indeed greatly reduce the enhancement near threshold, and the effect is most important at low energies.

As an alternative approach, the amplitude of the overall $pd \rightarrow {}^3He\,\omega$ reaction has been expressed in terms of $pp \rightarrow \pi^+ d$ and $\pi^+ n \rightarrow \omega p$ intermediate amplitudes using a two-step quantum model. Such a model reproduces the rapid rise from threshold, showing that the reduction effect can propagate from the $\pi^- p$ to the pd case. Furthermore, it is shown that the multiple scattering of the ω off the nucleons in ^3He, which might lead to a threshold enhancement, is suppressed through the ω decaying before it is multiply scattered.

Acknowledgments

My special thanks must go to my supervisor Professor C. Wilkin for many long, useful, and fruitful discussions, and for his hospitality which made me feel at home.

I am deeply indebted to my parents, who funded me throughout my 'A-levels' and BSc. studies in England, for their endless support and encouragement.

I would also like to thank the many people without whom this thesis would not have been possible: Professor L. Castillejo, Professor D. H. Davis, and Dr. D.N Tovee. My thanks also go to all my friends, especially Dr. O. Amin, for their help and support.

I am also indebted to the British Council, Overseas Research Council and the Department of Physics and Astronomy at University College London for funding me throughout the period of my research.

Contents

Chapter 1

Introduction

The near-threshold production of mesons and mesonic resonances in pion and proton-induced reactions has been studied in many experiments. However, there are severe complications when interpreting such data in cases where the meson produced is unstable and has an energy width comparable to the available energy in the final state. There are easily quantifiable effects, due to the final state phase space 'eating' into the width of the resonance, and corrections for this are normally carried out in the original experimental analysis when production cross sections are extracted. Even after accounting for such effects, experimental results show a striking energy dependence near threshold. It is the aim of this work to study different mechanisms which might lead to such non-smooth behaviour.

The ω resonance is a perfect candidate for such a study as it has a narrow width (8.43 MeV [1]), which makes it relatively easy to identify the corresponding peak in particle or nuclear production. Furthermore, there have been extensive measurements of its production at low energies in $\pi^- p \rightarrow \omega n$ [2, 3] and $pd \rightarrow {}^3He\,\omega$ [4, 5]. In both reactions the experimental results show a sharp suppression in the near-threshold region.

This thesis may be divided into four main parts. The first concentrates on

the properties of the ω and its production near threshold. The former is done in chapter 2, where we discuss the ω features within the framework of the quark model. We also derive the decay matrix element for the dominant decay mode $\omega \to \pi^+\pi^-\pi^0$. Although more emphasis is laid on the ω resonance, the η particle is also discussed, as its production amplitude in $\pi^- p \to \eta n$ plays a vital role in later chapters. Chapter 3 is entirely devoted to a review of the experimental results concerning the near-threshold ω production. Here, we reconstruct some of the experimentalists' discussions and briefly present some of the models they applied to explain their results.

The second part (chapters 4-5) tries to explain the reduction effect in terms of final-state interactions involving the ω-decay products and the recoil neutron (nucleus). This is first done in a simple semi-classical model using a Monte-Carlo simulation of the decay followed by final state interactions. Here, the ω mass is assumed to be always on shell, and its basic production amplitude is taken to be in an S-wave. On the other hand, the model takes account of the ω's finite lifetime and its decay probability distribution. Furthermore, the scattering of the decay products off the target nucleon (nucleus) is treated as that of macroscopic hard spheres. In chapter 5 we study the same effect in a more realistic quantum mechanical model which, unlike the semi-classical one, views the ω as a virtual particle, and all interaction amplitudes are calculated using quantum mechanical formalism. Here, for simplicity, we only consider the $\pi^- p \to \omega n$ process, where the ω decays radiatively, $\omega \to \pi^0\gamma$. Although the pion-nucleon interaction is P-wave dominated, we first derive the easier S-wave rescattering before moving on to the more complex P-wave case. Working in the limit where the $\pi^- p$ interaction at the initial production vertex is point-like, we make a rough estimate of the

suppression effect at the resonance energy.

The η production in $\pi^- p \to \eta n$ is enhanced due to an attractive (resonant) ηn interaction manifested in the formation of the $N^*(1535)$ S-wave resonance. Experimental results [2, 6] show that the ωn system from the $\pi^- p \to \omega n$ reaction to be in an S-wave. This leaves open the possibility that an S-wave $\omega - n$ resonance system could be formed if an attractive interaction between the ω and the neutron were possible. But such a system may then be destroyed due to the short lifetime of the ω. This is an alternative suppression mechanism which is independent of the ω decay channel. As a consequence it might explain the experimental observation [3] that the branching ratio of the $\omega \to \pi^+\pi^-\pi^0$ and $\omega \to \pi^0\gamma$ decay channels seems to be constant. In chapter 6 we investigate this hypothesis by developing an attractive (resonant) dynamical ωn interaction amplitude, which is then used to investigate the finite ω width on the resonance formation.

The fact that the ω particle can decay *via* strong interactions makes it difficult to obtain an experimentally determined ωn amplitude. Since our primary aim is to investigate the effect of a finite lifetime on the formation of a resonance, we might be justified in replacing the parameters of the ωn elastic channel by the corresponding ηn ones. There is in fact little alternative to making this crude *ansatz*. The effect of the finite width is then investigated by assuming a fictitious η particle with a width equals to that of the ω.

A one-term attractive S-wave potential does not support resonances. Consequently, in chapter 6 we adopt two different mechanisms which might lead to S-wave resonance production. In section 6.2 a two-term S-wave non-local potential, one attractive and the other repulsive, is considered. With such a potential we derive the ωn interaction amplitude by solving the Schrödinger equation. A more

successful description is however obtained in section 6.3, where we suggest that the resonance is trapped as a virtual state in a multi-channel scattering model. Three channels are here considered, ηn, $\pi^- p$ and $K\Lambda$ and, using multi-channel scattering formalism, we derive an amplitude for the ηn elastic scattering. This is then used to investigate the finite lifetime effect on the production amplitude.

The $pd \rightarrow {}^3He\,\eta$ reaction has previously been studied by considering double-scattering graphs in a quantum mechanical model [7]. In this model, the reaction is assumed to proceed in two stages. A pion beam created on one of the target nucleons *via* $pp \rightarrow d\pi^+$ is converted into an η-meson on the second nucleon through a $\pi^+ n \rightarrow \eta p$ reaction. After including strong final state interactions between the produced η and ${}^3He$, an enhancement factor of 2.2 was obtained near threshold. This is due to the η undergoing multiple scattering by the nucleons in the ${}^3He$ nucleus.

Unlike the η, the ω will be scattered once or at the most twice before it decays, especially at low energies. This is likely to kill the final-state related enhancement observed in the η case. In chapter 7 we modify the above model to take account of the finite ω lifetime, and study quantitatively its effect on the enhancement factor near threshold. In chapter 8, we apply the formalism of their two-step quantum model to express the ω production amplitude in the overall $pd \rightarrow {}^3He\,\omega$ reaction in terms of the amplitudes corresponding to $pp \rightarrow d\pi^+$ and $\pi^+ n \rightarrow \omega p$ intermediate reactions. This might shed light on whether the suppression effect can propagate from the $\pi^- p$ to the pd case, or if a common cause is behind the reduction in both reactions. The conclusions follow in chapter 9 where, as well as arguing that no one mechanism is sufficient to explain the experimental results, we discuss other possibilities that might engender a reduction effect.

Chapter 2

The ω Meson

2.1 The ω properties

The quark model successfully predicted the existence of two low-lying S-wave meson families which have been observed experimentally. One family is made up of nine particles with spin-parity $J^P = 0^-$ and is known as the pseudoscalar nonet, π, K, η and η'. The other is the vector meson nonet whose members have spin-parity $J^P = 1^-$. The particles of this group, ρ, K^*, ω and ϕ, can all decay *via* strong interactions and are seen as resonances in *e.g* $\pi\pi$ scattering.

The ω is a bound state of a linear combination of two quark-antiquark pairs. In terms of these, it is given by,

$$\omega = \sqrt{\frac{1}{2}}(u\bar{u} + d\bar{d}) \; .$$

The masses of the u and d quarks are almost equal. Then, in analogy with the proton and the neutron, they are viewed as different states of the same particle as an isospin doublet. Thus both quarks are assigned an isospin quantum number I = 1/2, while the value of the third component I_3 is 1/2 for the u quark, and $-1/2$ for the d. For antiquarks, the sign of I_3 is reversed, so that the $\bar{u}$ and $\bar{d}$ antiquarks have $I_3 = -1/2$ and a 1/2 respectively. Consequently, the ω has $I = I_3 = 0$ and so it is an antisymmetric isosinglet.

The η has the same quark constituents as the ω, and its wave function is,

$$\eta = \sqrt{\frac{1}{2}}(u\bar{u} + d\bar{d}) \; .$$

Despite this, the two mesons have different masses; M_ω = 782 MeV/c^2 and M_η = 549 MeV/c^2. This can be ascribed to the hyperfine interaction [8]. Consider two charged point fermions with magnetic dipole moments $\vec{\mu}_i$ and $\vec{\mu}_j$ separated by a distance r_{ij}. The magnetic interaction energy is proportional to $\vec{\mu}_i \cdot \vec{\mu}_j / r_{ij}^3$ [8]. For two particles in a relative S-state, the averaged interaction energy over all space is zero except at the origin. Now for a Dirac point-like fermion,

$$\vec{\mu}_i = \frac{e_i}{2m_i}\vec{\sigma}_i \; ,$$

where e_i and m_i are the electric charge and mass of the particle, $\vec{\sigma}_i$ its spin vector. The interaction energy due to this dipole-dipole interaction is then

$$\delta E = \frac{2\pi}{3}\frac{e_i e_j}{m_i m_j} \mid \psi(0) \mid^2 \vec{\sigma}_i \cdot \vec{\sigma}_j \; , \qquad (2.1.1)$$

with $\psi(0)$ being the wave function of the two particle system at $r_{ij} = 0$. The numerical factor arises from the angular integration for the S-state wave. This leads to an energy difference of $\approx$ 1 MeV in the quark case, which is significantly smaller than the 233 MeV/c^2 observed mass difference between the ω and the η. However, the colour magnetic interaction, which is of the same form as eq. (2.1.1) except that electric charges are replaced by colour charges, gives rise to much larger interaction energy. The numerical coefficient in the expression for δE depends on whether the interaction is between a quark pair or a quark-antiquark pair. These expressions are [8]

$$\delta E(q\bar{q}) = \frac{8\pi\alpha_s}{9m_i m_j} \mid \psi(0) \mid^2 \vec{\sigma}_i \cdot \vec{\sigma}_j \; , \qquad (2.1.2)$$

$$\delta E(qq) = \frac{4\pi\alpha_s}{9m_i m_j} \mid \psi(0) \mid^2 \vec{\sigma_i} \cdot \vec{\sigma_j} \ , \tag{2.1.3}$$

where α_s is the strong coupling constant. The size and sign of δE depends on the relative quark spin orientation. Denoting the spin vectors of the quarks by $\vec{s_i}$ and $\vec{s_j}$ and the total spin by $\vec{S} = \vec{s_i} + \vec{s_j}$, we get

$$\begin{aligned} \vec{\sigma_i} \cdot \vec{\sigma_j} \ = 4\vec{s_i} \cdot \vec{s_j} \ &= 2\{ \ S(S+1) - s_i(s_i+1) - s_j(s_j+1)\} \\ &= +1 \text{ for } S = 1, \\ &= -3 \text{ for } S = 0. \end{aligned}$$

The ω is a spin-triplet state (quark spins are parallel), while the η is a spin-singlet one (quark spins antiparallel). So taking $\bar{m} = m_u \approx m_d \approx 310$ MeV/c^2 we get

$$\delta E_\omega = \frac{K}{\bar{m}^2} \ ,$$

and

$$\delta E_\eta = -3\frac{K}{\bar{m}^2} \ .$$

Hence

$$M_\omega = 2\bar{m} + \frac{K}{\bar{m}^2} \ , \tag{2.1.4}$$

and

$$M_\eta = 2\bar{m} - 3\frac{K}{\bar{m}^2} \ , \tag{2.1.5}$$

where

$$K = \frac{8\pi\alpha_s}{9} \mid \psi(0) \mid^2 \ .$$

It should however be noted that the η is also thought to have an $s\bar{s}$ component, which also contributes to the mass difference between the two particles.

The ω was one of the first meson resonances to be discovered, and was found in an analysis of proton-antiproton annihilation into five pions,

$$p\bar{p} \rightarrow \pi^- \pi^+ \omega$$

$$\omega \rightarrow \pi^- \pi^+ \pi^0 ,$$

as a sharp peak in the $\pi^- \pi^+ \pi^0$ effective mass distribution. The absence of corresponding peaks in the $\pi^+ \pi^+ \pi^-$ and $\pi^+ \pi^- \pi^-$ spectra confirms the zero isospin of the ω.

The three pion decay mode is dominant, with a branching ratio of 90%. The average ω width $\Gamma_\omega = 8.43 \pm 0.10$ MeV/c^2 [1], corresponds to a mean lifetime of

$$\tau = \hbar/\Gamma_\omega = (7.81 \pm 0.09) \times 10^{-23} \text{ sec.}$$

This is considerably shorter than the η lifetime of 2×10^{-19} sec. The short ω lifetime indicates that it can decay *via* strong interactions. However, it is found that there is a 9% probability for the ω to decay *via* the electromagnetic interactions, as

$$\omega \rightarrow \pi^0 \gamma .$$

Other less important decay channels include,

$$\omega \rightarrow \pi^- \pi^+ ,$$

and

$$\omega \rightarrow e^- e^+ .$$

In what follows, we shall concentrate only on the dominant three-pion decay channel and the 9% radiative decay mode. The kinematics of the electromagnetic decay are simple since the π^0 and the γ are produced back-to-back with equal and opposite momenta in the ω rest frame. However, the 90% decay mode is more complicated and shall be studied in more detail below.

2.2 Three Body Phase Space

The three body phase space integral may in general be written as [9],

$$Q = \int \prod_{i=1}^{3} \frac{d^3p}{2E_i}\, \delta^3(\vec{P} - \sum_{i=1}^{3} \vec{p_i})\, \delta(\sqrt{s} - \sum_{i=1}^{3} E_i)\ , \tag{2.2.1}$$

where $\sqrt{s}$ and $\vec{P}$ are the total energy and momentum. In the ω rest frame $\vec{P} = 0$ and $\sqrt{s} = M_\omega$, where M_ω is the ω mass. In this frame, momentum conservation implies that the final pion momenta are coplanar. Defining $\vec{p}_-$, $\vec{p}_+$ and $\vec{p}_0$ to be the momenta of the π^-, π^+, π^0, and E_-, E_+, E_0 the corresponding energies, we get

$$\vec{p}_- + \vec{p}_+ + \vec{p}_0 = 0\ , \tag{2.2.2}$$

and

$$E_- + E_+ + E_0 = M_\omega\ . \tag{2.2.3}$$

In terms of the pion momenta and energies, the phase space integral can be expressed as

$$Q = \int \frac{d^3p_-}{2E_-} \frac{d^3p_+}{2E_+} \frac{d^3p_0}{2E_0}\, \delta^{(3)}(\vec{p}_- + \vec{p}_+ + \vec{p}_0)\, \delta(\sqrt{s} - E_+ - E_- - E_0)\ .$$

Since the detection of a charged particle is easier than that of a neutral one, we choose to integrate over $\vec{p}_0$ using the momentum δ-function. This results in,

$$Q = \int \frac{d^3p_-\, d^3p_+}{8E_+E_-E_0}\, \delta(\sqrt{s} - E_+ - E_- - E_0)\ ,$$

where the π^0 energy is now fixed by,

$$E_0^2 = \mid \vec{p}_+ + \vec{p}_- \mid^2 + m_{\pi^0}^2 = p_+^2 + p_-^2 + 2p_-p_+\cos\theta + m_{\pi^0}^2\ , \tag{2.2.4}$$

and θ is the angle between p_- and p_+. We further write

$$d^3p_-d^3p_+ = p_-^2\, dp_-\, d\Omega_- p_+^2\, dp_+ d\Omega_+\ , \tag{2.2.5}$$

where Ω_- is the solid angle that describes the orientation of $\vec{p}_-$ with respect to some fixed axis, while $\Omega_+ = (\theta, \phi)$ is that describing the orientation of $\vec{p}_+$ relative to $\vec{p}_-$. Substituting for $d^3p_- d^3p_+$ into Q, and using eq. (2.2.5), results in

$$Q = \frac{\pi}{4} \int \frac{p_-^2 dp_- d\Omega_- p_+^2 dp_+ d(\cos\theta)}{E_+ E_- E_0} \delta(\sqrt{s} - E_+ - E_- - E_0) \,, \tag{2.2.6}$$

where we have integrated over $d\phi$ to get the last equation. To simplify further we use,

$$E_i^2 = p_i^2 + m_i^2 \,, \tag{2.2.7}$$

which gives

$$E_- dE_- = p_- dp_- \,, \tag{2.2.8}$$

and

$$E_+ dE_+ = p_+ dp_+ \,. \tag{2.2.9}$$

Also, differentiating eq. (2.2.4) with respect to $\cos\theta$, we have

$$d(\cos\theta) = \frac{E_0 dE_0}{p_- p_+} \,. \tag{2.2.10}$$

The last equation is used to turn the integration over $d(\cos\theta)$ in eq. (2.2.6) to one over dE_0, enabling us to use the energy δ-function. We finally arrive at an expression for the phase space of the form,

$$Q = \frac{\pi}{4} \int dE_- dE_+ d\Omega_- \Theta(1 - \cos^2\theta) \,. \tag{2.2.11}$$

The step function Θ defines the limits of the physically accessible regions in the phase space. Using eq. (2.2.4), this requires

$$-1 \leq \frac{E_0^2 - p_-^2 - p_+^2 - m_{\pi^0}^2}{2p_- p_+} \leq +1 \,.$$

A further limit on the phase space is found by considering the integration over the energy δ-function carried out in eq. (2.2.6). There we required that

$$E_0 = (\sqrt{s} - E_+ - E_-) \, .$$

Squaring both sides and using eq. (2.2.4) gives

$$p_+^2 + p_-^2 + 2p_-p_+ \cos\theta + m_{\pi^0}^2 = (\sqrt{s} - E_+ - E_-)^2 \, .$$

Hence,

$$4(E_-^2 - m_{\pi^-}^2)(E_+^2 - m_{\pi^+}^2) = (2E_-E_+ - 2\sqrt{s}(E_- + E_+) + s + m_{\pi^-}^2 + m_{\pi^+}^2 - m_{\pi^0}^2)^2 \, . \tag{2.2.12}$$

To get the last result we substituted $\cos\theta = \pm 1$ and made use of eq. (2.2.7). Eq. (2.2.12) represents a closed curve in the $E_- - E_+$ plane and fixes the physical region in phase space. Since we are working in the ω rest frame, $\sqrt{s} = M_\omega$. In terms of this variable the above equation reads

$$4(E_-^2 - m_{\pi^-}^2)(E_+^2 - m_{\pi^+}^2) = (2E_-E_+ - 2M_\omega(E_- + E_+) + M_\omega^2 + m_{\pi^-}^2 + m_{\pi^+}^2 - m_{\pi^0}^2)^2 \, . \tag{2.2.13}$$

2.3 The Decay Matrix Element

As strong interactions conserve isospin, the three pion final state must be anti-symmetric under the exchange of any pair of pions, and must correspond to a state with $J = 1$ as the total angular momentum is conserved. The matrix element describing the ω decay into three pseudoscalar mesons must therefore be totally antisymmetric and parity conserving. The Lorentz-invariant form of such an element is [10]

$$T(s_z, P_+, P_0, P_-) = G_{\omega\pi^3} \epsilon_{\alpha\beta\gamma\delta} P_+^\alpha P_0^\beta P_-^\gamma \varepsilon^\delta(s_z) \, , \tag{2.3.1}$$

where P_+, P_0, P_- denote the 4-momenta of π^+, π^-, and π^0. The Levi-Civita symbol, $\epsilon_{\alpha\beta\gamma\delta}$, is totally antisymmetric in all four indices, each of which runs over the values 0, 1, 2, 3.

In the ω rest frame, eq. (2.3.1) reduces to

$$T(s_z, p_+, p_-, p_0) = G_{\omega\pi^3}\,\vec{\varepsilon}(s_z)\cdot\vec{n}\ .$$

Here $\vec{n}$ is a vector that lies along the normal to the decay plane,

$$\vec{n} = E_+(\vec{p}_0\times\vec{p}_-) + E_0(\vec{p}_-\times\vec{p}_+) + E_-(\vec{p}_+\times\vec{p}_0)\ . \tag{2.3.2}$$

$G_{\omega\pi^3}$ is the decay coupling constant, and the space components of the ω polarisation vector $\vec{\varepsilon}(s_z)$ may be written as,

$$\vec{\varepsilon}(\pm) = \begin{pmatrix} \mp\frac{1}{\sqrt{2}} \\ -\frac{i}{\sqrt{2}} \\ 0 \end{pmatrix}\ ,$$

and

$$\vec{\varepsilon}(0) = \begin{pmatrix} 0 \\ 0 \\ 1 \end{pmatrix}\ ,$$

corresponding to $s_z = \pm 1$ and 0 respectively (s_z is the spin projection in the ω rest frame). These vectors are orthonormal, *i.e*

$$\vec{\varepsilon}^{\,\dagger}(s_z)\cdot\vec{\varepsilon}(s_z') = \delta_{s_z,s_z'}\ , \tag{2.3.3}$$

and

$$\sum_{s_z}\varepsilon_i^\dagger(s_z)\,\varepsilon_j(s_z) = \delta_{i,j}\ . \tag{2.3.4}$$

When no information is recorded on the spin states of the incoming and outgoing particles, the resulting cross section is known as unpolarized. In order to

allow for scattering in all possible spin configurations, we must average over the spin states of the incoming particles and sum over the spin projections of the particles in the final state. In our case,

$$\mid T \mid^2 \rightarrow \overline{\mid T \mid^2} = \frac{1}{2s+1} \sum_{spins} \mid T \mid^2 ,$$

where, for simplicity, we have written $T(s_z, p_+, p_0, p_-)$ as T. Since the ω has s = 1, for the three pion decay we get,

$$\overline{\mid T \mid^2} = \frac{\mid G_{\omega\pi^3} \mid^2}{3} \sum_{s_z} n_\mu \, \varepsilon_\mu(s_z) \, n_\nu \, \varepsilon^\dagger_\nu(s_z) = \frac{\mid G_{\omega\pi^3} \mid^2}{3} n_\mu \, n_\nu \delta_{\mu,\nu}$$

where summation over repeated indices is understood. This results in

$$\overline{\mid T \mid^2} = \mid G_{\omega\pi^3} \mid^2 \mid \vec{n} \mid^2 \quad . \tag{2.3.5}$$

In the ω rest frame, the momenta of the decay products are coplanar and their total energy equals M_ω. Hence

$$\vec{n} = (E_+ + E_- + E_0)(\vec{p}_- \times \vec{p}_+) = M_\omega(\vec{p}_- \times \vec{p}_+) ,$$

The modulus squared of $\vec{n}$ is therefore given by,

$$\mid \vec{n} \mid^2 = M_\omega^2 p_-^2 p_+^2 \sin^2\theta , \tag{2.3.6}$$

where θ is the angle between $\vec{p}_-$ and $\vec{p}_+$. Substituting for $\mid \vec{n} \mid^2$ in eq. (2.3.5), we get a final expression for the matrix element, which is

$$\overline{\mid T \mid^2} = \mid G_{\omega\pi^3} \mid^2 M_\omega^2 p_-^2 p_+^2 \sin^2\theta . \tag{2.3.7}$$

Now we are in a position to write down the decay rate of the ω in terms of a phase space element dQ, and $\overline{\mid T \mid^2}$ namely,

$$\Gamma = \int dQ \, \overline{\mid T \mid^2} .$$

Using eq. (2.2.11) and eq. (2.3.7), Γ is given by,

$$\Gamma = \frac{\pi}{4} \mid G_{\omega\pi^3} \mid^2 M_\omega^2 \int dE_- dE_+ d\Omega_- p_-^2 p_+^2 \sin^2\theta \, \Theta(1-\cos^2\theta) \, .$$

Here p_-^2 and p_+^2 are functions of E_- and E_+ and so we must write them in terms of their corresponding energies using eq. (2.2.7). Our final expression reads,

$$\Gamma = \pi^2 \mid G_{\omega\pi^3} \mid^2 M_\omega^2 \int (E_-^2 - m_{\pi^-}^2) dE_- (E_+^2 - m_{\pi^+}^2) dE_+ \sin^2\theta \, \Theta(1-\cos^2\theta) \, .$$

This is equivalent to,

$$\Gamma = \pi^2 \mid G_{\omega\pi^3} \mid^2 M_\omega^2 \int d\left(\frac{E_-^3}{3} - m_{\pi^-}^2 E_-\right) \, d\left(\frac{E_+^3}{3} - m_{\pi^+}^2 E_+\right) \sin^2\theta \, \Theta(1-\cos^2\theta) \, . \tag{2.3.8}$$

Chapter 3

ω Production Near Threshold

3.1 Experimental Data

The ω-meson can decay *via* strong interactions. Therefore, it has a relatively large width of 8.43 MeV/c^2 [1] compared to that of the η, which has essentially zero width. Therefore, when defining an ω production amplitude, one has to state clearly with respect to which mass, in the ω spectrum, the amplitude is defined. We shall briefly discuss the simpler η production amplitude before moving on to the more difficult ω case.

For the η production in the reaction $\pi^- p \rightarrow \eta n$, we can define an averaged amplitude squared in terms of the c.m. differential cross section by,

$$\mid F_\eta \mid^2 = \frac{p_p^*}{p_\eta^*} \times \left(\frac{d\sigma}{d\Omega^*} \right) ,$$

where the phase space ratio of outgoing to incident centre-of-mass momenta has been factored out. Experimentally, the η production seems to be enhanced in the vicinity of its threshold, *i.e.* F_η increases steadily as p_η^* gets smaller.

Similarly, for the reaction $\pi^- p \rightarrow \omega n$ we can define an averaged square amplitude $\mid F_\omega \mid^2$ which applies only to a narrow mass bin, ΔM say, in the ω mass spectrum. With this in mind, an experimental group [2] determined $\mid F_\omega \mid^2$ as

a function of the incident beam energy. They implemented the 'threshold crossing technique', which requires varying the pion beam momentum in very small steps such that they scanned the whole of the ω mass spectrum. Then, for each value of the missing mass ΔM, the corresponding recoil neutron was detected as the beam crossed a momentum value just above the threshold for its production. The recoil neutrons were detected at a mean angle of 2.8^0 relative to the incident pion beam. For each value of p^*_ω this resulted in a peak profile, which had a Breit-Wigner shape with a resonable width. With p^*_ω fixed, the value of p^*_p varied slightly for the different mass bins.

They defined an averaged amplitude squared, $\mid f_\omega \mid^2$, for the production of the whole ω state as the integral over the peak profile. *i.e*,

$$\mid f_\omega \mid^2 = \int \mid F_\omega \mid^2 dM \ .$$

For a narrow resonance, their definition implies that the cross section behaviour with p^*_ω be the same for each mass interval within the resonance.

In contrast to the η case, the experimental results given in [3], which are illustrated in fig. (3.1), show a rapid rise in σ/p^*_ω from threshold to a maximum value of about 8 mb/(GeV/c) at $p^*_\omega \approx 160$ MeV/c, decreasing thereafter. Despite this, the data showed almost no forward/backward asymmetry up to $p^*_\omega \approx 140$ MeV/c, suggestive of S-wave production. It is crucial to note that the suppression near threshold is in no way due to phase space cutting into the ω width as this was taken into account in the experimental analysis.

The experimental results [4, 5] illustrated in fig. (3.2) show the same type of behaviour for the reaction $p\,d \rightarrow {}^3He\,\omega$.

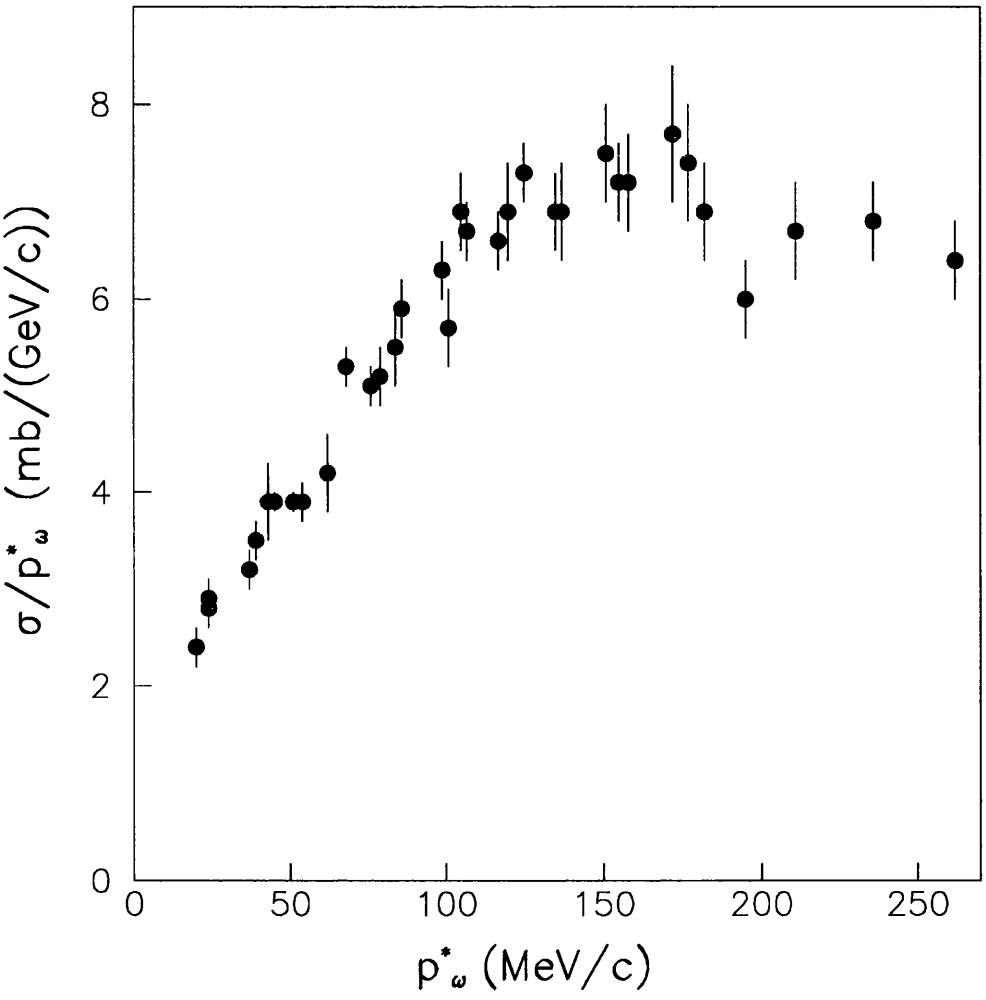

Figure 3.1: $\pi^- p \to n\omega$. σ/p^*_ω *versus* the centre-of-mass momentum p^*_ω.

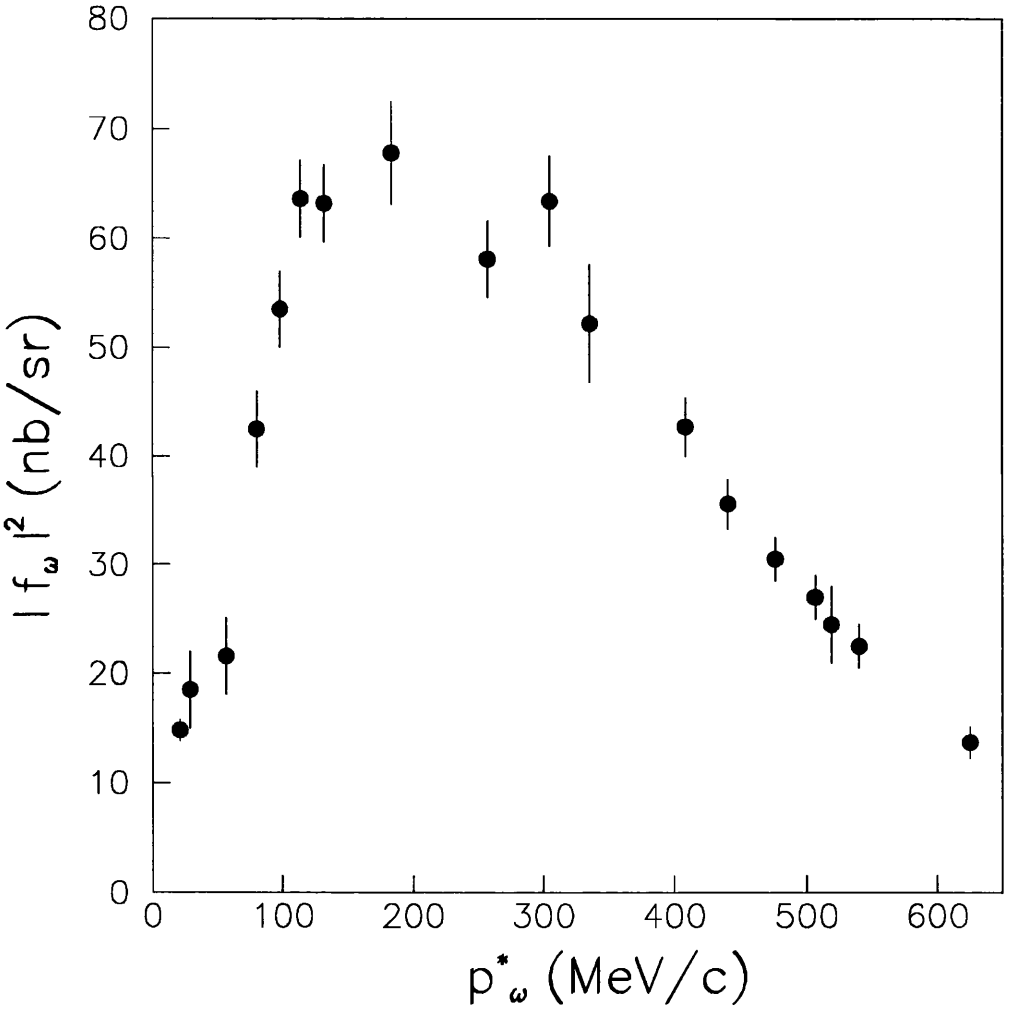

Figure 3.2: $pd \rightarrow {}^3He\,\omega$. The average amplitude squared, $|f_\omega|^2$, versus the centre-of-mass momentum p^*_ω.

3.2 Experimentalists' Analysis

In the dominant decay mode $\omega \rightarrow \pi^+\pi^-\pi^0$, the pions have an average momentum of 220 MeV/c in the ω rest frame which, at threshold, coincides with that of the neutron. This momentum is near the peak of the πN cross section. For $p^*_\omega = 20$ MeV/c, the ω and the neutron may have a total separation of ≈ 1 fm before the ω decays. This is within the range of interaction with the neutron. Thus, the probability of at least one of the decay pions interacting with the recoil neutron is high. The rescattering of such a pion would almost certainly knock the event out of the relatively narrow ω peak and into the background continuum, resulting in the determination of a lower cross section. Hence, the decay of an ω followed by Final State Interaction (**FSI**) effects seems to be a possible cause of the reduced production observed near threshold. To investigate this possibility the experimental group adopted a simple model where they assumed;

1. The ω production occurs in an S wave with respect to the neutron.

2. There is an effective distance R, such that all ω's decaying before travelling this distance from the neutron are assumed to be associated with scattered pions and hence be removed from the event rate. Those decaying beyond R are not affected and therefore contribute to the cross section.

Semiclassically, the probability of decay of the ω as a function of the ωn separation x can be written as,

$$P(x) \propto \exp\left(-\Gamma_\omega\, t\right) = \exp\left(\frac{-\Gamma_\omega\, x}{v}\right) \cdot \qquad (3.2.1)$$

Here

$$v = \left(\frac{p^*_\omega}{m_{red}}\right) ,$$

is the relative speed in the ωn centre-of-mass frame, and

$$m_{red} = \frac{m_\omega\, m_n}{m_\omega + m_n} ,$$

is the reduced mass of the ωn system. Therefore eq. (3.2.1) becomes

$$P(x) \propto \exp\left(-\frac{\Gamma_\omega\, m_{red}\, x}{p^*_\omega}\right) . \qquad (3.2.2)$$

The factor $\Gamma_\omega\, m_{red} = 8.43 \times 426.90 = 18.2$ MeV/c fm^{-1}. The experimental group actually used a value of $\approx$ 22 MeV/c fm^{-1} corresponding to an ω width of 10 MeV/c^2, and found a good fit to their data with $R = 1.5$ fm. Thus, for $\Gamma_\omega = 8.43$ MeV/c^2 [1], $R = 1.8$ fm. The final expression for the decay probability is,

$$P(x) \propto \exp\left(-\frac{18.2R}{p^*_\omega}\right) ,$$

where p^*_ω is measured in MeV/c.

The fit, shown in fig. (3.3), only reproduces the rapid rise from zero up to $p^*_\omega \approx 180$ MeV/c, and does not try to explain the decrease in σ/p^*_ω thereafter.

In their subsequent work [3], extra counters were introduced to differentiate between the dominant $\omega \rightarrow \pi^+\pi^-\pi^0$ and the 10% $\pi^0\gamma$ decay channels. Their new results lead them to abandon the earlier decay hypothesis for two reasons;

1. The ω width seemed to be independent of the value of p^*_ω. If decay + FSI were important the width should perhaps be larger nearer threshold where the decay is more likely to occur within the volume of radius R.

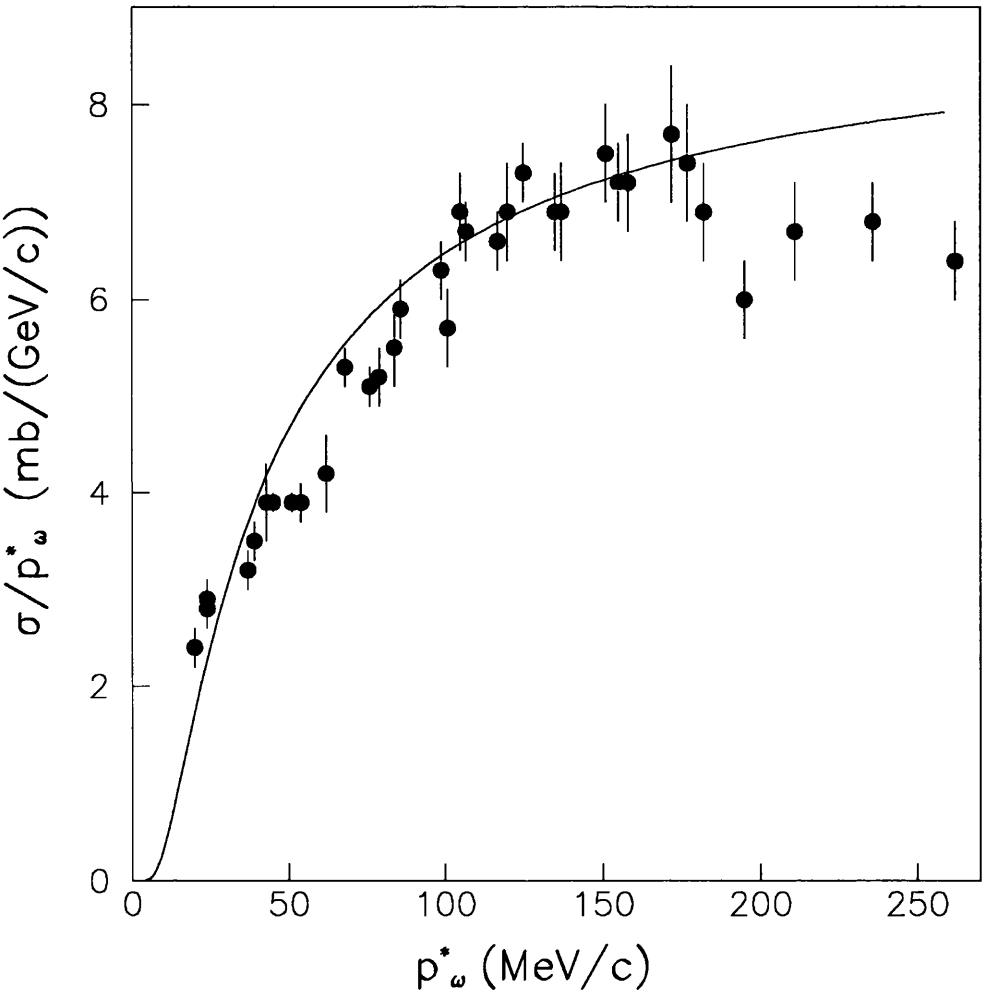

Figure 3.3: $\pi^- p \to n\omega$. σ/p^*_ω *versus* the centre-of-mass momentum p^*_ω. The solid line is a fit to the data corresponding to $P(x) = 9\exp(-18.2R/p^*_\omega)$. The value of R is 1.8 fm.

2. The relative branching ratios of the above decay channels seemed to be independent of p^*_ω, whereas one would expect the decay followed by the FSI to be more important in the three-pion case than for the radiative one due to the larger number of pions. A final-state interaction might also distort the ω mass spectrum, but no such effect was detected in their experiment.

The group tried other models in the hope of explaining the $d\sigma/d\Omega$ behaviour, which we shall outline below,

1. It was suggested that the effect could be caused by ρ exchange in the t channel, due to the vanishing of the spin-flip term at threshold. However, detailed study of the ρ-exchange model, conducted at the time, showed that it could not explain the effect.

2. The group sought an alternative explanation in terms of the S-channel partial-wave amplitudes. For a particular final-state orbital angular momentum L, the contribution to the cross section as $p^*_\omega \to 0$ behaves as,

$$\sigma \propto (p^*_\omega)^{2L+1} ,$$

There was therefore an *a priori* expectation that only S and P waves would be important in their energy region. The rapid rise in σ/p^*_ω suggests a significant contribution coming from the P waves. However, S waves are also required as the data are inconsistent with a parabolic rise from zero. However, they had to reconcile the inclusion of P waves with their data which showed an almost isotropic cross section normally associated with pure S-wave production. For the ωn system,

labeling the amplitudes by LL$'$(2S$'$)(2J), where L and L$'$ are the initial and final orbital angular momenta, S$'$ is the final spin, and J is the total angular momentum, then the seven parity-conserving amplitudes with L$'$= 0 or 1 and L = 0, 1, 2, or 3 are (SS11), (DS33), (PP11), (PP31), (PP13), (PP33) and (FP35). Of the possible S- and P-wave combinations, (SS11) + (PP31) and (DS33) + (PP11) can lead to the observed isotropic angular distribution with suitable combinations of coefficients. They fit their data using a combination of S and P waves, which resulted in good agreement with the data. Furthermore, their fit corresponded to a surprisingly large P-wave contribution, dominating over the S-wave even very close to threshold. As an example, at p^*_ω = 160 MeV/c, where $\mid f_\omega \mid^2$ reaches it maximum, the S-wave contribution to the cross section is 0.4 mb, while that of the P-wave is 0.85 mb. They speculated that the large P-wave contribution was due to a $\pi^- p$ resonance coupling to the ωn system near threshold. Now considering the only two possible combinations (SS11) + (PP31) and (DS33) + (PP11) that give an isotropic angular distribution, a possible candidate for the $\pi^- p$ resonance near threshold with J = $\frac{1}{2}$ and L = 1 is the P11(1720). They suggested that the resonance couples to the P-wave parts of the allowed amplitude combinations above. This hypothesis is not completely satisfactory as the resonance would be expected to feed both (PP31) and (PP11) amplitudes, resulting in an interference with a final-state S-wave amplitude. Hence, to maintain an isotropic angular distribution one of the final-state P waves and one of the final-state S waves would have to be suppressed.

3. In their subsequent work [6], they suggested a mechanism whereby the above desired suppression could be attained. They argued that in an $SU(6)_W$ model the decay of P11(1720) into (PP31) is strongly favoured over that into (PP11). If so, then the remaining S-wave part of σ/p^*_ω must be (SS11). The most likely way of producing an (SS11) final state is the presence of S11(1650) resonance in the $\pi^- p$ system.

One problem with their mechanism is that the photoproduction of P11(1720) shows only a small coupling to γ - N and so, by vector meson dominance, this is likely also to be the case for ω - N. A second difficulty is that exactly the same type of threshold reduction is seen in $pd \rightarrow {}^3He\,\omega$ data. Since their resonance mechanism depends on the relative coupling to the P11(1720) and S11(1650) being 'just right', it is unlikely that this would propagate through to the ${}^3He\,\omega$ system with sufficient precision.

On the other hand, the decay-FSI effect must exist at some level of importance. Therefore, we estimated its size in a more realistic but still *classical* model in the Monte-Carlo simulation of the decay followed by FSI, described in the next chapter.

Chapter 4

The Semi–Classical Model

4.1 The Monte-Carlo Simulation

We have written a Monte-Carlo simulation of the decay + FSI process based on the following assumptions,

1. Near threshold the basic ω-production amplitude is independent of p^*_ω and corresponds to S-wave production.

2. At time t=0 an ω and a neutron are produced at r=0 with equal and opposite momenta p^*_ω.

3. In the centre-of-mass frame of the decaying particle, the highest momentum of a decay product in a three body system occurs when two particles are moving in an opposite direction to the third. Labelling the three particles by a, b, and c, this momentum can be written in terms of the centre-of-mass energy s and the masses of the particles involved as

$$p^2_{max} = \frac{1}{4s}\left\{ \left(s - (m_a + m_{bc})^2\right)\left(s - (m_a - m_{bc})^2\right)\right\} \quad ,$$

where m_{bc} is the mass of the two particles moving in an opposite direction to third, whose mass is m_a. Thus, in the ω rest frame $p_{max} = 327$

MeV/c, corresponding to a central value of the ω mass of 782 MeV. On the other hand, for the radiative decay the the π^0 and γ are produced back to back with equal and opposite momenta, which is $\approx$ 379 MeV/c in the ω rest frame.

4. The normal to the decay plane $\vec{n}$ is chosen randomly in space. In the rest frame of the ω a distribution of the form,

$$| \vec{p}_- \times \vec{p}_+ |^2 = p_-^2 p_+^2 \sin^2\theta \ ,$$

is taken (see eq. (2.3.6)), which leads to an ω decay rate given by eq. (2.3.8).

5. Random values are generated for the functions

$$f(E_-) = \left(\frac{E_-^3}{3} - m_{\pi^-}^2 E_- \right) \ ,$$

and

$$f(E_+) = \left(\frac{E_+^3}{3} - m_{\pi^+}^2 E_+ \right) \ .$$

From the values of these two functions, the values of E_- and E_+ are determined by linear interpolation between two points using a table of $f(E_i)$ at equal intervals *versus* E_i. Then E_0 and the pion momenta are calculated by conserving energy and momentum according to equations (2.2.2) and (2.2.3), namely

$$\vec{p}_- + \vec{p}_+ + \vec{p}_0 = 0 \ ,$$

and

$$E_- + E_+ + E_0 = M_\omega \ .$$

6. A distribution in the $\omega-n$ separation x is taken according to eq. (3.2.1), namely

$$P(x) \propto \exp\left(\frac{-\Gamma_\omega x}{v}\right) ,$$

and events are drawn at random in x.

7. All momenta are then transformed to the neutron rest frame.

8. The total pion-neutron cross section, $\sigma_t(\pi^i n)$, is taken as a circular disc which defines a solid angle Ω at the distance x away from the recoil neutron where the ω decays.

9. The angle each pion makes with the line joining the ω and the neutron is calculated.

10. The crucial dynamical assumption is that if the pion angle α_i ($i = +, -, 0$) falls within the solid angle defined above, then we assume the pion is rescattered and hence the ω signal is destroyed. Otherwise, the ω's escape freely and the corresponding signals contribute to the cross section.

11. For the $\omega \to \pi^+\pi^-\pi^0$ decay channel, our *semiclassical* model implies that at least one or a *maximum* of two pions can be rescattered off the recoil neutron since it is not possible to have all three pions pointing towards the target as total momentum is conserved. For the radiative case only the π^0 can interact with the neutron significantly.

12. In the $\omega \to \pi^-\pi^+\pi^0$ decay mode the pions have an average momentum of about 220 MeV/c in the ω rest frame, which at threshold coincides with that of the neutron. This momentum corresponds to an incident

pion laboratory kinetic energy of ≈ 122 MeV. The total pion-neutron cross sections, $\sigma_t(\pi^+ n)$, $\sigma_t(\pi^- n)$, are taken to be constant at their values corresponding to the above kinetic energy [11]. Then $\sigma_t(\pi^0 n)$ was obtained using the isospin ratio (see appendix A) according to

$$\sigma_t(\pi^+ n) : \sigma_t(\pi^0 n) : \sigma_t(\pi^- n) = 3 : 2 : 1 \ .$$

The same is done in the radiative decay case except that the π^0 is produced at a momentum of 379 MeV/c.

13. An array of bins, each of width 1 MeV/c, is set up for values of p^*_ω starting from 0 up to 350 MeV/c. Corresponding to each one, we set up a further eight bins. They are SUM, three of the type P_i $(i = +, -, 0)$, and a further three P_{ij} with $j = +, -, 0$ but $i \neq j$. The last is P_0 for the π^0 in the radiative decay case. As could be seen from eq. (2.3.8), each event is weighted by the factor $\sin^2\theta$. The values of $\sin^2\theta$ corresponding to all physical events are stored in bin SUM. However, this factor is stored in bin P_i *only* when the angle α_i of pion π^i satisfies our dynamical assumption. When α_i and α_j, corresponding to π^i and π^j respectively, fall within the solid angle Ω the weighting factor is stored in bin P_{ij}.

    All eight bins are initialized with the value 0. For each p^*_ω bin we generated 5×10^4 random events. So each time a physical event was obtained, the value of SUM was updated as

$$\text{SUM} = \text{SUM} + \sin^2\theta \ .$$

Providing that one of the pion angles α_i falls within the solid angle subtended by σ_{π^i} at a distance x away from the neutron then,

$$P_i = P_i + \sin^2\theta \ .$$

Similarly, when α_i *and* α_j satisfy our dynamical assumption then,

$$P_{ij} = P_{ij} + \sin^2\theta \ .$$

Only if an interaction is possible are the values of the corresponding bins updated. Separate programmes were run for the three-pion and radiative decay channels, since the kinematics of these modes are different. We define the probability of only one pion scattering as,

$$P_i' = \frac{P_i}{\mathrm{SUM}}$$

and that of two pions scattering as,

$$P_{ij}' = \frac{P_{ij}}{\mathrm{SUM}}$$

14. In the limiting case $p_\omega^* \to 0$ the $\omega - n$ separation $x \to 0$ also. This corresponds to 2π solid angle subtended by σ_{π^i} at x. As a result the probability of one pion interacting is 0.5 depending on whether it is moving towards or away from the neutron. So

$$\sum_i P_i' = 1.5 \ .$$

On the other hand, in any physical event we must have two particles moving towards the neutron and the third away from it, or *vice versa.* Both cases are equally likely. As a consequence

$$\sum_{i \neq j} P_{ij}' = 0.5 \ ,$$

which means that $P'_{ij} \approx 0.16$. Therefore, by standard probability argument, the total probability of any final state interaction at all, is

$$P_{tot} = \sum_i P'_i - \sum_{i \neq j} P'_{ij} = 1.0 \; . \tag{4.1.1}$$

15. Defining P_ω to be the probability of observing an ω if it is produced, we can write down an expression for P_ω in terms of P_{tot} of the form,

$$P_\omega = 1 - P_{tot} \; . \tag{4.1.2}$$

16. Exactly the same procedure is carried out for the case $pd \rightarrow {}^3He\,\omega$, except that the pion-target cross section is evaluated for each event as a function of the incident pion beam momentum. This produced very similar results to those obtained when the cross section (for the same reaction) was taken to be independent of the initial state energy at a value corresponding to the average initial energy.

4.2 Results and Discussion

The predictions of the Monte-Carlo simulation for the decay followed by FSI in $\pi^- p$ and pd are shown in fig. (4.1) and fig. (4.2) respectively with an arbitrary normalization but no other free parameters.

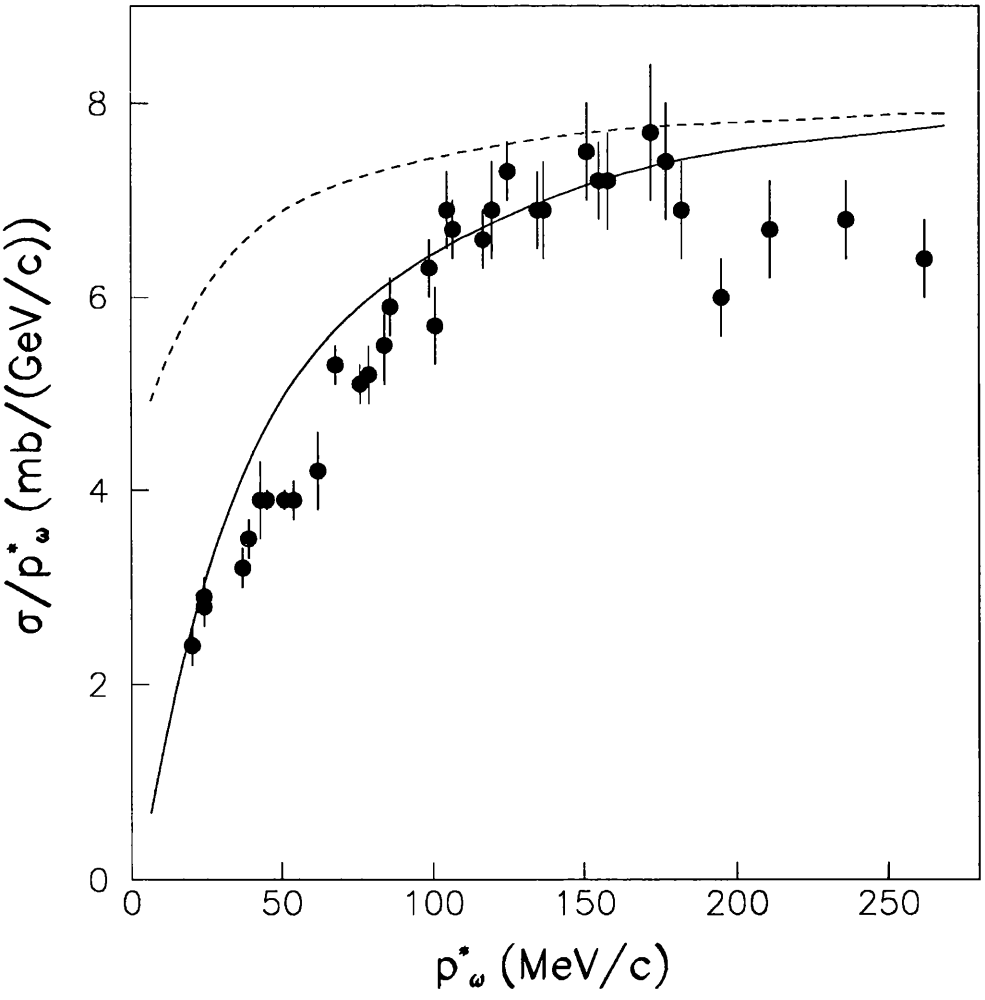

Figure 4.1: $\pi^- p \rightarrow n\omega$. σ/p^*_ω *versus* the centre-of-mass momentum p^*_ω. The solid line represents the three pion case, while the broken line is for the radiative branch.

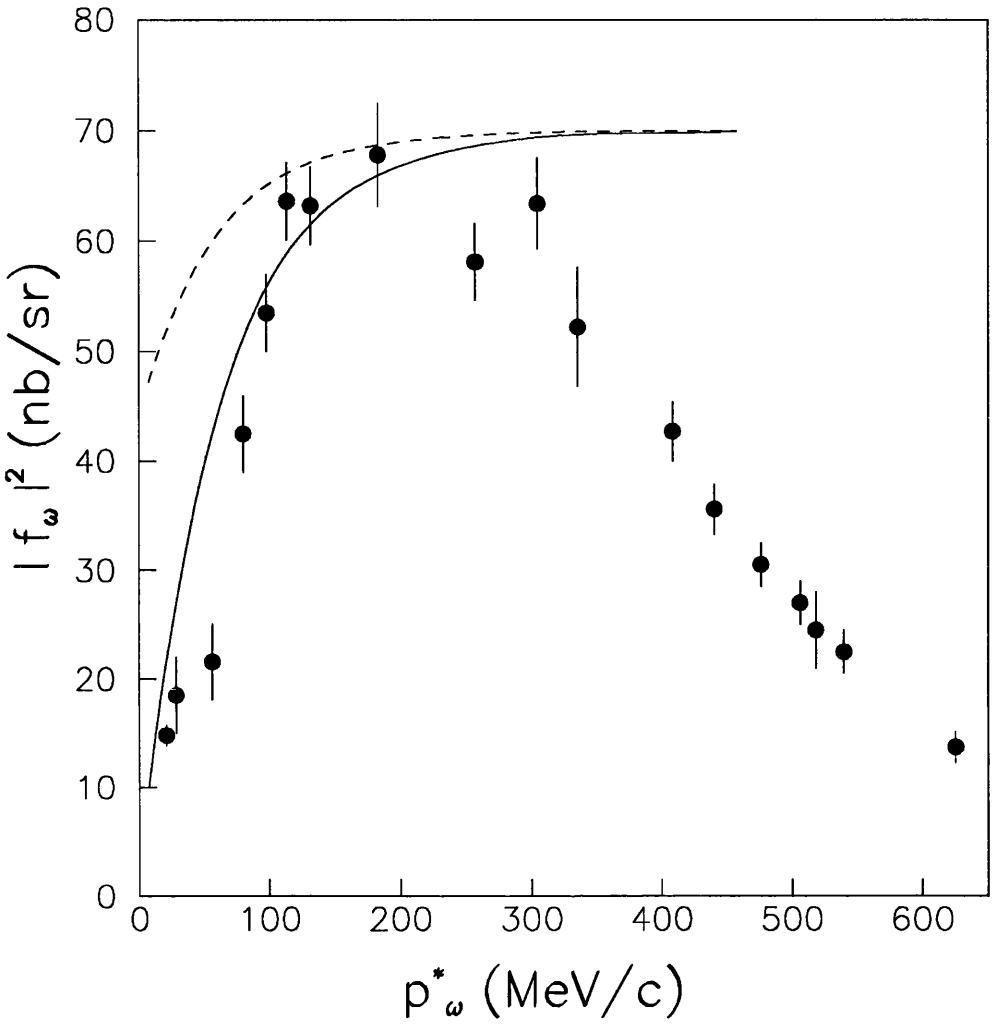

Figure 4.2: $pd \rightarrow {}^3He\,\omega$. The average amplitude square $\mid f_\omega \mid^2$, *versus* the centre-of-mass momentum p^*_ω. The solid line represents the three-pion case, while the broken one relates to the radiative case.

The behaviour of the Monte-Carlo predictions can be explained in terms of the solid angles subtended by σ_{π^i} at a distance x from the neutron. Large solid angles imply a high probability of the pions being scattered, resulting in a reduced observed ω amplitude. Conversely, small subtended solid angles reduce the chance of the decay pions interacting with the neutron, hence increasing the probability

of observing an ω. For example, consider the solid angle Ω_- subtended by σ_{π^-} at a distance x away from the neutron target. Then,

$$\Omega_- = \frac{\sigma_{\pi^-}}{x^2} \tag{4.2.1}$$

is inversely proportional to the square of the distance away from the target. Small p^*_ω results in the ω decaying in the near vicinity of the neutron leading to a reduction in the ω detection amplitude. On the other hand, for large p^*_ω the ω travels a longer distance on average before decaying, resulting in a large $\mid f_\omega \mid^2$. For very large x, *i.e* $p^*_\omega \geq 400$ MeV/c, the σ_{π^i} correspond to a negligible Ω_i and the probability of detecting an ω-meson tends to unity.

Clearly, the rapid fall-off for small p^*_ω has been quantitatively reproduced, as well as the scale of the effect in p^*_ω. As speculated earlier, in our Monte Carlo simulation the reduction effect is more important in the dominant three pion decay channel than the $\pi^0\gamma$ radiative case. It is worth mentioning that the difference is not a naive factor of three, since momentum conservation in the earlier case implies a maximum number of two pions scattering off the recoil neutron. However, our semi-classical model is a crude one and has many limitations. These include

1. The model violates the uncertainty principle as it simultaneously defines the position and momentum of the ω at the production vertex.

2. The ω-meson is always assumed to be on shell, and so off-shell effects were totally ignored.

3. For the three-pion case our model prohibits more than two pions to scatter off the neutron in any one event. This may not be the case in the quantum mechanical model, which we shall now study.

Chapter 5

Final–State Interaction Effects in $\pi^- p \rightarrow \omega n$

5.1 Introduction

In chapter 4 we developed a semi-classical model to estimate the effect of final-state interactions, between the ω decay products and the recoil neutron, on near-threshold ω production in the $\pi^- p \rightarrow \omega n$ process. The results reproduced well the sharp suppression at low energies. Although the ω lifetime, its decay probability distribution, the π-nucleon amplitudes *etc.* were all taken into account, this is still a simple model and has severe limitations. It viewed the ω as a real particle, and treated the scattering of its decay products as that of macroscopic hard spheres. Further, it did not take account of the smearing of the initial ω production vertex, as required by the uncertainty principle. Therefore, we decided to investigate the decay/FSI effects in a more realistic quantum model using Feynman diagrams.

In considering $\pi^- p \rightarrow \omega n$, where $\omega \rightarrow \pi^0 \gamma$, we shall treat the ω as a virtual particle, and calculate the strong final-state interaction amplitude between the π^0 and the recoil nucleon using quantum mechanical formalism. Although the pion-nucleon interaction is P-wave dominated, we shall first derive the easier S-wave amplitude and then move later to the more complex P-wave case. In both the

S and P-wave calculations we have not accounted for spin effects. These were of course also neglected in the classical approach.

In section 5.2.5 we present the quantum mechanical model results, which show $\approx$ 9% near-threshold reduction in the ω production amplitude due to the decay/FSI effects. The fact that a reduction is obtained is in line with experimental results [2, 3]. However, the suppression size is too small to account for the 70% effect observed experimentally.

5.2 The Quantum Mechanical Model

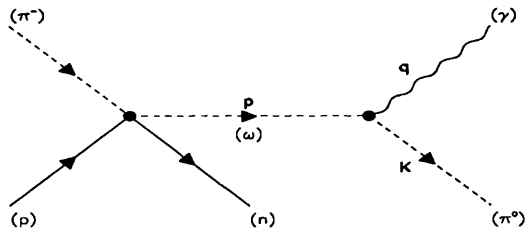

Figure 5.1: $\pi^- p \rightarrow \omega n$. Feynman diagram for ω production followed by its subsequent decay. No final state interactions are included. Characters in bold face are vectors in the overall c.m. system.

The ω production can be represented in terms of two Feynman graphs. The first corresponds to the production and subsequent decay of the ω, as shown in fig. (5.1). The second is shown in fig. (5.2), which is essentially the same as the first but extended to include final-state interactions between one of the ω decay products and the recoil neutron.

All momenta and energies are in the overall c.m. unless otherwise stated. To

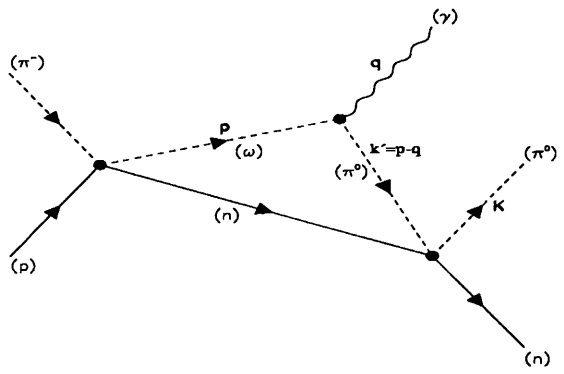

Figure 5.2: $\pi^- p \to \omega n$. Feynman diagram for ω production followed by its subsequent decay. Final-state interaction between π^0 and the recoil neutron is also included. Characters in bold face are vectors in the overall c.m. system.

simplify the presentation we have denoted p^*_ω by p.

5.2.1 Production Amplitude

As both fig. (5.1) and fig. (5.2) contribute to the ω production, it is their relative normalization which is critical and must be determined. For this purpose, we turn to the wave function of the final π^0, which is given by [12]

$$\Psi_K^{(+)}(\vec{r}) = \exp(i\vec{K}\cdot\vec{r}) + \int \frac{d^3k'}{(2\pi)^3} \frac{e^{i\vec{k'}\cdot\vec{r}}\, T(\vec{k'},\vec{K})}{E(K) - E(k') + i\epsilon}\,, \tag{5.2.1}$$

here

$$T(\vec{k'},\vec{K}) = -(4\pi/2M_{\pi^0}) f(\vec{k'},\vec{K})\,, \tag{5.2.2}$$

where $f(\vec{k'},\vec{K})$ is the pion-nucleon amplitude, which in general depends on the magnitude and direction of the momenta of the incident and scattered pions. $E(k')$ and $E(K)$ are the energies of the incident and rescattered π^0 respectively. Furthermore, the superscript plus indicates the outgoing wave boundary condition of $\Psi(\vec{r})$, and the subscript K indicates the physical scattering configuration with a beam of momentum K.

In momentum space, eq. (5.2.1) transforms into

$$\begin{aligned}\Psi_K^{(+)}(\vec{k}) &= \frac{1}{(2\pi)^{3/2}} \int d^3r\ e^{-i\vec{k}\cdot\vec{r}}\ \Psi_K^{(+)}(\vec{r}) \\ &= \frac{1}{(2\pi)^{3/2}} \left[(2\pi)^3\ \delta^{(3)}(\vec{k}-\vec{K}) + \int \frac{\delta^{(3)}(\vec{k}-\vec{k}')\ T(\vec{k}',\vec{K}) d^3k'}{E(K)-E(k')+i\epsilon} \right] .\end{aligned}$$

Hence

$$\Psi_K^{(+)}(\vec{k}) = \frac{1}{(2\pi)^{3/2}} \left[(2\pi)^3\, \delta^{(3)}(\vec{k}-\vec{K}) + \frac{T(\vec{k},\vec{K})}{E(K)-E(k)+i\epsilon} \right] \qquad (5.2.3)$$

The first term on the right relates to fig. (5.1), while the second term is associated with fig. (5.2) where final-state interactions take place. The above equation fixes the relative contributions of the two graphs to the ω production cross section.

For an infinitely heavy nucleon, and treating the ω production and pion-nucleon interaction vertices as point interactions, the ω production amplitude, F, can be expressed as

$$F = \frac{g}{(2\pi)^{3/2}} \int d^3p \left[\frac{1}{E_{\pi^-} - E_\omega} \left\{ (2\pi)^3\ \delta^{(3)}(\vec{k}-\vec{K}) - \frac{2\pi}{M_{\pi^0}}\ \frac{f(\vec{k},\vec{K})}{E(K)-E(k)+i\epsilon} \right\} \right] ,$$

where M_{π^0} is the π^0 mass and g is the ω decay coupling constant corresponding to the $\pi^0\gamma$ channel. The first integral on the right corresponds to the non-scattering case for which $\vec{K} = \vec{p} - \vec{q}$, while the second one is associated with the scattering case where $\vec{k} = \vec{p} - \vec{q}$. After carrying out the first integral, F is given by

$$F = \frac{g}{(2\pi)^{3/2}} \left[\frac{(2\pi)^3}{E_{\pi^-} - E_\omega} - \frac{2\pi}{M_{\pi^0}} \int d^3p \frac{f(\vec{k},\vec{K})}{(E_{\pi^-} - E_\omega)(E(K)-E(k)+i\epsilon)} \right] . \qquad (5.2.4)$$

The terms

$$\frac{1}{E_{\pi^-} - E_\omega} = \frac{1}{E_{\pi^-} - \left(\sqrt{p^2 + M_\omega^2} - i\Gamma_\omega/2\right)} ,$$

and

$$\frac{1}{E(K) - E(k) + i\epsilon} ,$$

are the ω and π^0 propagators respectively.

We can easily substitute for $E_{\pi^-} - E_\omega$ in the first term of eq. (5.2.4) but not in the second (scattering) term as $\sqrt{p^2 + M_\omega^2}$ would complicate the integration procedure. Instead, we write

$$\frac{1}{E_{\pi^-} - \sqrt{p^2 + M_\omega^2} + i\Gamma_\omega/2} = \frac{E_{\pi^-} + \sqrt{p^2 + M_\omega^2}}{E_{\pi^-}^2 - p^2 - M_\omega^2 + (i\Gamma_\omega/2)(E_{\pi^-} + \sqrt{p^2 + M_\omega^2})} . \tag{5.2.5}$$

We expect the scattering term to be small at high p as an ω would then escape from the nucleon field before decaying. This is in line with the experimental data, which show the suppression effect to be important only at low p. Consequently, we take

$$\sqrt{p^2 + M_\omega^2} \approx M_\omega , \quad p \ll M_\omega .$$

Therefore

$$\frac{1}{E_{\pi^-} - \sqrt{p^2 + M_\omega^2} + i\Gamma_\omega/2} \approx \frac{E_{\pi^-} + M_\omega}{(E_{\pi^-}^2 - p^2 - M_\omega^2 + i\Gamma_\omega(E_{\pi^-} + M_\omega)/2)} .$$

Defining $p_0^2 = (E_{\pi^-}^2 - M_\omega^2)$ and $\alpha = \Gamma_\omega(E_{\pi^-} + M_\omega)/2$, we finally get

$$\frac{1}{E_{\pi^-} - E_\omega} \approx \frac{E_{\pi^-} + M_\omega}{p_0^2 - p^2 + i\alpha} .$$

The $E(K) - E(k) + i\epsilon$ term can be expressed non-relativistically as

$$E(K) - E(k) + i\epsilon = -\frac{1}{2M_{\pi^0}} \left((\vec{p} - \vec{q})^2 - K^2 - i\epsilon \right) .$$

In terms of the above, the production amplitude becomes

$$F = \frac{g}{(2\pi)^{3/2}} \left[\frac{(2\pi)^3}{E_{\pi^-} - \sqrt{p^2 + M_\omega^2} + i\Gamma_\omega/2} - 4\pi \int \frac{(E_{\pi^-} + M_\omega)\, f(\vec{k}, \vec{K})\, d^3p}{(p^2 - p_0^2 - i\alpha)((\vec{p} - \vec{q})^2 - K^2 - i\epsilon)} \right] . \tag{5.2.6}$$

At threshold the π^0 and the γ are produced back to back with equal and opposite momenta of $\approx$ 379 MeV/c. This implies that our non-relativistic approximation of $E(K) - E(k) + i\epsilon$ is not valid in this energy range. On the other hand, putting in the exact energy expressions makes it almost impossible to obtain an analytical closed form for F. Therefore, we decided to expand $E(K) - E(k) + i\epsilon$ using the eikonal approximation [13], where we assume $\vec{K} - (\vec{p} - \vec{q})$ to be small *i.e.* small angle scattering. Hence,

$$\begin{aligned}(\vec{p} - \vec{q})^2 &= \left[(\vec{p} - \vec{q} - \vec{K}) + \vec{K})\right]^2 , \\ &= K^2 + 2\vec{K} \cdot (\vec{p} - \vec{q} - \vec{K}) + (\vec{p} - \vec{q} - \vec{K})^2 , \\ &\approx 2\vec{K} \cdot \vec{p} - 2\vec{K} \cdot \vec{q} - K^2 . \end{aligned} \tag{5.2.7}$$

To get our last expression, we neglected the small $(\vec{p} - \vec{q} - \vec{K})^2$ term. This should be a better approximation at higher energies. Finally

$$(\vec{p} - \vec{q})^2 - K^2 = 2(\vec{K} \cdot \vec{p} - \vec{K} \cdot \vec{q} - K^2) . \tag{5.2.8}$$

Substituting for $(\vec{p} - \vec{q})^2 - K^2$ in eq. (5.2.6) results in

$$F = \frac{g}{(2\pi)^{3/2}} \left[\frac{(2\pi)^3}{E_{\pi^-} - \sqrt{p^2 + M_\omega^2} + i\Gamma_\omega/2} - 2\pi \int \frac{(E_{\pi^-} + M_\omega)\, f(\vec{k}, \vec{K})\, d^3p}{(p^2 - p_0^2 - i\alpha)(\vec{K} \cdot \vec{p} - \vec{K} \cdot \vec{q} - K^2 - i\epsilon)} \right] . \tag{5.2.9}$$

The above integral is logarithmically divergent due to having taken point interactions. This problem may be dealt with by introducing form factors describing the size of the two-particle systems at the pion-nucleon and ω production interaction vertices. The first may be taken as

$$f_1 = \frac{(K^2 + \beta^2)^2}{(k^2 + \beta^2)^2} , \tag{5.2.10}$$

and, for simplicity, we shall take the second as

$$f_2 = \frac{(p_0^2 + \delta^2)}{(p^2 + \delta^2)} \,. \tag{5.2.11}$$

At threshold, $p_0 = p = 0$, and hence f_2 reduces to unity. Furthermore, the denominator of f_1 can be written as

$$\begin{aligned} k^2 + \beta^2 - i\epsilon &= (\vec{p} - \vec{q})^2 + \beta^2 - i\epsilon \,, \\ &= [(\vec{p} - \vec{q} - \vec{K}) + \vec{K}]^2 + \beta^2 - i\epsilon \,, \\ &\approx K^2 + 2\vec{K} \cdot (\vec{p} - \vec{q} - \vec{K}) + \beta^2 - i\epsilon \,, \end{aligned} \tag{5.2.12}$$

so that

$$f_1 \approx \frac{(K^2 + \beta^2)^2}{2\vec{K} \cdot \vec{p} - 2\vec{K} \cdot \vec{q} - K^2 + \beta^2 - i\epsilon} \,. \tag{5.2.13}$$

The finite nucleon mass also modifies the kinematics, leading to

$$E_{ext} = \sqrt{M_p^2 + p_p^2} + \sqrt{M_{\pi^-}^2 + p_p^2} \,, \tag{5.2.14}$$

and

$$E_{int} = \sqrt{M_n^2 + p^2} + \sqrt{M_\omega^2 + p^2} - i\Gamma_\omega/2 \,, \tag{5.2.15}$$

where E_{ext} (E_{int}) are the external (internal) total c.m. energies, and p_p is the proton momentum in the overall c.m. system.

This has the result of changing the ω propagator according to

$$\begin{aligned} \frac{1}{E_{\pi^-} - E_\omega} &\rightarrow \frac{1}{E_{ext} - E_{int}} \,, \\ &= \frac{1}{E_{ext} - \sqrt{M_n^2 + p^2} - \sqrt{M_\omega^2 + p^2} + i\Gamma_\omega/2} \,. \end{aligned} \tag{5.2.16}$$

As before, the above expression is exact and can be used in the non-scattering term. But once again we are going to make an approximation which applies in

the low p limit where the suppression effect is most important. For $p \ll M_\omega$ we can write

$$\begin{aligned} E_{int} &= \sqrt{M_n^2 + p^2} + \sqrt{M_\omega^2 + p^2} - i\Gamma_\omega/2 \,, \\ &\approx M_\omega + M_n + p^2/2M_r - i\Gamma_\omega/2 \,, \end{aligned} \tag{5.2.17}$$

where

$$M_r = \frac{M_n M_\omega}{M_n + M_\omega} \,,$$

is the reduced mass of the ω-n system.

This redefines our earlier values of p_0 and α as following

$$\begin{aligned} \frac{1}{E_{ext} - M_\omega - M_n - p^2/2M_r + i\Gamma_\omega/2} &= \frac{2M_r}{2M_r(E_{ext} - M_\omega - M_n) - p^2 + iM_r\Gamma_\omega} \,, \\ &= -\frac{2M_r}{p^2 - p_0^2 - i\alpha} \,. \end{aligned} \tag{5.2.18}$$

Obviously, p_0 and α are now given by

$$p_0^2 = 2M_r(E_{ext} - M_\omega - M_n) \,, \quad \alpha = M_r\Gamma_\omega \,.$$

Our final expression for F then reads

$$\begin{aligned} F &= \frac{g}{(2\pi)^{3/2}} \left[\frac{(2\pi)^3}{E_{ext} - \sqrt{p^2 + M_n^2} - \sqrt{p^2 + M_\omega^2} + i\Gamma_\omega/2} \right. \\ &- 4\pi M_r f(\vec{K}, \vec{K}) \int d^3p \frac{(p_0^2 + \delta^2)}{(p^2 + \delta^2)(2\vec{K}\cdot\vec{p} - 2\vec{K}\cdot\vec{q} - K^2 + \beta^2 - i\epsilon)^2} \times \\ &\left. \frac{(K^2 + \beta^2)^2}{(p^2 - p_0^2 - i\alpha)(\vec{K}\cdot\vec{p} - \vec{K}\cdot\vec{q} - K^2 - i\epsilon)} \right] \,, \end{aligned} \tag{5.2.19}$$

where we have replaced the half off-shell $f(\vec{k}, \vec{K})$ by the on shell $f(\vec{K}, \vec{K})$, and taken it out of the integral. This manner of estimating $f(\vec{k}, \vec{K})$ is in line with the eikonal approximation where the quantity $\vec{K} - \vec{k}$ was taken to be small; i.e forward scattering.

A Breit-Wigner fit for the total cross section for the $\pi^+ p$ interaction in our energy range is [11]

$$\sigma_{tot}(W) = \frac{8\pi}{k^2} \frac{W_0^2 \Gamma^2}{(W_0^2 - W^2)^2 + W_0^2 \Gamma^2} \,, \tag{5.2.20}$$

where W is the $\pi-$nucleon c.m. energy, and Γ is an energy dependent width.

This is a P-wave dominated cross section. To determine the parameters for the S-wave calculation, we took the cross section to be constant at its value in the forward direction and used the optical theorem to obtain the $\pi-$nucleon scattering amplitude *viz.*

$$\mathrm{Im}(f) = \frac{k}{4\pi}\sigma_{tot} = \frac{2}{k} \frac{W_0^2 \Gamma^2}{(W_0^2 - W^2)^2 + W_0^2 \Gamma^2} \,, \tag{5.2.21}$$

which implies that

$$f = \frac{2}{k} \frac{W_0 \Gamma}{(W_0^2 - W^2) - i W_0 \Gamma} \tag{5.2.22}$$

Defining

$$I = \int \frac{(p_0^2 + \delta^2)(K^2 + \beta^2)^2 d^3p}{(p^2 + \delta^2)(p^2 - p_0^2 - i\alpha)(\vec{K}\cdot\vec{p} - \vec{K}\cdot\vec{q} - K^2 - i\epsilon)(2\vec{K}\cdot\vec{p} - 2\vec{K}\cdot\vec{q} - K^2 + \beta^2 - i\epsilon)^2}, \tag{5.2.23}$$

then

$$F = \frac{g}{(2\pi)^{3/2}} \left[\frac{(2\pi)^3}{E_{ext} - \sqrt{p^2 + M_n^2} - \sqrt{p^2 + M_\omega^2} + i\Gamma_\omega/2} - 4\pi M_r f(\vec{K}, \vec{K})\, I \right] . \tag{5.2.24}$$

As mentioned earlier, we shall start with the easier S-wave πN amplitude, though the first term on the right (non-scattering term) is common to both the S and P-wave calculations.

5.2.2 S-Wave Amplitude

For the S-wave case we have

$$F_S = \frac{g}{(2\pi)^{3/2}} \left[\frac{(2\pi)^3}{E_{ext} - \sqrt{p^2 + M_n^2} - \sqrt{p^2 + M_\omega^2} + i\Gamma_\omega/2} - 4\pi M_r \, f(\vec{K}, \vec{K}) \, I_S \right] \tag{5.2.25}$$

where

$$I_S = \int \frac{(p_0^2 + \delta^2)\,(K^2 + \beta^2)^2 d^3p}{(p^2 + \delta^2)\,(p^2 - p_0^2 - i\alpha)(\vec{K}\cdot\vec{p} - \vec{K}\cdot\vec{q} - K^2 - i\epsilon)(2\vec{K}\cdot\vec{p} - 2\vec{K}\cdot\vec{q} - K^2 + \beta^2 - i\epsilon)^2}. \tag{5.2.26}$$

For simplicity, we start with

$$\begin{aligned} I'_S &= \int \frac{d^3p}{(p^2 + \delta^2)\,(p^2 - p_0^2 - i\alpha)(\vec{K}\cdot\vec{p} - \vec{K}\cdot\vec{q} - K^2 - i\epsilon)(2\vec{K}\cdot\vec{p} - 2\vec{K}\cdot\vec{q} - K^2 + \beta^2 - i\epsilon)}, \\ &= \frac{1}{K^2 + \beta^2} \int \frac{d^3p}{(p^2 - p_0^2 - i\alpha)(p^2 + \delta^2)} \times \\ &\quad \left[\frac{1}{\vec{K}\cdot\vec{p} - \vec{K}\cdot\vec{q} - K^2 - i\epsilon} - \frac{2}{2\vec{K}\cdot\vec{p} - 2\vec{K}\cdot\vec{q} - K^2 + \beta^2 - i\epsilon} \right]. \end{aligned}$$

Therefore

$$I'_S = \frac{1}{K^2 + \beta^2} \left[I'_{S1} - I'_{S2} \right], \tag{5.2.27}$$

with

$$I'_{S1} = \int \frac{d^3p}{(p^2 - p_0^2 - i\alpha)(p^2 + \delta^2)(\vec{K}\cdot\vec{p} - \vec{K}\cdot\vec{q} - K^2 - i\epsilon)}, \tag{5.2.28}$$

and

$$I'_{S2} = \int \frac{2\ d^3p}{(p^2 - p_0^2 - i\alpha)(p^2 + \delta^2)(2\vec{K}\cdot\vec{p} - 2\vec{K}\cdot\vec{q} - K^2 + \beta^2 - i\epsilon)}. \tag{5.2.29}$$

The relation between I_S and I'_S is

$$I_S = -\frac{1}{2\beta} \frac{\partial I'_S}{\partial \beta}. \tag{5.2.30}$$

Starting with I'_{S1} and letting $z = \cos\theta$, where θ is the angle between $\vec{K}$ and $\vec{p}$, we have

$$\begin{aligned} I'_{S1} &= 2\pi \int_0^{+\infty} \frac{p^2 dp}{(p^2 - p_0^2 - i\alpha)(p^2 + \delta^2)} \int_{-1}^{+1} \frac{dz}{Kpz - \vec{K}\cdot\vec{q} - K^2 - i\epsilon}\,, \\ &= \frac{2\pi}{K} \int_0^{+\infty} \frac{p\,dp}{(p^2 - p_0^2 - i\alpha)(p^2 + \delta^2)} \left[\ln(Kpz - \vec{K}\cdot\vec{q} - K^2 - i\epsilon)\right]_{-1}^{+1}\,, \\ &= \frac{2\pi}{K} \int_0^{+\infty} \frac{p\,dp}{(p - \sqrt{p_0^2 + i\alpha})(p + \sqrt{p_0^2 + i\alpha})(p - i\delta)(p + i\delta)} \times \\ &\quad \ln\left(\frac{Kp - KqH - K^2 - i\epsilon}{-Kp - KqH - K^2 - i\epsilon}\right)\,. \end{aligned} \tag{5.2.31}$$

Here, H is the cosine of the angle between $\vec{K}$ and $\vec{q}$. To do the above integral, we differentiate I'_{S1} with respect to q to obtain

$$\begin{aligned} \frac{\partial I'_{S1}}{\partial q} &= -\pi H \int_{-\infty}^{+\infty} \frac{p\,dp}{(p - \sqrt{p_0^2 + i\alpha})(p + \sqrt{p_0^2 + i\alpha})(p - i\delta)(p + i\delta)} \times \\ &\quad \left(\frac{1}{Kp - KqH - K^2 - i\epsilon} + \frac{1}{Kp + KqH + K^2 + i\epsilon}\right)\,. \end{aligned}$$

As the last expression is symmetric around $p = 0$, we extend the integration down to $-\infty$ and compensate for this by multiplying by a factor of $1/2$. Further, we can write

$$\frac{\partial I'_{S1}}{\partial q} = -\pi H \left(\frac{\partial I'_{S11}}{\partial q} + \frac{\partial I'_{S12}}{\partial q}\right)\,. \tag{5.2.32}$$

where

$$\frac{\partial I'_{S11}}{\partial q} = \frac{1}{K} \int_{-\infty}^{+\infty} \frac{p\,dp}{(p - \sqrt{p_0^2 + i\alpha})(p + \sqrt{p_0^2 + i\alpha})(p - i\delta)(p + i\delta)(p - qH - K - i\epsilon)}\,,$$

and

$$\frac{\partial I'_{S12}}{\partial q} = \frac{1}{K} \int_{-\infty}^{+\infty} \frac{p\,dp}{(p - \sqrt{p_0^2 + i\alpha})(p + \sqrt{p_0^2 + i\alpha})(p - i\delta)(p + i\delta)(p + qH + K + i\epsilon)}\,.$$

Contour integration results in

$$\frac{\partial I'_{S11}}{\partial q} = \frac{2\pi i}{K}\left[\frac{1}{2(p_0^2+i\alpha+\delta^2)(\sqrt{p_0^2+i\alpha}-qH-K)}\right.$$

$$- \frac{1}{2(p_0^2+i\alpha+\delta^2)(i\delta-qH-K)}$$

$$\left. + \frac{K+qH}{[(K+qH)^2-p_0^2-i\alpha][(K+qH)^2+\delta^2]}\right] . \qquad (5.2.33)$$

Similarly,

$$\frac{\partial I'_{S12}}{\partial q} = \frac{2\pi i}{K}\left[\frac{1}{2(p_0^2+i\alpha+\delta^2)(\sqrt{p_0^2+i\alpha}+qH+K)}\right.$$

$$\left. - \frac{1}{2(p_0^2+i\alpha+\delta^2)(i\delta+qH+K)}\right] .$$

Substituting for $\partial I'_{S12}/\partial q$ and $\partial I'_{S12}/\partial q$ in eq. (5.2.32) results in

$$\frac{\partial I'_{S1}}{\partial q} = -\frac{2\pi^2 iH}{K}\left[\frac{1}{2(p_0^2+i\alpha+\delta^2)(K+qH-i\delta)}\right.$$

$$-\frac{1}{2(p_0^2+i\alpha+\delta^2)(K+qH-\sqrt{p_0^2+i\alpha})} + \frac{K+qH}{[(K+qH)^2-p_0^2-i\alpha][(K+qH)^2+\delta^2]}$$

$$\left. + \frac{1}{2(p_0^2+i\alpha+\delta^2)(K+qH+\sqrt{p_0^2+1\alpha})} - \frac{1}{2(p_0^2+i\alpha+\delta^2)(K+qH+i\delta)}\right] . \qquad (5.2.34)$$

By taking

$$\frac{1}{p_0^2+i\alpha+\delta^2} ,$$

as a common factor and rearranging, we arrive at

$$\frac{\partial I'_{S1}}{\partial q} = -\frac{2\pi^2 iH}{K(p_0^2+i\alpha+\delta^2)}\left[\frac{1}{K+qH+\sqrt{p_0^2+i\alpha}} - \frac{1}{K+qH+i\delta}\right] ,$$

which yields

$$I'_{S1} = -\frac{2\pi^2 i}{K(p_0^2 + i\alpha + \delta^2)} \ln\left(\frac{K + qH + \sqrt{p_0^2 + i\alpha}}{K + qH + i\delta}\right) + C\,, \qquad (5.2.35)$$

Repeating the above procedure for the second integral, we find

$$I'_{S2} = -\frac{2\pi^2 i}{K(p_0^2 + i\alpha + \delta^2)} \ln\left(\frac{K/2 + qH - \beta^2/2K + \sqrt{p_0^2 + i\alpha}}{K/2 + qH - \beta^2/2K + i\delta}\right) + C'\,. \quad (5.2.36)$$

Here C and C' are infinite constants which cancel out when I'_{S1} and I'_{S2} are substituted into eq. (5.2.27). This gives

$$I'_S = \frac{2\pi^2 i}{K(p_0^2 + i\alpha + \delta^2)(K^2 + \beta^2)} \times$$

$$\left[\ln\left(\frac{K + qH + i\delta}{K/2 + qH - \beta^2/2K + i\delta}\right) - \ln\left(\frac{K + qH + \sqrt{p_0^2 + i\alpha}}{K/2 + qH - \beta^2/2K + \sqrt{p_0^2 + i\alpha}}\right)\right]\,. \qquad (5.2.37)$$

Differentiating I'_S with respect to β and using eq. (5.2.30) we finally get

$$I_S = \frac{2\pi^2 i}{K} \frac{(p_0^2 + \delta^2)}{(p_0^2 + i\alpha + \delta^2)} \times$$

$$\left[\frac{(K^2 + \beta^2)}{2K}\left(\frac{1}{K/2 + qH - \beta^2/2K + \sqrt{p_0 + i\alpha}} - \frac{1}{K/2 + qH - \beta^2/2K + i\delta}\right)\right.$$

$$\left. + \ln\left(\frac{K/2 + qH - \beta^2/2K + \sqrt{p_0^2 + i\alpha}}{K + qH + \sqrt{p_0^2 + i\alpha}}\right) + \ln\left(\frac{K + qH + i\delta}{K/2 + qH - \beta^2/2K + i\delta}\right)\right]\,. \qquad (5.2.38)$$

Using eq. (5.2.25), our final expression for the S-wave amplitude reads

$$F_S = (2\pi)^{3/2} g \left\{ \frac{1}{E_{ext} - \sqrt{p^2 + M_n^2} - \sqrt{p^2 + M_\omega^2} + i\Gamma_\omega/2} - iM_r \frac{f(\vec{K},\vec{K})}{K} \frac{(p_0^2 + \delta^2)}{(p_0^2 + i\alpha + \delta^2)} \times \right.$$

$$\left[\frac{(K^2 + \beta^2)}{2K} \left(\frac{1}{K/2 + qH - \beta^2/2K + \sqrt{p_0 + i\alpha}} - \frac{1}{K/2 + qH - \beta^2/2K + i\delta} \right) \right.$$

$$\left. \left. + \ln \left(\frac{K/2 + qH - \beta^2/2K + \sqrt{p_0^2 + i\alpha}}{K + qH + \sqrt{p_0^2 + i\alpha}} \right) + \ln \left(\frac{K + qH + i\delta}{K/2 + qH - \beta^2/2K + i\delta} \right) \right] \right\}. \tag{5.2.39}$$

5.2.3 P-Wave Amplitude

We now turn to the more realistic but complicated P-wave case. In analogy with the S-wave case, the P-wave ω production amplitude may be expressed as

$$F_P = \frac{g}{(2\pi)^{3/2}} \left[\frac{(2\pi)^3}{E_{ext} - \sqrt{p^2 + M_n^2} - \sqrt{p^2 + M_\omega^2} + i\Gamma_\omega/2} - 4\pi M_r \frac{f(\vec{K},\vec{K})}{K^2} I_P \right] \tag{5.2.40}$$

where

$$I_P = \int \frac{(p_0^2 + \delta^2)(K^2 + \beta^2)^2 \vec{K} \cdot \vec{k}\, d^3p}{(p^2 + \delta^2)(p^2 - p_0^2 - i\alpha)(2\vec{K} \cdot \vec{p} - 2\vec{K} \cdot \vec{q} - K^2 + \beta^2 - i\epsilon)^2 (\vec{K} \cdot \vec{p} - \vec{K} \cdot \vec{q} - K^2 - i\epsilon)}. \tag{5.2.41}$$

Substituting $\vec{k} = \vec{p} - \vec{q}$ gives

$$I_P = \int \frac{(p_0^2 + \delta^2)(K^2 + \beta^2)^2\ \vec{K} \cdot (\vec{p} - \vec{q})\, d^3p}{(p^2 + \delta^2)(p^2 - p_0^2 - i\alpha)(2\vec{K} \cdot \vec{p} - 2\vec{K} \cdot \vec{q} - K^2 + \beta^2 - i\epsilon)^2 (\vec{K} \cdot \vec{p} - \vec{K} \cdot \vec{q} - K^2 - i\epsilon)}. \tag{5.2.42}$$

If we define

$$I'_P = \int d^3p \frac{\vec{K} \cdot \vec{p}}{(p^2 + \delta^2)(p^2 - p_0^2 - i\alpha)(2\vec{K} \cdot \vec{p} - 2\vec{K} \cdot \vec{q} - K^2 + \beta^2 - i\epsilon)(\vec{K} \cdot \vec{p} - \vec{K} \cdot \vec{q} - K^2 - i\epsilon)}, \tag{5.2.43}$$

where I_S is given by eq. (5.2.26). Then

$$I_P = (p_0^2 + \delta^2)(K^2 + \beta^2)^2 \left(-\frac{1}{2\beta}\frac{\partial I'_p}{\partial \beta}\right) - \vec{K}\cdot\vec{q}\, I_S \,, \tag{5.2.44}$$

We introduced K^2 in the denominator of the second term in eq. (5.2.40) to compensate for the $\vec{K}\cdot\vec{k}$ term in eq. (5.2.41). Using partial fractions, I'_P may be expressed as

$$I'_P = \frac{1}{K^2+\beta^2}\left(I'_{P1} - I'_{P2}\right) \,, \tag{5.2.45}$$

where

$$I'_{P1} = \int d^3p \frac{\vec{K}\cdot\vec{p}}{(p^2 - p_0^2 - i\alpha)(p^2+\delta^2)(\vec{K}\cdot\vec{p} - \vec{K}\cdot\vec{q} - K^2 - i\epsilon)} \,, \tag{5.2.46}$$

and

$$I'_{P2} = \int d^3p \frac{2\vec{K}\cdot\vec{p}}{(p^2 - p_0^2 - i\alpha)(p^2+\delta^2)(2\vec{K}\cdot\vec{p} - 2\vec{K}\cdot\vec{q} - K^2 + \beta^2 - i\epsilon)} \,. \tag{5.2.47}$$

We shall start by evaluating I'_{P1}, where we add and subtract the term

$$(\vec{K}\cdot\vec{q} + K^2 + i\epsilon) \,, \tag{5.2.48}$$

from the the numerator of eq. (5.2.46) to get

$$\begin{aligned} I'_{P1} &= \int d^3p \frac{\vec{K}\cdot\vec{p} - (\vec{K}\cdot\vec{q} + K^2 + i\epsilon) + (\vec{K}\cdot\vec{q} + K^2 + i\epsilon)}{(p^2 - p_0^2 - i\alpha)(p^2+\delta^2)(\vec{K}\cdot\vec{p} - \vec{K}\cdot\vec{q} - K^2 - i\epsilon)} \,, \\ &= \int \frac{d^3p}{(p^2 - p_0^2 - i\alpha)(p^2+\delta^2)} + (\vec{K}\cdot\vec{q} + K^2)\, I'_{S1} \,, \end{aligned} \tag{5.2.49}$$

with I'_{S1} given in eq. (5.2.28). By integrating the first term on the right and then using eq. (5.2.35), we arrive at

$$I'_{P1} = \frac{2\pi^2 i}{(p_0^2 + i\alpha + \delta^2)}\left[\sqrt{p_0^2 + i\alpha} - i\delta - \frac{(\vec{K}\cdot\vec{q} + K^2)}{K}\ln\left(\frac{K + qH + \sqrt{p_0^2 + i\alpha}}{K + qH + i\delta}\right)\right] + D \,. \tag{5.2.50}$$

Similarly

$$I'_{P2} = \int \frac{d^3p}{(p^2 - p_0^2 - i\alpha)(p^2 + \delta^2)} + (2\vec{K}\cdot\vec{q} + K^2 - \beta^2)\frac{I'_{S2}}{2} ,$$

$$= \frac{2\pi^2 i}{(p_0^2 + i\alpha + \delta^2)} \left[\sqrt{p_0^2 + i\alpha} - i\delta - \frac{1}{2K}(2\vec{K}\cdot\vec{q} + K^2 - \beta^2) \times \right.$$

$$\left. \ln\left(\frac{K/2 + qH - \beta^2/2K + \sqrt{p_0^2 + i\alpha}}{K/2 + qH - \beta^2/2K + i\delta}\right)\right] + D' .$$

Eq. (5.2.36) was used to get the last result. Substituting for I'_{P1} and I'_{P2} into eq. (5.2.45) eliminates the (infinite) D and D' constants and results in

$$I'_P = \frac{\pi^2 i}{K(K^2 + \beta^2)(p_0^2 + i\alpha + \delta^2)} \times$$

$$\left[(2\vec{K}\cdot\vec{q} + K^2 - \beta^2)\ln\left(\frac{K/2 + qH - \beta^2/2K + \sqrt{p_0^2 + i\alpha}}{K/2 + qH - \beta^2/2K + i\delta}\right) - \right.$$

$$\left. 2(\vec{K}\cdot\vec{q} + K^2)\ln\left(\frac{K + qH + \sqrt{p_0^2 + i\alpha}}{K + qH + i\delta}\right)\right] .$$

Differentiating I'_P with respect to β and using eq. (5.2.38), eq. (5.2.44) becomes

$$I_P = \pi^2 i \frac{(p_0^2 + \delta^2)}{K^3(p_0^2 + i\alpha + \delta^2)} \times$$

$$\left[\frac{K^4 - \beta^4}{2K}\left(\frac{1}{K/2 + qH - \beta^2/2K + \sqrt{p_0^2 + i\alpha}} - \frac{1}{K/2 + qH - \beta^2/2K + i\delta}\right) + 2K^2 \right.$$

$$\left. \left\{\ln\left(\frac{K/2 + qH - \beta^2/2K + \sqrt{p_0^2 + i\alpha}}{K + qH + \sqrt{p_0^2 + i\alpha}}\right) + \ln\left(\frac{K + qH + i\delta}{K/2 + qH - \beta^2/2K + i\delta}\right)\right\}\right] . \tag{5.2.51}$$

According to eq. (5.2.40), the total near-threshold P-wave production ampli-

tude for the ω meson may now be written as

$$F_P = \frac{(2\pi)^{3/2} g}{E_{ext} - \sqrt{p^2 + M_n^2} - \sqrt{p^2 + M_\omega^2} + i\Gamma_\omega/2} - (2\pi)^{3/2} g \frac{iM_r}{2} \frac{f(\vec{K}, \vec{K})}{K^3} \frac{(p_0^2 + \delta^2)}{(p_0^2 + i\alpha + \delta^2)} \times$$

$$\left\{ \frac{K^4 - \beta^4}{2K} \left(\frac{1}{K/2 + qH - \beta^2/2K + \sqrt{p_0^2 + i\alpha}} - \frac{1}{K/2 + qH - \beta^2/2K + i\delta} \right) + 2K^2 \right.$$

$$\left. \left[\ln \left(\frac{K/2 + qH - \beta^2/2K + \sqrt{p_0^2 + i\alpha}}{K + qH + \sqrt{p_0^2 + i\alpha}} \right) + \ln \left(\frac{K + qH + i\delta}{K/2 + qH - \beta^2/2K + i\delta} \right) \right] \right\} . \tag{5.2.52}$$

5.2.4 Phase Space Factors

In chapter 2 we developed the three particle phase space for the final state pions π^-, π^+ and π^0, though we did not necessarily assume equal masses at that stage. According to eq. (2.2.11), the phase space is given by

$$dQ = \frac{\pi}{4} dE_- dE_+ d\Omega_- \Theta(1 - \cos^2\theta) .$$

In our present case, the final state particles are n, π^0 and γ. Therefore, by making the correspondence $\pi^- \rightarrow n$, $\pi^+ \rightarrow \pi^0$ and $\pi^0 \rightarrow \gamma$, we get

$$dQ = \frac{\pi}{4} dE_n \, dE(K) \, d\Omega_n . \tag{5.2.53}$$

We have omitted the step function on the understanding that $\cos^2\theta \leq 1$, where θ is the angle between the recoil neutron momentum and $\vec{K}$. E_n and $E(K)$ are the neutron and π^0 energies respectively, and $d\Omega_n$ is the solid angle describing the orientation of the neutron momentum with respect to some axis in space.

Using the relation $E_n \, dE_n = P_n \, dP_n$, where $P_n = p$ is the internal neutron

momentum in the overall c.m. system, we can rewrite dQ as

$$dQ = \frac{\pi}{4}\frac{p}{E_n}\, dE(K)\, dp\, d\Omega_n \ . \tag{5.2.54}$$

In terms of the phase space and the ω production amplitude F, the cross section for the threshold ω production can be expressed as

$$\sigma = \frac{\pi}{4}\int \frac{p}{E_n} \mid F \mid^2 \ dE(K)\, d\Omega_n dp \ . \tag{5.2.55}$$

Therefore

$$\frac{\partial^2\sigma}{\partial p\, \partial\Omega_n} = \frac{\pi}{4}\int_{E(K)^{min}}^{E(K)^{max}} \frac{p}{E_n} \mid F \mid^2 \ dE(K) \ . \tag{5.2.56}$$

Apart from averaging over initial spin states and summing over the final ones, eq. (5.2.56) is the theoretical prediction for the experimental results given in [3] which we displayed in chapter 3. The curve in the $E_n - E(K)$ plane, which bounds the physically accessible region in phase space is given by eq. (2.2.12) after making the same final state particle correspondence as above. Hence it is given by

$$4(E_n^2 - m_n^2)(E_K^2 - m_{\pi^0}^2) = (2E_nE(K) - 2\sqrt{s}(E_n + E(K)) + s + m_n^2 + m_{\pi^0}^2)^2 \ . \tag{5.2.57}$$

In line with the threshold crossing technique followed in the experiment, we varied the pion beam energy such that we scanned the ω mass for constant p.

5.2.5 Results of the Quantum Mechanical Model

The results of the our quantum mechanical model are shown below. Fig. (5.3) and Fig. (5.4) correspond to the S-wave case. The solid line relates to the production and subsequent decay only, whereas the broken line corresponds to the case where final state interactions of the decaying pions are included. In Fig. (5.5) and Fig. (5.6) we show the results corresponding to the more realistic P-wave πN

interaction. All graphs correspond to $\alpha = 3599\ (\mathrm{MeV/c^2})^{-2}$ and $\beta = 1682$ MeV/c (see appendix B).

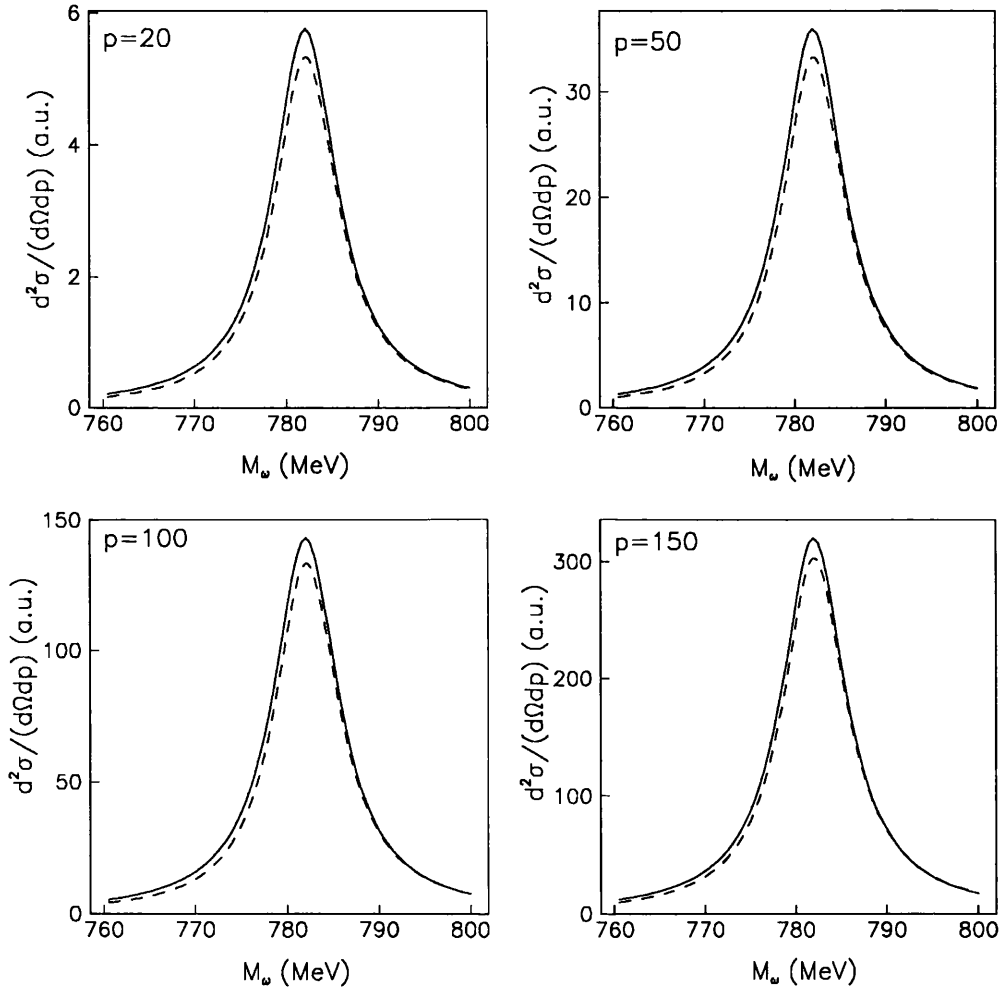

Figure 5.3: $\pi^- p \to \omega n$. The S-wave theoretical prediction of eq. (5.2.56). The solid line represents the production followed by subsequent decay only. The broken line corresponds to the case where final state interactions are included.

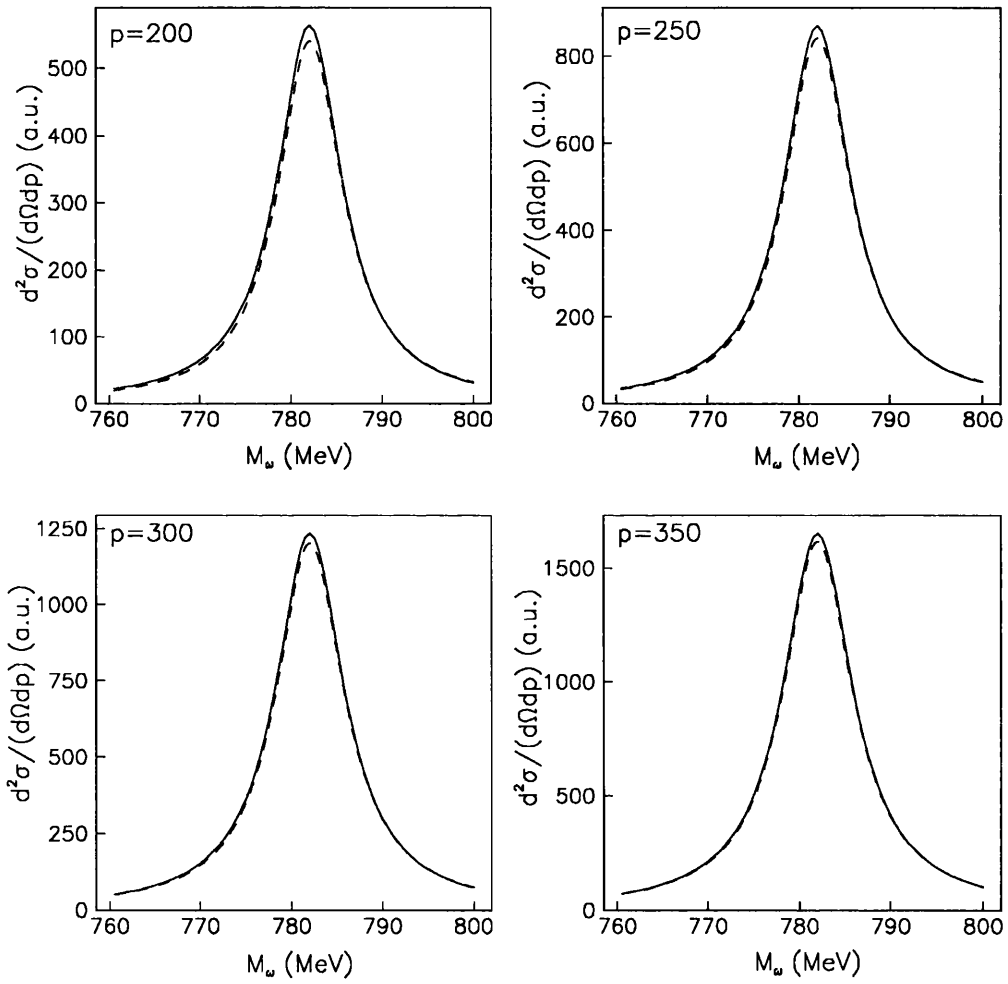

Figure 5.4: $\pi^- p \to \omega n$. The S-wave theoretical prediction of eq. (5.2.56). The solid line represents the production followed by subsequent decay only. The broken line corresponds to the case where final state interactions are included.

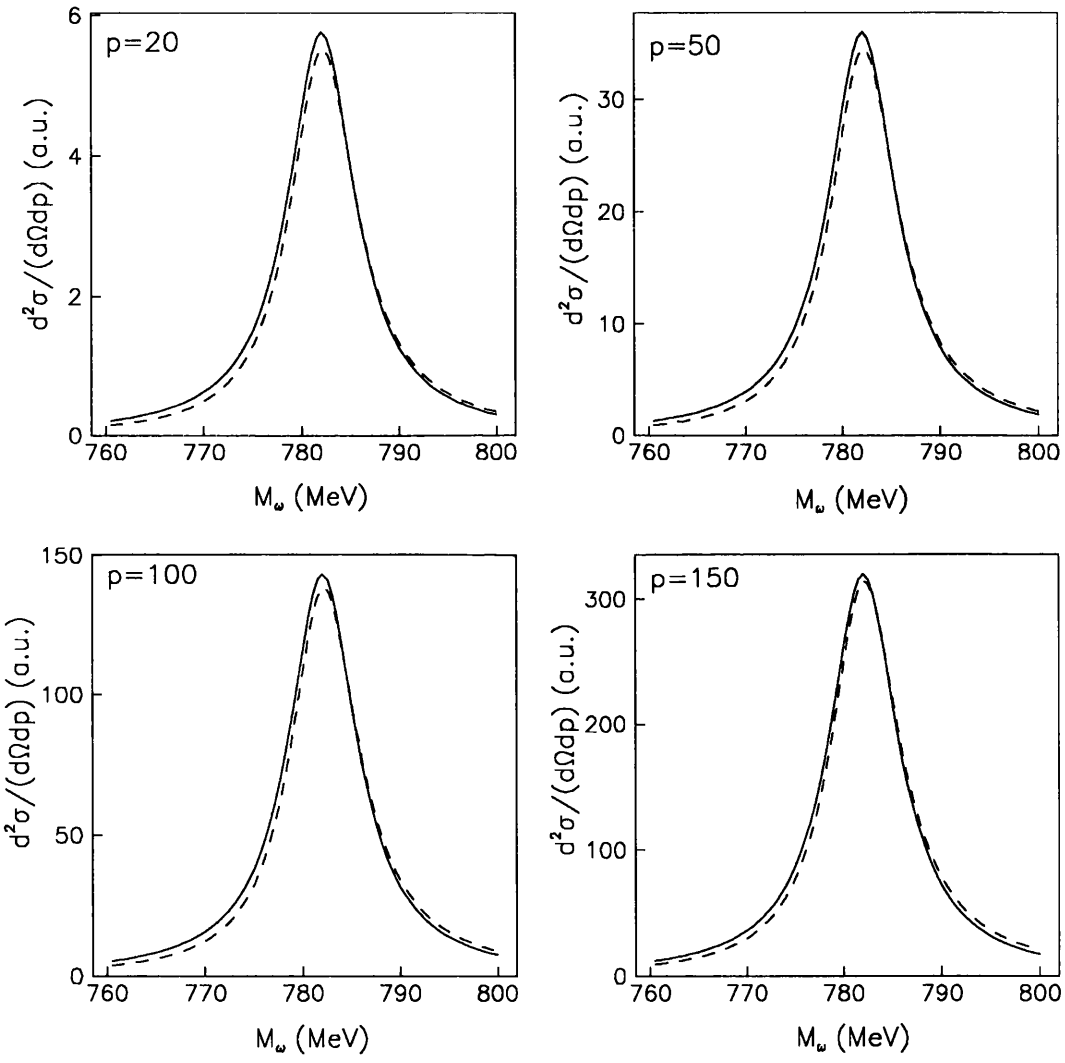

Figure 5.5: $\pi^- p \to \omega n$. The P-wave theoretical prediction of eq. (5.2.56). The solid line represents the production followed by subsequent decay only. The broken line corresponds to the case where final state interactions are included.

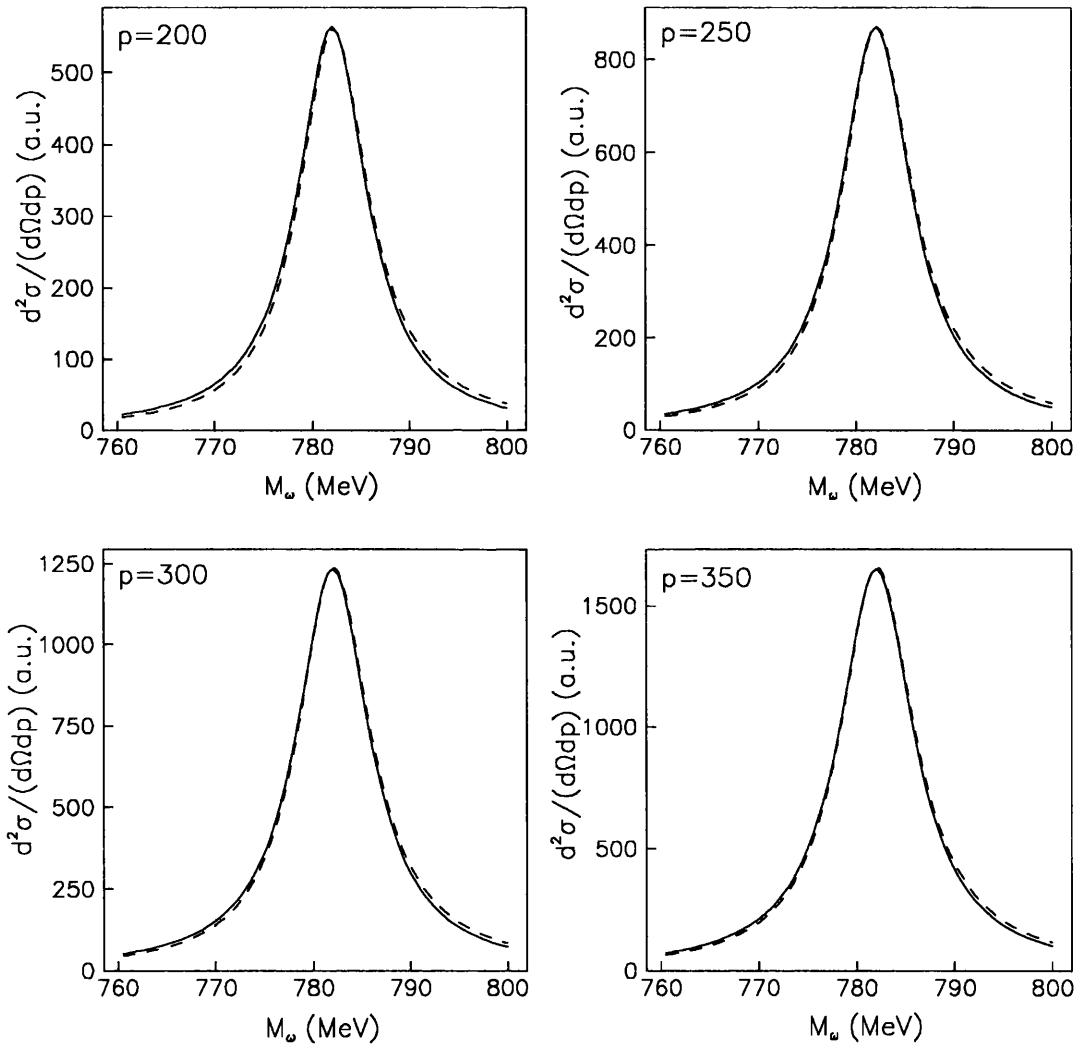

Figure 5.6: $\pi^- p \to \omega n$. The P-wave theoretical prediction of eq. (5.2.56). The solid line represents the production followed by subsequent decay only. The broken line corresponds to the case where final state interactions are included.

5.3 Analysis and Discussion

As can be clearly seen from figs. (5.3)– (5.6), the decay of the ω followed by final-state interactions leads to a reduction in the near-threshold production cross section in both the S and P-wave models. This reduction is in line with the experimental results. However, the size of the suppression near threshold is much too small, and its variation with p is very slow. The suppression effect, albeit small, decreases as p gets larger until it nearly vanishes at $p \approx 350$ MeV/c. This is more evident in the more realistic P-wave case. This sort of behaviour is expected for large p, as an ω meson would be expected to travel far enough to escape the neutron before it decays.

The total production amplitude F can be expressed as

$$\begin{aligned} F &= F_N + F_S \,, \\ &= [\mathrm{Re}(F_N) + \mathrm{Re}(F_S)] + i[\mathrm{Im}(F_N) + \mathrm{Im}(F_S)] \,, \\ &= \mathrm{Re}(F) + i\mathrm{Im}(F) \,, \end{aligned} \tag{5.3.1}$$

where F_N is the amplitude corresponding to the ω production and F_S includes final-state interactions. The reduction effect is a direct consequence of interference between $\mathrm{Re}(F_N)$ and $\mathrm{Re}(F_S)$ on one hand, and that between $\mathrm{Im}(F_N)$ and $\mathrm{Im}(F_S)$ on the other. A destructive (suppression) or constructive (enhancement) interference may take place depending on the relative signs of the terms involved. The size of the effect is a reflection of the relative magnitudes of the interfering terms.

In fig. (5.7) we show the real and imaginary parts of F_N and F_S on the same graph for each of the S and P-wave cases. Graphs (a), (b), (c), and (d) all correspond to a constant $p = 20$ MeV/c. As can be seen from graphs (a) and (b),

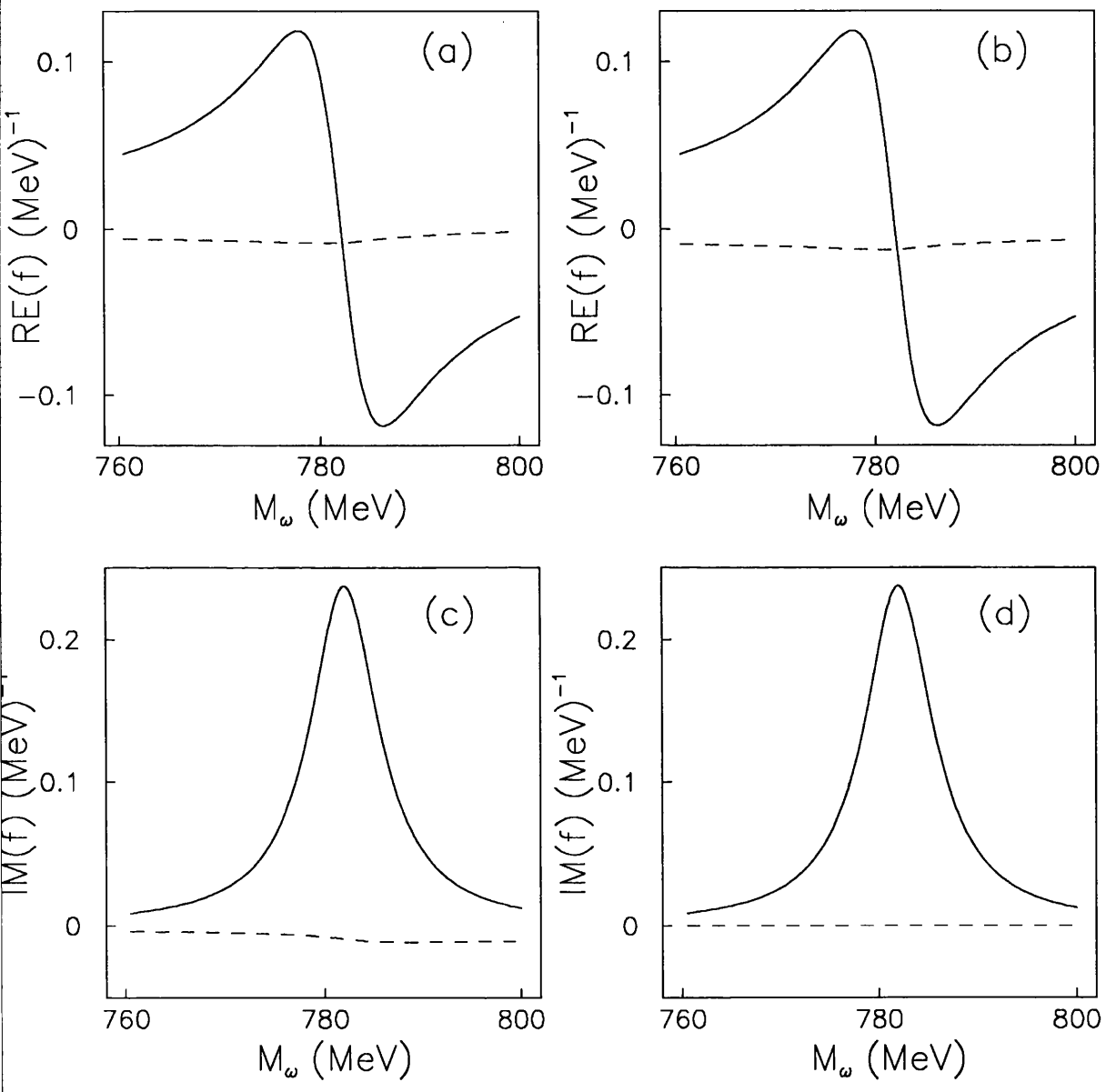

Figure 5.7: $\pi^- p \to \omega n$. (a) S-wave: Solid line is the real part of the amplitude corresponding to the ω production followed by its decay. Broken line is the real part of the amplitude which incorporates final-state interactions. (b) The corresponding P-wave case. (c) S-wave: Solid line is the imaginary part of the amplitude corresponding to the ω production followed its decay. Broken line is the imaginary part of the amplitude which incorporates final-state interactions. (d) The corresponding P-wave. All four graphs are obtained at a constant $p = 20$ MeV/c.

$\mathrm{Re}(F_N) = 0$ at $M_\omega = 782$ MeV/c, and so at this point there is no interference between the real parts. On the other hand, in graphs (c) and (d) the positive $\mathrm{Im}(F_N)$ term and negative $\mathrm{Im}(F_S)$ interfere destructively resulting in a cross section reduction. However, since $\mathrm{Im}(F_S) \ll \mathrm{Im}(F_N)$, the reduction effect is small. This small suppression effect is clearly seen in in the graphs corresponding to $p = 20$ MeV/c in fig. (5.3) and fig. (5.5). Fig (5.7) (a)–(d) also show that the pure final-state interaction term shows no reflection of the narrow ω peak, leading to a smooth variation of the amplitude as a function of p.

5.3.1 Simplified Estimate of the Decay-FSI effect

In what follows, we shall derive a rough estimate of the decay-FSI effect in the limit $p = 0$, $p_0 = 0$. For simplicity, we shall take $\delta \to \infty$, which corresponds to a very short pion-nucleon interaction range and write $f(\vec{K}, \vec{K})$ as $f(K)$. Under such conditions, $\vec{K} = -\vec{q}$ and, apart from an overall constant, eq. (5.2.52) becomes

$$F_P = \frac{2}{i\Gamma_\omega} - iM_r \frac{f(K)}{K} \left[\frac{(K^2+\beta^2)(K^2-\beta^2)}{4K^3(\sqrt{i\alpha} - (K^2+\beta^2)/2K)} + \ln\left(\frac{\sqrt{i\alpha} - (K^2+\beta^2)/2K}{\sqrt{i\alpha}} \right) \right] . \tag{5.3.2}$$

Now $\sqrt{\alpha} \ll (K^2+\beta^2)/2K$, and hence

$$\frac{(K^2+\beta^2)(K^2-\beta^2)}{4K^3(\sqrt{i\alpha} - (K^2+\beta^2)/2K)} \to -\frac{(K^2-\beta^2)}{2K^2} , \tag{5.3.3}$$

and

$$\ln\left(\frac{\sqrt{i\alpha} - (K^2+\beta^2)/2K}{\sqrt{i\alpha}} \right) \approx \ln\left(\frac{-(K^2+\beta^2)/2K\sqrt{\alpha}}{e^{i\pi/4}} \right) . \tag{5.3.4}$$

The minus sign in the numerator of the last equation gives rise to a phase of $e^{i\pi}$, and therefore

$$\ln\left(\frac{-(K^2+\beta^2)/2K\sqrt{\alpha}}{e^{i\pi/4}} \right) = \ln\left(\frac{K^2+\beta^2}{2K\sqrt{\alpha}}\, e^{3i\pi/4} \right) = \ln\left(\frac{K^2+\beta^2}{2K\sqrt{\alpha}} \right) + \frac{3i\pi}{4} . \tag{5.3.5}$$

Hence

$$F_p \approx \frac{2}{i\Gamma_\omega} - iM_r \frac{f(K)}{K}\left[\ln\left(\frac{K^2+\beta^2}{2K\sqrt{\alpha}}\right) - \frac{(K^2-\beta^2)}{2K^2} + \frac{3i\pi}{4}\right] . \qquad (5.3.6)$$

Letting

$$A = \ln\left(\frac{K^2+\beta^2}{2K\sqrt{\alpha}}\right) - \frac{(K^2-\beta^2)}{2K^2} , \qquad (5.3.7)$$

we can write F_P as

$$F_p \approx \frac{2}{i\Gamma_\omega} - iM_r \frac{f(K)}{K}\left(A + \frac{3i\pi}{4}\right) , \qquad (5.3.8)$$

$$= \frac{2}{i\Gamma_\omega} + \frac{M_r}{K}\left([A\,\mathrm{Im}f(K) + \frac{3\pi}{4}\mathrm{Re}f(K)] - i[A\,\mathrm{Re}f(K) - \frac{3\pi}{4}\mathrm{Im}f(K)]\right) , \qquad (5.3.9)$$

At $p = 0$ and $p_0 = 0$

$$f(K) = (-0.00227 + 0.00323\,i)\ (\mathrm{MeV/c})^{-1} , \qquad (5.3.10)$$

so that both the real and imaginary terms between parentheses in eq. (5.3.9) are small compared to $2/i\Gamma_\omega = -0.2433\,i\ (\mathrm{MeV})^{-1}$. Furthermore, as the real term corresponding to fig. (5.1) is zero at the ω peak, the small real part above will not interfere with other terms. Hence its contribution to $\mid F_P \mid^2$ is obtained by squaring it, which results in a quantity that we may safely ignore. According to eq. (5.3.10), $\mathrm{Re}(f) = -0.7\,\mathrm{Im}(f)$, which allows us to rewrite eq. (5.3.9) as

$$F_p \approx \frac{2}{i\Gamma_\omega} - \frac{1}{i}M_r\frac{\mathrm{Im}f(K)}{K}\left(0.7A + \frac{3\pi}{4}\right) ,$$

$$= \frac{2}{i\Gamma_\omega} - \frac{1}{i}M_r\frac{\sigma_t}{4\pi}\left(0.7A + \frac{3\pi}{4}\right) . \qquad (5.3.11)$$

We have used the optical theorem to arrive at the last expression. In the present limit the π^0 and γ are produced back to back with equal and opposite momenta,

i.e. $K \approx 379$ MeV/c. This results in $A \approx 13.5$ if we use $\beta = 1682$ MeV/c and $\alpha = 3599$ $(\text{MeV/c}^2)^{-2}$. Consequently, the two imaginary terms above interfere destructively, leading to a reduction near threshold. Taking $2/i\Gamma_\omega$ as a common factor gives

$$F_p \approx \frac{2}{i\Gamma_\omega}\left[1 - \frac{\Gamma_\omega}{2} M_r \frac{\sigma_t}{4\pi}\left(0.7A + \frac{3\pi}{4}\right)\right] . \tag{5.3.12}$$

The second term between the square brackets is a rough estimate of the decay followed by FSI effect. If we define a reduction factor, R, as

$$R = \frac{\Gamma_\omega}{2} M_r \frac{\sigma_t}{4\pi}\left(0.7A + \frac{3\pi}{4}\right) , \tag{5.3.13}$$

then near threshold and in the limit $\delta \rightarrow \infty$ the amplitude is suppressed by a factor of $R \approx 0.18$ for an average $\sigma_t \approx 4.2$ fm^2. Near threshold the volume of phase space is small and we may rewrite eq. (5.2.56) as

$$\frac{\partial^2\sigma}{\partial p \partial\Omega_n} \approx \mid F \mid^2 \approx \frac{4}{\Gamma_\omega^2}\left[1 - \Gamma_\omega M_r \frac{\sigma_t}{4\pi}\left(0.7A + \frac{3\pi}{4}\right)\right] . \tag{5.3.14}$$

In terms of R,

$$\frac{\partial^2\sigma}{\partial p \partial\Omega_n} \approx \frac{4}{\Gamma_\omega^2}[1 - 2R] , \tag{5.3.15}$$

where we have ignored the small term in R^2. This implies that $\partial^2\sigma/\partial p\partial\Omega_n$ is reduced by a factor of $\approx 36\%$ near threshold. This is large compared to the $\approx 9\%$ reduction obtained for $\delta = 500$ MeV/c which is shown in fig. (5.5).

In fig. (5.8) we show the results of our quantum mechanical model in the limit $\delta \rightarrow \infty$. At threshold the reduction is $\approx 30\%$, which is close to that predicted by eq. (5.3.14). Further, the rapid variation of the size of the effect with p has somewhat been reproduced . However, the large δ limit cannot be realistically accepted for (i) this corresponds to a point-like $\omega - n$ system which is not reasonable at such intermediate energies, and (ii) the integral given in eq. (5.2.42) becomes logarithmically divergent.

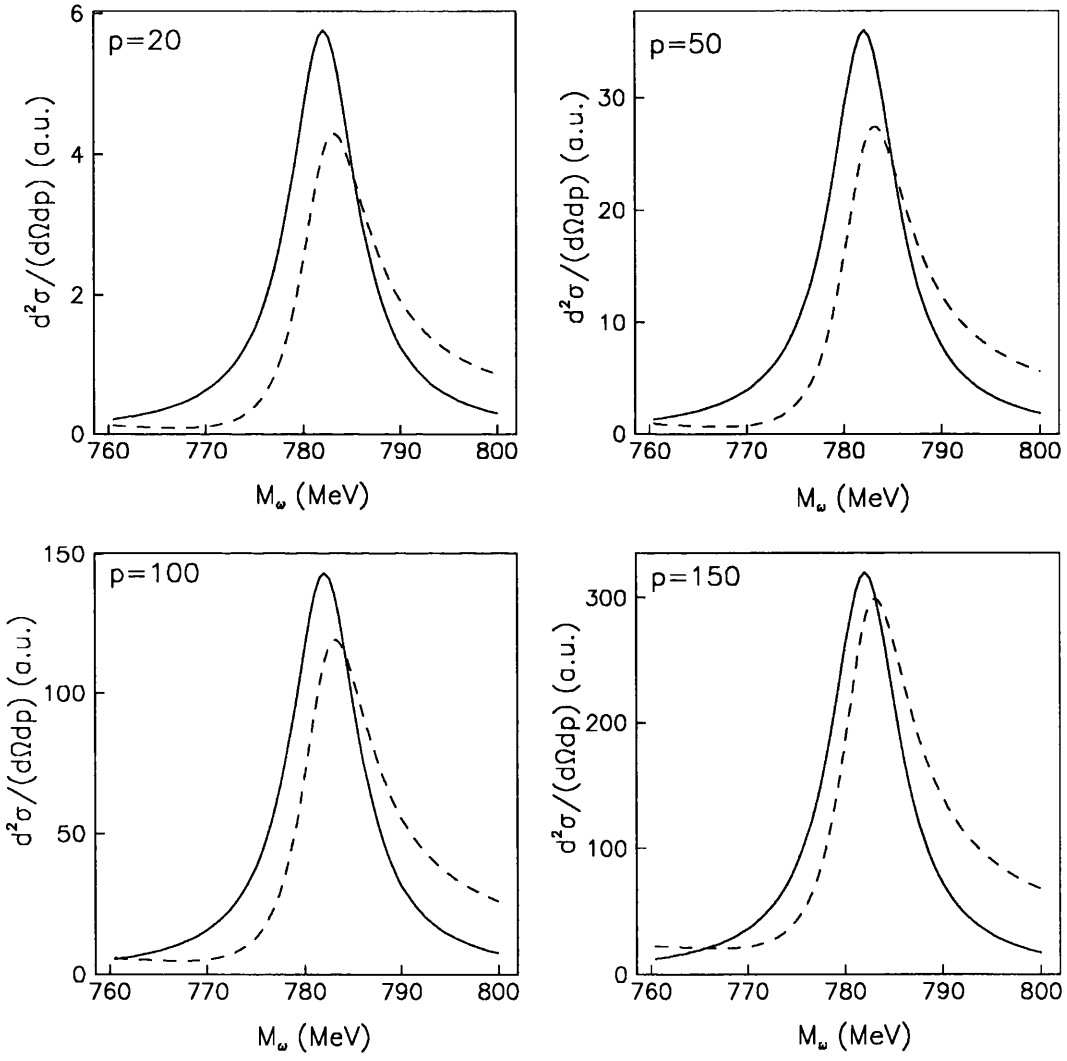

Figure 5.8: $\pi^- p \to \omega n$. The P-wave theoretical prediction of eq. (5.3.14). in the limit $\delta \to \infty$. The solid line represents the production followed by subsequent decay only. The broken line corresponds to the case where final state interactions are included.

The much smaller FSI effect found at $\delta \approx 500$ MeV/c can be understood by considering a simple physical picture. A low value of δ corresponds to a relatively large $\omega - n$ system, so that the ω may be produced at larger distances away from the neutron. This initial separation helps the ω to escape from the nucleon before it decays, and as a result the final-state interactions have a smaller effect. This same picture may also explain the 40% suppression effect we obtained in our semi-classical model results for the $\pi^0\gamma$ channel, where the $\omega - n$ system was taken to be point-like. One improvement to the classical model would be to smear the point-like production vertex and allow the ω to be produced at a random initial separation away from the nucleon.

5.4 Conclusions

In the reaction $\pi^- p \rightarrow \omega n$, our quantum mechanical model results show the ω production cross section to be reduced by a factor of $\approx 9\%$ near threshold. This is due to final-state interactions between π^0, arising from $\omega \rightarrow \pi^0\gamma$, and the recoil neutron. The fact that a reduction is obtained is in line with experimental observations. However, the size of the effect and its rate of variation with the c.m. momentum p are both too small to account for the results obtained experimentally. The data show that $\mid f_\omega \mid^2$ for all decay channels is suppressed by $\approx 70\%$ near threshold.

Nevertheless, in the limit where the $\omega - n$ system is taken to be point-like ($\delta \rightarrow \infty$), our quantum mechanical model predicts a near-threshold reduction of $\approx 36\%$ but only $\approx 9\%$ at $\delta = 500$ MeV/c. This limit is implicit in our semi-classical model, where we took the neutron and the ω to be produced at time $t = 0$ at position $x = 0$. As was pointed earlier, the semi-classical model reproduced

well the size of the reduction as well as its variation with p. Both models produce roughly similar results in the same limit. However, it is unreasonable to accept the assumption of the point-like initial production vertex, and a size of ≈ 1 fm, which is comparable to the range of nucleon potential, would seem more sensible. At threshold, taking the neutron to be at the centre of a sphere of radius 1 fm means that the ω may be produced anywhere within this sphere. This offers the ω an initial separation distance from the neutron, which may help it to escape the neutron even at low energies. The effect is as if p has been increased.

The 70% reduction effect observed experimentally is significantly larger than that obtained using our quantum model. Consequently, even if spin effects were included, the results of the quantum model would not be expected to be in line with experiment. In view of this, we feel that the near-threshold reduction due to the $\pi^-\pi^+\pi^0$ decay mode may safely be assumed to have an upper limit of $\approx 27\%$, which is still less than half of that found experimentally. This may be justified as following.

As the ω meson has a relatively narrow width [1], the rescattering of one pion off the recoil neutron is most likely to throw the corresponding event out of the ω peak. Consequently, more than one pion interacting with the neutron will either push the event even further into the continuum, or knock it back into the ω peak. Therefore, double or triple scattering do not contribute to the reduction in the former case, but could *increase* the ω production in the latter one. Hence, the leading term contributing to the reduction near threshold is expected to come from single pion scattering. This has been estimated in the $\omega \to \pi^0\gamma$ decay channel, and resulted in a 9% reduction near threshold. Although the kinematics of the three-pion and radiative decay channels are different, one would not expect the

reduction effect due to the former to differ much from three times that due to the latter, where the factor of 3 arises because there are three pions rather than one.

The fact that a large enough effect was not found, and final-state interactions are not expected to give a constant $\pi^-\pi^+\pi^0$ and $\pi^0\gamma$ decay modes branching ratio has lead us to consider other mechanisms, which will be presented in the next chapter, to explain the experimental results.

Chapter 6

S–Wave Resonance Production

As we have seen in the last chapter, final-state interactions do not seem sufficient to be solely responsible for the sharp suppression in the ω production near threshold. Therefore, we shall now consider other mechanisms which might explain the experimental results.

In sharp contrast to the ω case, η production in $\pi^- p \to \eta n$ is enhanced near threshold. This is due to an attractive ηn interaction leading to the formation of the $N^*(1535)$ S-wave resonance. In the $\pi^- p \to \omega n$ process, the ω and the neutron also exist in an S-wave [2, 6]. Consequently, there is a possibility that an S-wave resonance could be formed if the ω and the neutron interacted *via* an attractive (resonant) potential. But, unlike the η, the ω has a short lifetime which could destroy the resonance system. This is an alternative suppression mechanism which is independent of the ω decay channel *i.e.* it affects the $\pi^-\pi^+\pi^0$ and $\pi^0\gamma$ decay modes equally the same. In this chapter we shall investigate this hypothesis by deriving a dynamical ωn attractive interaction amplitude, and then using it to investigate the short lifetime effect on resonance formation.

The ω dominantly decays *via* strong interactions, which accounts for most of its 8.43 MeV [1] width. Furthermore, its short lifetime is partly responsible for the

absence of an experimentally determined interaction amplitude with the neutron. If such an amplitude existed, we would have used it to fit the theoretically derived one. Nevertheless, as our primary aim is to examine the effect of a short lifetime on resonance formation, we might be justified in replacing the parameters of the ωn elastic channel by the corresponding ηn ones, which are presented in appendix C. There is little alternative to making this crude *ansatz*. The finite lifetime effect is then investigated by assuming the η to have a finite width equals to that of the ω.

In section 6.1 we argue that a one-term S-wave attractive potential does not support resonances. Consequently, we consider two different mechanisms which might lead to the production of an S-wave resonance. The first is presented in section 6.2 where we take a two-term S-wave separable non-local potential to describe the interaction between the ω and the neutron. One term is attractive and the other repulsive but both with complex coupling constants as only the elastic ωn channel is considered. Using such a potential, we solve the Schrödinger equation, and extract an ωn dynamical amplitude. A more sophisticated approach is considered in section 6.3, where the resonance is assumed to be trapped as a virtual state in a quantum multi-channel scattering model. Three channels are here considered, ηn, $\pi^- p$ and $K\Lambda$, where we note that the first has replaced the ωn one. Using multi-channel scattering formalism we derive a dynamical ηn amplitude, then fit it to a simple Breit-Wigner form.

It is worth noting that our primary aim is to investigate the effect of a short lifetime on resonance formation and not to fit the ηn elastic scattering data using a multi-channel scattering model.

6.1 Resonances

The radial part of the Schrödinger equation is given by

$$\left[\frac{d^2}{dr^2} + k^2 - \frac{l(l+1)}{r^2} - U(r)\right] u_l(k,r) = 0 \,, \tag{6.1.1}$$

where $u_l(k,r)$ is the radial wave function corresponding to an angular momentum quantum number l, $U(r)$ is a reduced local potential and the $l(l+1)/r^2$ is the reduced centrifugal barrier term. If we define an effective potential $U_{\text{eff}}(r)$ by

$$U_{\text{eff}}(r) = \frac{l(l+1)}{r^2} + U(r) \,, \tag{6.1.2}$$

then the Schrödinger equation now reads

$$\left[\frac{d^2}{dr^2} + k^2 - U_{\text{eff}}(r)\right] u_l(k,r) = 0 \,. \tag{6.1.3}$$

Essentially, $U_{\text{eff}}(r)$ is made up of two parts; the first may be attractive corresponding to $U(r)$ and the other is the repulsive centrifugal barrier term. Fig. (6.1) depicts a typical shape of $U_{\text{eff}}(r)$ for a well behaved attractive potential $U(r)$. At small r the potential is dominated by the repulsive $l(l+1)/r^2$ term. As this distance increases the attractive term becomes more important and $U_{\text{eff}}(r)$ attains its minimum value of U_{min}. Further increase in r results in the potential barrier with a maximum of U_{max} before reaching an asymptotic value of U_{asm} as $r \to \infty$. For an incident particle of energy E, four different cases must be distinguished depending on the value of E.

1. $\underline{E < U_{\text{min}}}$: no physical solutions can be found as wave functions are not finite at infinity.

2. $\underline{U_{\text{min}} < E < U_{\text{asm}}}$: bound states of discrete energy levels may be obtained, that is the energy of a particle is quantized.

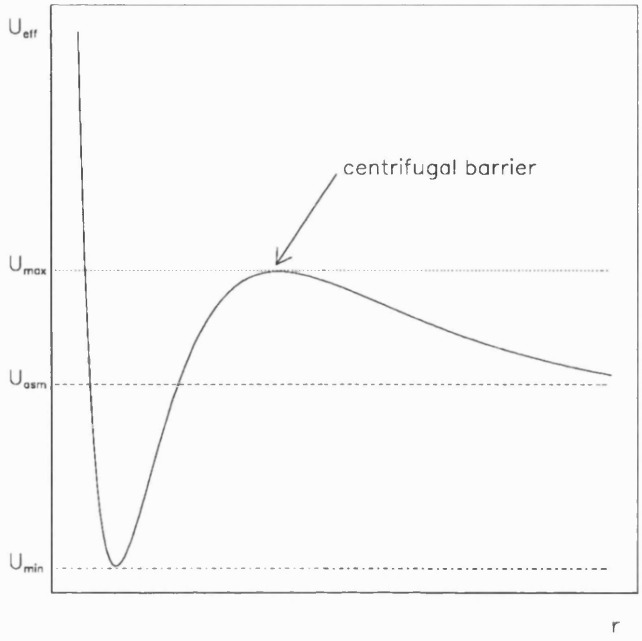

Figure 6.1: A typical shape of $U_{\text{eff}}(r)$. For an incident particle of energy E four different cases are possible depending on the magnitude of E; (i) $E < U_{\text{min}}$: No physical states are possible. (ii) $U_{\text{min}} < E < U_{\text{asm}}$: Bound states of discrete energies are formed. (iii) $U_{\text{asm}} < E < U_{\text{max}}$: short-lived bound states are formed (resonances). (iv) $E > U_{\text{max}}$ the particle will be scattered off the potential. States in (iii) and (iv) are said to form a continuum as their energies are not quantized.

3. $\underline{U_{\text{asm}} < E < U_{\text{max}}}$: The physically acceptable wave functions represent almost bound states that decay (by tunneling through the centrifugal barrier) shortly after formation *i.e.* they are *resonances.* The existence of the centrifugal barrier, which is a direct consequence of the $l(l+1)/r^2$ term is vital for the formation of resonances.

4. $\underline{E > U_{\text{max}}}$: In such a case particles scatter off the potential. In this and the previous case, the energies of the particles are said to form a continuum as they are not quantized.

The experimental data [2, 6] suggest that in the reaction $\pi^- p \to \omega n$ the ωn system exists in an S-wave, *i.e.* $l = 0$, and therefore the effective potential reduces to

$$U_{\text{eff}}(r) = U(r) \, .$$

Such a purely attractive potential could not, on its own, produce a potential barrier which is crucial in the formation of resonances. In the next section we shall consider other potential models which introduce an *ad hoc* potential barrier. In such a case S-wave resonance production is possible.

6.2 S-wave Non-local Separable Potential

One way of obtaining a potential barrier to confine the wave function of a resonance in an S-wave system is by considering a non-local separable potential consisting of two terms, one attractive and the other repulsive both with complex coupling constants as only the ωn channel is considered. The repulsive part plays the role of the centrifugal barrier discussed in the last section. With such a potential we shall solve the non-homogeneous Schrödinger equation

$$(\nabla^2 + k^2)\Psi(\vec{r}) = \int 2mV(\vec{r},\vec{r}')\Psi(\vec{r}')d^3r' \, , \qquad (6.2.1)$$

where $V(\vec{r},\vec{r}')$ is an S-wave non-local separable potential, and m is the reduced mass of the interacting particles. Our ansatz for the corresponding reduced potential is

$$U(\vec{r},\vec{r}') = 2mV(\vec{r},\vec{r}') = [\lambda_1 u(r)u(r') + \lambda_2 v(r)v(r')]Y_0^0(\hat{r})Y_0^{0*}(\hat{r}') \, , \qquad (6.2.2)$$

We take the $u(r)$ and $v(r)$ terms to be Yamaguchi potentials, which in r space are

$$u(r) = \sqrt{\frac{\pi}{2}}\,\frac{e^{-\beta_1 r}}{r} \, , \quad u(r') = \sqrt{\frac{\pi}{2}}\,\frac{e^{-\beta_1 r'}}{r'} \, ,$$

$$v(r) = \sqrt{\frac{\pi}{2}}\,\frac{e^{-\beta_2 r}}{r}\,, \quad v(r') = \sqrt{\frac{\pi}{2}}\,\frac{e^{-\beta_2 r'}}{r'}\,.$$

Further, we used the notation

$$Y_l^m(\hat{r}) \equiv Y_l^m(\theta,\phi)\,, \tag{6.2.3}$$

where $Y_l^m(\hat{r})$ are the spherical harmonic functions. For $l = 0$

$$Y_0^0(\hat{r}) = Y_0^{0*}(\hat{r}') = \frac{1}{\sqrt{4\pi}}\,, \tag{6.2.4}$$

With the above definitions $U(r,r')$ becomes

$$U(r,r') = \frac{\pi}{2}\left(\lambda_1 \frac{e^{-\beta_1 r}}{r}\,\frac{e^{-\beta_1 r'}}{r'} + \lambda_2 \frac{e^{-\beta_2 r}}{r}\,\frac{e^{-\beta_2 r'}}{r'}\right) Y_0^0(\hat{r})\, Y_0^0(\hat{r}')\,, \tag{6.2.5}$$

with $\mathrm{Re}(\lambda_1) > 0$ (repulsive), $\mathrm{Re}(\lambda_2) < 0$ (attractive) and $\beta_1 < \beta_2$.

Consequently, eq. (6.2.1) now reads

$$(\nabla^2 + k^2)\Psi(\vec{r}) = \int U(r,r')\Psi(\vec{r}')d^3r'\,.$$

Substituting for $U(r,r')$ gives

$$(\nabla^2 + k^2)\Psi(\vec{r}) = \frac{\pi}{2}\lambda_1 \int u(r)u(r')\Psi(\vec{r}')\,d^3r' + \frac{\pi}{2}\lambda_2 \int v(r)v(r')\Psi(\vec{r}')\,d^3r'\,. \tag{6.2.6}$$

6.2.1 One-Term Separable Potential

The two integrals on the right hand side of our last equation have the same form. In order to avoid evaluating the same type of integral twice, we shall solve the general equation

$$(\nabla^2 + k^2)\Phi(\vec{r}) = \lambda \int U_1(r,r')\,\Phi(\vec{r}')\,d^3r'\,, \tag{6.2.7}$$

and use the answer to write the desired solution for eq. (6.2.6). Here $U_1(r,r')$ is a reduced potential of the form

$$U_1(r,r') = \lambda\, g(r)\, g(r')\, Y_0^0(\hat{r})\, Y_0^{0*}(\hat{r}')\,. \tag{6.2.8}$$

The terms $g(r)$ and $g(r')$ have similar definitions to that of $u(r)$ and $u(r')$ above, namely

$$g(r) = \sqrt{\frac{\pi}{2}}\,\frac{e^{-\beta r}}{r}\ , \quad g(r') = \sqrt{\frac{\pi}{2}}\,\frac{e^{-\beta r'}}{r'}\ . \tag{6.2.9}$$

The general solution for equation (6.2.7) may be given as

$$\Phi(\vec{r}) = e^{i\vec{k}\cdot\vec{r}} + \int G(\vec{r},\vec{r}')\,U_1(r',r'')\Phi(\vec{r}'')d^3r'd^3r''\ . \tag{6.2.10}$$

Here $G(\vec{r},\vec{r}')$ is a Green's function given by

$$\begin{aligned} -G(\vec{r},\vec{r}') &= \frac{1}{4\pi}\frac{e^{ik|\vec{r}-\vec{r}'|}}{|\,\vec{r}-\vec{r}'\,|}\ , \\ &= ik\sum_{l=0}^{\infty} j_l(kr)\,h_l^{(1)}(kr')\sum_{m=-l}^{l} Y_l^m(\hat{r})\,Y_l^{m*}(\hat{r}'),\quad r\le r'\ , \qquad (6.2.11) \\ &= ik\sum_{l=0}^{\infty} j_l(kr')\,h_l^{(1)}(kr)\sum_{m=-l}^{l} Y_l^m(\hat{r})\,Y_l^{m*}(\hat{r}'),\quad r> r'\ , \qquad (6.2.12) \end{aligned}$$

with $j_l(kr)$ and $h_l^{(1)}(kr)$ being spherical Bessel and Hankel functions. Hence the general solution now reads

$$\Phi(\vec{r}) = e^{i\vec{k}\cdot\vec{r}} - \frac{\lambda}{4\pi}\int \frac{e^{ik|\vec{r}-\vec{r}'|}}{|\,\vec{r}-\vec{r}'\,|}\,g(r')g(r'')Y_0^0(\hat{r}')\,Y_0^{0*}(\hat{r}'')\,\Phi(\vec{r}'')d^3r'd^3r''\ . \tag{6.2.13}$$

If we define

$$I = \frac{1}{4\pi}\int \frac{e^{ik|\vec{r}-\vec{r}'|}}{|\,\vec{r}-\vec{r}'\,|}\,g(r')g(r'')Y_0^0(\hat{r}')\,Y_0^{0*}(\hat{r}'')\,\Phi(\vec{r}'')d^3r'd^3r''\ . \tag{6.2.14}$$

then, according to the Green function expansion in eqs. (6.2.11,6.2.12), I may be written as a sum of two terms

$$I = I(r\le r') + I(r> r')\ . \tag{6.2.15}$$

(i) Case $r \leq r'$

In this case we have

$$I(r \leq r') = ik \int \sum_{l=0}^{\infty} j_l(kr)\, h_l^{(1)}(kr') \sum_{m=-l}^{l} Y_l^m(\hat{r}) \left[Y_0^0(\hat{r}')\, Y_l^{m*}(\hat{r}') \right] Y_0^{0*}(\hat{r}'') \times$$

$$g(r')g(r'')\Phi(\vec{r}'')d^3r'd^3r'' \,. \tag{6.2.16}$$

Using the orthogonality condition

$$\int Y_l^m(\hat{r})\, Y_{l'}^{m'*}(\hat{r})d\Omega = \delta_{ll'}\delta_{mm'} \tag{6.2.17}$$

the term

$$\int Y_0^0(\hat{r}')\, Y_l^{m*}(\hat{r}')d\Omega' = 1 \text{ for } l = m = 0 \,,$$

$$= 0 \text{ for } l \neq 0 \,. \tag{6.2.18}$$

Thus the S-wave separable potential selects the terms corresponding to $l = 0$ only.

i.e

$$I(r \leq r') = ikj_0(kr)Y_0^0(\hat{r}) \int_r^{\infty} h_0^{(1)}(kr')Y_0^{0*}(\hat{r}'')g(r')g(r'')\Phi(\vec{r}'')r'^2dr'd^3r'' \,.$$

This may be written as

$$I(r \leq r') = ikCY_0^0(\hat{r})j_0(kr) \int_r^{\infty} h_0^{(1)}(kr')g(r')r'^2dr' \,. \tag{6.2.19}$$

Where C is a constant given by

$$C = \int \Phi(\vec{r}'')g(r'')Y_0^{0*}(\hat{r}'')d^3r'' \,. \tag{6.2.20}$$

Substituting for

$$j_0(kr) = \frac{\sin kr}{kr} \,, \tag{6.2.21}$$

and

$$h_0^{(1)}(kr') = \frac{\sin kr'}{kr'} - i\frac{\cos kr'}{kr'} \,, \tag{6.2.22}$$

into the expression for $I(r \leq r')$ results in

$$\begin{aligned} I(r \leq r') &= \frac{iC}{2\sqrt{2}} \frac{\sin kr}{kr} \int_r^\infty (\sin kr' - i\cos kr')\, e^{-\beta r'}\, dr' \\ &= \frac{C}{2\sqrt{2}} \frac{\sin kr}{kr} \int_r^\infty e^{(ik-\beta)r'} dr' = \frac{1}{2\sqrt{2}} \frac{C}{(ik-\beta)} \frac{\sin kr}{kr} \left[e^{(ik-\beta)r'}\right]_r^\infty \,. \end{aligned} \tag{6.2.23}$$

As $r' \to \infty$, the term

$$e^{(ik-\beta)r'} = e^{ikr'}\, e^{-\beta r'} \to 0 \,.$$

Hence

$$I(r \leq r') = -\frac{1}{2\sqrt{2}} \frac{C}{(ik-\beta)} \frac{\sin kr}{kr}\, e^{(ik-\beta)r} \,. \tag{6.2.24}$$

(ii) Case $r > r'$

Here

$$\begin{aligned} I(r > r') &= ikCY_0^0(\hat{r}) h_0^{(1)}(kr) \int_0^r j_0(kr') g(r') r'^2 dr' \,, \\ &= \frac{iC}{2\sqrt{2}} \left(\frac{\sin kr}{kr} - i\frac{\cos kr}{kr}\right) \int_0^r e^{-\beta r'} \sin kr'\, dr' \,, \\ &= \frac{C}{2\sqrt{2}} \frac{e^{ikr}}{kr} \int_0^r e^{-\beta r'} \sin kr'\, dr' \,, \\ &= \frac{1}{2\sqrt{2}} \frac{C}{(\beta^2+k^2)} \frac{e^{ikr}}{kr} \left(k - e^{-\beta r}\left(\beta \sin kr + k\cos kr\right)\right) . \end{aligned} \tag{6.2.25}$$

To get the last result we have used the general relation

$$\int e^{ax} \sin bx\, dx = \frac{e^{ax}}{a^2+b^2} \left(a\sin bx - b\cos bx\right) \,. \tag{6.2.26}$$

According to eq. (6.2.15) the sum of the two terms is

$$
\begin{aligned}
I &= -\frac{1}{2\sqrt{2}}\frac{C}{(ik-\beta)}\frac{\sin kr}{kr}\,e^{(ik-\beta)r} + \frac{1}{2\sqrt{2}}\frac{C}{(\beta^2+k^2)}\frac{e^{ikr}}{kr}\left(k - e^{-\beta r}(\beta\sin kr + k\cos kr)\right) , \\
&= \frac{C}{2\sqrt{2}}\frac{e^{ikr}}{kr}\frac{1}{(\beta^2+k^2)}\left(k - e^{-\beta r}[\beta\sin kr + k\cos kr] + (ik+\beta)\sin kr\, e^{-\beta r}\right) , \\
&= \frac{C}{2\sqrt{2}}\frac{1}{(\beta^2+k^2)}\left(\frac{e^{ikr}-e^{-\beta r}}{r}\right) . \qquad (6.2.27)
\end{aligned}
$$

With this form of I, the total wave function $\Phi(\vec{r})$ in eq. (6.2.13) now reads

$$
\Phi(\vec{r}) = e^{i\vec{k}\cdot\vec{r}} - \frac{C}{2\sqrt{2}}\frac{\lambda}{(\beta^2+k^2)}\left(\frac{e^{ikr}-e^{-\beta r}}{r}\right) . \qquad (6.2.28)
$$

To determine C we need to substitute the above expression in eq. (6.2.20), *i.e.*

$$
\begin{aligned}
C &= \frac{1}{2\sqrt{2}}\int\left[e^{i\vec{k}\cdot\vec{r}\,''} - \frac{C}{2\sqrt{2}}\frac{\lambda}{(\beta^2+k^2)}\left(\frac{e^{ikr''}-e^{-\beta r''}}{r''}\right)\right]\frac{e^{-\beta r''}}{r''}d^3r'' , \\
&= \frac{1}{2\sqrt{2}}\int\frac{e^{-\beta r''}}{r''}e^{i\vec{k}\cdot\vec{r}\,''}d^3r'' - \frac{\lambda C}{8(\beta^2+k^2)}\int\frac{e^{-\beta r''}}{r''}\left(\frac{e^{ikr''}-e^{-\beta r''}}{r''}\right)d^3r'' . \\
&= \frac{\sqrt{2}\pi}{\beta^2+k^2} - \frac{\lambda\pi C}{4\beta(ik-\beta)^2} \qquad (6.2.29)
\end{aligned}
$$

Thus

$$
C = \frac{\sqrt{2}\pi}{\beta^2+k^2}\left[1 + \frac{\pi\lambda}{4\beta(ik-\beta)^2}\right]^{-1} . \qquad (6.2.30)
$$

Finally, $\Phi(\vec{r})$ has the form

$$
\Phi(\vec{r}) = e^{i\vec{k}\cdot\vec{r}} + \left[-2\frac{(\beta^2+k^2)}{\pi\lambda} + \frac{(k^2-\beta^2)}{2\beta} - ik\right]^{-1}\left(\frac{e^{ikr}-e^{-\beta r}}{r}\right) . \qquad (6.2.31)
$$

6.2.2 Two-Term Separable potential

We now return to our original differential equation given in (6.2.6). In analogy with eq. (6.2.7), its solution may be written as

$$\Psi(\vec{r}) = e^{i\vec{k}\cdot\vec{r}} - \frac{\lambda_1}{4\pi}\int \frac{e^{ik|\vec{r}-\vec{r}'|}}{|\vec{r}-\vec{r}'|}\, u(r')u(r'')Y_0^0(\hat{r}')\, Y_0^{0*}(\hat{r}'')\Psi(\vec{r}'')d^3r'd^3r''$$

$$-\frac{\lambda_2}{4\pi}\int \frac{e^{ik|\vec{r}-\vec{r}'|}}{|\vec{r}-\vec{r}'|}\, v(r')v(r'')Y_0^0(\hat{r}')\, Y_0^{0*}(\hat{r}'')\Psi(\vec{r}'')d^3r'd^3r'' \,. \tag{6.2.32}$$

Each of the two integrals on the right hand side has the same form as in equation (6.2.14). Hence, using eq. (6.2.27), the wave function $\Psi(\vec{r})$ becomes

$$\Psi(\vec{r}) = e^{i\vec{k}\cdot\vec{r}} - \frac{1}{2\sqrt{2}}\,\frac{\lambda_1 C_1}{\beta_1^2+k^2}\left(\frac{e^{ikr}-e^{-\beta_1 r}}{r}\right) - \frac{1}{2\sqrt{2}}\,\frac{\lambda_2 C_2}{\beta_2^2+k^2}\left(\frac{e^{ikr}-e^{-\beta_2 r}}{r}\right) . \tag{6.2.33}$$

Generalizing eq. (6.2.20), the constant C_1 is given by

$$\begin{aligned} C_1 &= \sqrt{\frac{\pi}{2}}\int \Psi(\vec{r}'')u(r'')Y_0^{0*}(\hat{r}'')d^3r'' \,, \\ &= \frac{1}{2\sqrt{2}}\int\left[e^{i\vec{k}\cdot\vec{r}''} - \frac{1}{2\sqrt{2}}\,\frac{\lambda_1 C_1}{\beta_1^2+k^2}\left(\frac{e^{ikr''}-e^{-\beta_1 r''}}{r''}\right)\right. \\ &\quad \left. - \frac{1}{2\sqrt{2}}\frac{\lambda_2 C_2}{\beta_2^2+k^2}\left(\frac{e^{ikr''}-e^{-\beta_2 r''}}{r''}\right)\right]\frac{e^{-\beta_1 r''}}{r''}d^3r'' \,. \end{aligned}$$

Therefore

$$C_1 = \frac{\sqrt{2}\pi}{\beta_1^2+k^2} - \frac{\pi\lambda_1 C_1}{4\beta_1(ik-\beta_1)^2} - \frac{\pi\lambda_2 C_2}{2(ik-\beta_1)(ik-\beta_2)(\beta_1+\beta_2)} \,. \tag{6.2.34}$$

Similarly

$$C_2 = \frac{\sqrt{2}\pi}{\beta_2^2+k^2} - \frac{\pi\lambda_2 C_2}{4\beta_2(ik-\beta_2)^2} - \frac{\pi\lambda_1 C_1}{2(ik-\beta_2)(ik-\beta_1)(\beta_2+\beta_1)} \,. \tag{6.2.35}$$

The above are two simultaneous equations coupling the constants C_1 and C_2, and are symmetric under the exchange of the labels 1 and 2. This is a reflection of the same symmetry of the differential equation in eq.(6.2.6).

The scattering amplitude may be extracted by considering the asymptotic behaviour of $\Psi(\vec{r})$ in eq. (6.2.33).

$$\lim_{r\to\infty} \Psi(\vec{r}) = -\frac{1}{2\sqrt{2}} \left(\frac{\lambda_1 C_1}{\beta_1^2 + k^2} + \frac{\lambda_2 C_2}{\beta_2^2 + k^2} \right) \frac{e^{ikr}}{r} , \qquad (6.2.36)$$

which means that the amplitude is given by

$$f(k) = -\frac{1}{2\sqrt{2}} \left(\frac{\lambda_1 C_1}{\beta_1^2 + k^2} + \frac{\lambda_2 C_2}{\beta_2^2 + k^2} \right) = -\frac{1}{2\sqrt{2}} (\lambda_1 D_1 + \lambda_2 D_2) , \qquad (6.2.37)$$

where

$$D_1 = \frac{C_1}{\beta_1^2 + k^2} , \quad D_2 = \frac{C_2}{\beta_2^2 + k^2} . \qquad (6.2.38)$$

Our expression for $f(k)$ contains six unknown parameters, β_1, β_2 and the complex coupling constants λ_1 and λ_2. To determine these fit parameters, we shall fit $f(k)$ to the ηN scattering amplitude.

According to [7] the ηn amplitude may be parameterized in an effective range expansion as

$$[f(\eta n \to \eta n)]^{-1} = \frac{1}{a_0} + \frac{1}{2} r_0 k^2 , \qquad (6.2.39)$$

where the ηn scattering length and effective range are

$$a_0 = (0.481 + 0.289i)\,\mathrm{fm}, \qquad r_0 = (-3.16 - 0.13i)\,\mathrm{fm}.$$

This is a second order polynomial in k which reproduces well the energy dependence of the cross section. This suggests that terms $O(k^4)$ and higher have little significance. We therefore expand the two simultaneous equations coupling D_1 and D_2 in powers of k up to and including k^2, to give

$$\begin{aligned} D_1 &= \sqrt{2}\pi \left(\frac{1}{\beta_1^4} - \frac{2k^2}{\beta_1^6} \right) - \frac{\pi \lambda_1 D_1}{4\beta_1^3} \left(1 + \frac{2ik}{\beta_1} - \frac{3k^2}{\beta_1^2} \right) \\ &- \frac{\pi \lambda_2 D_2}{2\beta_1^3(\beta_1 + \beta_2)} \left(\beta_2 + ik\frac{\beta_1 + \beta_2}{\beta_1} - k^2 \frac{\beta_1 + 2\beta_2}{\beta_1^2} \right) . \qquad (6.2.40) \end{aligned}$$

Similarly

$$D_2 = \sqrt{2}\pi\left(\frac{1}{\beta_2^4} - \frac{2k^2}{\beta_2^6}\right) - \frac{\pi\lambda_2 D_2}{4\beta_2^3}\left(1 + \frac{2ik}{\beta_2} - \frac{3k^2}{\beta_2^2}\right)$$

$$- \frac{\pi\lambda_1 D_1}{2\beta_2^3(\beta_2+\beta_1)}\left(\beta_1 + ik\frac{\beta_2+\beta_1}{\beta_2} - k^2\frac{\beta_2+2\beta_1}{\beta_2^2}\right) . \qquad (6.2.41)$$

We solved for D_1 and D_2 using *Mathematica.* Hence, by eq. (6.2.37), $f(k)$ is determined in terms of the β_i, λ_i and k. But the forms of D_1 and D_2 turned out to be very complex which deterred us from presenting them here.

Fitting $f(k)$ using the parameterized ηn amplitude provides us with four equations to fix six parameters. At $k = 0$

$$f(0) = a_0 . \qquad (6.2.42)$$

For $k = 1$ fm^{-1}

$$[f(1)]^{-1} = \frac{1}{a_0} + \frac{1}{2}r_0 . \qquad (6.2.43)$$

As $f(k)$, a_0 and r_0 are all complex quantities the last two equations give rise to four constraints, which are not *a priori* enough to determine all six parameters uniquely. Nevertheless, for chosen real values of β_1 and β_2 we tried to solve eqs. (6.2.42) and (6.2.43), hoping to find a set of (β_i, λ_i) that reproduces the correct variation of the amplitude as a function of k. Although it has been possible to solve the first of our two equations, no solution could be obtained for (6.2.43) despite searching over a wide area in the (β_1, β_2) space. This may well be a reflection of the difficulty of obtaining a resonance using an S-wave potential unless singular repulsive potentials are included.

In what follows we shall consider a more sophisticated model where an S-wave production of a resonance, which fits the ηN data, may actually be possible.

6.3 Multi–Channel Scattering

A channel is a possible mode of fragmentation of a composite system during a collision. If the final state after the collision is allowed by energy conservation and quantum numbers then that channel is open; otherwise it is closed. In this chapter we shall restrict ourselves to channels where the number of particles in the initial and final states is the same and equal to two.

In the multi-channel formalism, the Schrödinger equation for channel i is given by

$$\left(\frac{1}{2m_i}\nabla^2 + E_i - V_i(r)\right)\Psi_i = \sum_{j\neq i} V_{ij}(r)\Psi_j \,, \tag{6.3.1}$$

where m_i is the reduced mass in channel i.

Apart from the terms on the right hand side (RHS), the above is the Schrödinger equation for the elastic scattering in channel i. The inhomogenious terms on the right describe the coupling to the other j channels. That is to say, the wave function and hence the scattering amplitude in any one channel is dependent on the interactions in all other channels. In practice it is not possible to consider all channels, so that approximation schemes that only consider the most important ones are normally adopted.

It is worth noting that closed channels may still contribute to eq. (6.3.1) as virtual states and quantum tunneling is possible in quantum mechanics. This could provide a mechanism by which a resonance state is possible in an S-wave production. The resonance may be temporarily trapped in a virtual state, which in turn decays into the physical resonance state through quantum tunnelling.

6.3.1 Multi–Channel Scattering Formalism

Defining the reduced potential, $U_{ij}(r)$, and the momentum wave number, k_i, as

$$U_{ij}(r) = 2m_i V_{ij}(r) \ , \tag{6.3.2}$$

and

$$k_i^2 = 2m_i E_i \ , \tag{6.3.3}$$

equation (6.3.1) has the form

$$\left(\nabla^2 + k_i^2 - U_i(r)\right) \Psi_i = \sum_{j \neq i} U_{ij}(r)\, \Psi_j \ . \tag{6.3.4}$$

Now, the inhomogeneous differential equation

$$(\nabla^2 + k_i^2) G_i(\vec{r}, \vec{r}\,') = \delta^{(3)}(\vec{r} - \vec{r}\,') \ , \tag{6.3.5}$$

has a solution of the form

$$G_i(\vec{r}, \vec{r}\,') = -\frac{1}{4\pi} \frac{e^{ik_i|\vec{r}-\vec{r}\,'|}}{|\ \vec{r} - \vec{r}\,'\ |} \ . \tag{6.3.6}$$

For an incident wave in channel j, the total wave function may be written in terms of the incident plane wave and an outgoing spherical wave, in analogy with the single channel case, as

$$\Psi_i(\vec{r}) = e^{i\vec{k_j}\cdot\vec{r}}\delta_{ij} - \frac{2m_i}{4\pi} \sum_l \int \frac{e^{ik_i|\vec{r}-\vec{r}\,'|}}{|\ \vec{r} - \vec{r}\,'\ |} V_{il}(r')\, \Psi_l(\vec{r}\,')\, d^3r' \ . \tag{6.3.7}$$

The asymptotic behaviour is then given by

$$\begin{aligned} \Psi_i(\vec{r}) \ &\rightarrow \ e^{i\vec{k_j}\cdot\vec{r}}\delta_{ij} - \frac{2m_i}{4\pi} \frac{e^{ik_i r}}{r} \sum_l \int e^{-\vec{k_i}\cdot\vec{r}\,'} V_{il}(r')\, \Psi_l(\vec{r}\,')\, d^3r' \ , \\ &= \ e^{i\vec{k_j}\cdot\vec{r}}\delta_{ij} + \sqrt{\frac{m_i}{m_j}} \frac{e^{ik_i r}}{r} f_{ij}(\vec{k_i}, \vec{k_j}) \ , \end{aligned} \tag{6.3.8}$$

where $f_{ij}(\vec{k_i}, \vec{k_j})$ is the scattering amplitude given by

$$f_{ij}(\vec{k_i}, \vec{k_j}) = -2\frac{\sqrt{m_i m_j}}{4\pi} \sum_l \int e^{-\vec{k_i}\cdot\vec{r}'} V_{il}(r')\, \Psi_l(\vec{r}')\, d^3r' \,. \qquad (6.3.9)$$

In terms of this, the differential cross section is

$$\left(\frac{d\sigma}{d\Omega}\right)_{ij} = \frac{v_i}{v_j}\left|\sqrt{\frac{m_i}{m_j}} f_{ij}(\vec{k_i}, \vec{k_j})\right|^2 = \frac{k_i}{k_j} \mid f_{ij}(\vec{k_i}, \vec{k_j}) \mid^2 \qquad (6.3.10)$$

The first term in the Born series approximates $\Psi_l(\vec{r}')$ by a plane wave. Hence the first Born approximation for the scattering amplitude is given by

$$f^B_{ij}(\vec{k_i}, \vec{k_j}) = -2\frac{\sqrt{m_i m_j}}{4\pi} \sum_l \int e^{-\vec{k_i}\cdot\vec{r}'} V_{ij}(r')\, e^{-\vec{k_j}\cdot\vec{r}'}\, d^3r' \,. \qquad (6.3.11)$$

If we define

$$T_{ij}(\vec{k_i}, \vec{k_j}) = -\frac{4\pi}{2\sqrt{m_i m_j}} f_{ij}(\vec{k_i}, \vec{k_j}) \,, \qquad (6.3.12)$$

then in Born approximation,

$$T^B_{ij}(\vec{k_i}, \vec{k_j}) = V_{ij}(\vec{k_i}, \vec{k_j}) = \int e^{-\vec{k_i}\cdot\vec{r}'} V_{ij}(r')\, e^{\vec{k_j}\cdot\vec{r}'} d^3r' \,. \qquad (6.3.13)$$

In general, the $T_{ij}(\vec{k_i}, \vec{k_j})$ elements are given by

$$T_{ij}(\vec{k_i}, \vec{k_j}) = \sum_l \int e^{-i\vec{k_i}\cdot\vec{r}'} V_{il}(r')\, \Psi_l(\vec{r}')\, d^3r' \,. \qquad (6.3.14)$$

Substituting for $\Psi_l(\vec{r}')$ using eq. (6.3.7) we get

$$\begin{aligned} T_{ij}(\vec{k_i}, \vec{k_j}) &= \sum_l \int e^{-i\vec{k_i}\cdot\vec{r}'} V_{il}(r') \left[e^{i\vec{k_j}\cdot\vec{r}'}\delta_{lj} - \frac{2m_l}{4\pi} \sum_n \int \frac{e^{ik_l|\vec{r}'-\vec{r}''|}}{|\,\vec{r}' - \vec{r}''\,|} V_{ln}(r'')\, \Psi_n(\vec{r}'') \right] d^3r' d^3r'' \\ &= V_{ij}(\vec{k_i}, \vec{k_j}) - \frac{1}{4\pi} \sum_{nl} \int e^{-\vec{k_i}\cdot\vec{r}'} V_{il}(r') \frac{e^{ik_l|\vec{r}'-\vec{r}''|}}{|\,\vec{r}' - \vec{r}''\,|} 2m_l\, V_{ln}(r'')\, \Psi_n(\vec{r}'')\, d^3r'\, d^3r'' \,. \end{aligned}$$

Using

$$\int \frac{e^{ik'\cdot(\vec{r}'-\vec{r}'')}}{k'^2 - k_l^2 - i\epsilon}\, d^3k' = 2\pi^2 \frac{e^{ik_l|\vec{r}'-\vec{r}''|}}{|\,\vec{r}' - \vec{r}''\,|} \,, \qquad (6.3.15)$$

our last equation for $T_{ij}(\vec{k_i}, \vec{k_j})$ reads

$$T_{ij}(\vec{k_i}, \vec{k_j}) = V_{ij}(\vec{k_i}, \vec{k_j}) - \frac{1}{(2\pi)^3} \sum_{nl} \int e^{-i\vec{k_i}\cdot\vec{r}'} V_{il}(r') \frac{e^{ik'\cdot(\vec{r}'-\vec{r}'')}}{k'^2 - k_l^2 - i\epsilon} 2m_l V_{ln}(r'') \Psi_n(\vec{r}'') \, d^3r' \, d^3r'' \, d^3k'. \tag{6.3.16}$$

By equations (6.3.13) and (6.3.14) our expression in eq. (6.3.16) may be written as

$$T_{ij}(\vec{k_i}, \vec{k_j}) = V_{ij}(\vec{k_i}, \vec{k_j}) - \frac{1}{(2\pi)^3} \sum_{l} \int \frac{d^3k'}{k'^2 - k_l^2 - i\epsilon} 2m_l V_{il}(\vec{k_i}, \vec{k'}) \, T_{lj}(\vec{k'}, \vec{k_j}) \, d^3k' \, . \tag{6.3.17}$$

Using the relation in eq. (6.3.15), the total wave function $\Psi_i(\vec{r})$ given in (6.3.7) reads

$$\begin{aligned} \Psi_i(\vec{r}) &= e^{i\vec{k_j}\cdot\vec{r}}\delta_{ij} - \frac{2m_i}{(2\pi)^3} \sum_{l} \int \frac{e^{i\vec{k'}\cdot(\vec{r}-\vec{r}')}}{k'^2 - k_l^2 - i\epsilon} V_{il}(r') \, \Psi_l(\vec{r}') d^3r' d^3k' \\ &= e^{i\vec{k_j}\cdot\vec{r}}\delta_{ij} - \frac{2m_i}{(2\pi)^3} \int \frac{e^{i\vec{k'}\cdot\vec{r}}}{k'^2 - k_l^2 - i\epsilon} T_{ij}(\vec{k'}, \vec{k_j}) d^3k' \, . \end{aligned} \tag{6.3.18}$$

To get our last expression, we substituted for $T_{ij}(\vec{k_i}, \vec{k_j})$ using eq. (6.3.14).

6.3.2 Separable Potential Ansatz

If we take a potential of the form

$$V_{ij}(\vec{k_i}, \vec{k_j}) = v(k_i) \, A_{ij} \, v(k_j) \, , \tag{6.3.19}$$

and try the solution

$$T_{ij}(\vec{k_i}, \vec{k_j}) = v(k_i) \, \tau_{ij} \, v(k_j) \, , \tag{6.3.20}$$

then, by eq. (6.3.17), we have

$$\begin{aligned} \tau_{ij} &= A_{ij} - \frac{1}{(2\pi)^3} \sum_{l} 2m_l A_{il} \, \tau_{lj} \int \frac{(v(k'))^2}{k'^2 - k_l^2 - i\epsilon} \, d^3k' \, , \\ &= A_{ij} - \sum_{l} A_{il} \, \tau_{lj} \, \Delta_{ll} \, , \end{aligned} \tag{6.3.21}$$

where

$$\Delta_{ll} = \frac{2m_l}{(2\pi^3)} \int \frac{(v(k'))^2}{k'^2 - k_l^2 - i\epsilon} d^3k' = \frac{m_l}{\pi^2} \int \frac{(v(k'))^2}{k'^2 - k_l^2 - i\epsilon} k'^2 dk' \ . \tag{6.3.22}$$

For a Yamaguchi potential

$$v(k') = \frac{1}{(k'^2 + \beta^2)} \ , \tag{6.3.23}$$

Δ_{ll} is given by

$$\Delta_{ll} = \frac{m_l}{4\pi\beta(\beta - ik_l)^2} \ . \tag{6.3.24}$$

In the next section we shall describe our multi-channel resonance model, where the formalism developed in this section will be applied.

6.4 The Multi-Channel Resonance Model

As discussed in section (6.1), an S-wave scattering in an attractive potential does not lead to resonances as the centrifugal barrier is absent. However experiment shows that the ω production is isotropic up to $p^*_\omega \approx 200$ MeV/c [2, 6]. This led us to look for other ways where S-wave production of a resonance is feasible. In multi-channel scattering we suggest that the resonance state is actually an S-wave bound state in a closed channel. The virtual state corresponding to such a channel then decays through the open channels giving rise to the physical resonance state. Since the ωn scattering length and effective range are not known, the corresponding ηn parameters will be used instead. In this model we shall make make two approximations; the first is to consider only three elastic channels, namely

$$\eta n \rightarrow \eta n \ ,$$

$$\pi^- p \rightarrow \pi^- p \ ,$$

and

$$K\Lambda \rightarrow K\Lambda \, .$$

Below a centre-of-mass energy of $\approx$ 1610 MeV the $K\Lambda$ channel is closed, but the state is believed to be strongly coupled to the ηn elastic channel [14]. After deriving the scattering amplitude we shall investigate the effect of the finite lifetime by assuming the η particle to have a finite width equals to that of the ω.

6.4.1 Amplitude Derivation

We take a factorisable form for A_{ij}, namely

$$A_{ij} = -\lambda_i \lambda_j \, . \tag{6.4.1}$$

A minus sign means that $V_{ij}(\vec{k_i}, \vec{k_j})$ is attractive. With the aid of eq. (6.3.21), τ_{ij} is then given by

$$\tau_{ij} = -\lambda_i \, \lambda_j + \sum_l \lambda_i \, \lambda_l \, \Delta_{ll} \, \tau_{lj} \, . \tag{6.4.2}$$

A possible solution for τ_{ij} is

$$\tau_{ij} = C \lambda_i \lambda_j \, , \tag{6.4.3}$$

where C is the same in all channels. Substituting for τ_{ij} results in

$$\begin{aligned} C\lambda_i \, \lambda_j &= -\lambda_i \, \lambda_j + \sum_l \lambda_i \, \lambda_l \, \Delta_{ll} \, (C \lambda_l \, \lambda_j) \, , \\ &= -\lambda_i \, \lambda_j + C \lambda_i \, \lambda_j \sum_l \lambda_l^2 \, \Delta_{ll} \, . \end{aligned} \tag{6.4.4}$$

Hence

$$C = \frac{1}{\sum_l \lambda_l^2 \, \Delta_{ll} - 1} \tag{6.4.5}$$

and therefore,

$$\tau_{ij} = \frac{\lambda_i \, \lambda_j}{\sum_l \lambda_l^2 \, \Delta_{ll} - 1} \, . \tag{6.4.6}$$

Substituting for τ_{ij} in eq. (6.3.20) we have

$$T_{ij}(\vec{k_i}, \vec{k_j}) = \frac{\lambda_i \lambda_j \, v(k_i) \, v(k_j)}{\sum_l \lambda_l^2 \, \Delta_{ll} - 1} \, , \tag{6.4.7}$$

From equation (6.3.12), the scattering amplitude is then given by

$$f_{ij}(\vec{k_i}, \vec{k_j}) = \frac{\sqrt{m_i \, m_j}}{2\pi} \, \frac{\lambda_i \, \lambda_j \, v(k_i) \, v(k_j)}{1 - \sum_l \lambda_l^2 \Delta_{ll}} \, . \tag{6.4.8}$$

For clarity, we shall label the coupling constants λ_i and the Δ_{ll} terms as $(\lambda_\eta, \, \Delta_\eta)$, $(\lambda_\pi, \, \Delta_\pi)$ and (λ_K, Δ_K), corresponding to the ηn, $\pi^- p$ and $K\lambda$ elastic channels respectively.

We are now in a position to write down the scattering amplitude for the process

$$\eta n \rightarrow \eta n \, ,$$

which according to eq. (6.4.8) reads

$$f_{\eta n \rightarrow \eta n} = \frac{m_\eta}{2\pi} \, \frac{\lambda_\eta^2 \, (v(k_\eta))^2}{1 - \sum_l \lambda_l^2 \, \Delta_{ll}} \, , \tag{6.4.9}$$

where k_η is the centre-of-mass momentum. For simplicity, we have omitted the explicit dependence of the amplitude on the momentum vectors. Equation (6.4.9) contains three real unknowns, λ_η, λ_π and λ_K, as well as three range parameters. Therefore we need three independent equations to determine them, even if the range parameters are taken as given. Our second approximation is to take the same value of the range parameter β to describe the interactions in all channels.

6.4.2 Determination of the Coupling Constants

In an S-wave production, the Breit-Wigner form of the transition amplitude from channel i to channel j is given by

$$f_{ij}(\vec{k_i}, \vec{k_j}) = \frac{1}{\sqrt{k_i k_j}} \frac{M_R \sqrt{\Gamma_i \Gamma_j}}{M_R^2 - W^2 - i\Gamma(W) M_R} \, , \tag{6.4.10}$$

where, as explained in Appendix C, M_R is the resonance mass and Γ_i is the partial width corresponding to channel i. $\Gamma(W)$ is the $N^*(1535)$ width, which is given by

$$\Gamma(W) = \Gamma_R \left(0.50 \frac{k_\eta}{k_\eta^R} \Theta(k_\eta^2) + 0.40 \frac{k_\pi}{k_\pi^R} \Theta(k_\pi^2) + 0.10 \right) , \tag{6.4.11}$$

where the centre-of-mass momenta of the η and π at a total energy W are k_η and k_π respectively. The momenta k_η^R and k_π^R are those evaluated at the resonance position $W = M_R$, where the branching ratios to the ηn, πn and $\pi\pi N$ channels were imposed to be 0.50, 0.40 and 0.10 respectively. Finally Γ_R is the total width of the resonance = (134.6 $\pm$ 5.6) MeV. The step functions imply that the channels contribute to the total width only when they are open. But in our model we are not considering the $\pi\pi N$ channel, which according to equation (6.4.11) has a 10% partial width. To get the right value of Γ_R we could divide the 0.10 between the ηN and πN channels equally. However, as k_η varies more rapidly than k_π in the neighbourhood of the threshold η production we choose to leave the ηN partial width unchanged but modify that of the πN channel such that

$$\Gamma(W) = \Gamma_R \left(0.50 \frac{k_\eta}{k_\eta^R} \Theta(k_\eta^2) + 0.50 \frac{k_\pi}{k_\pi^R} \Theta(k_\pi^2) \right) . \tag{6.4.12}$$

Using eq. (6.4.12) the ηn partial width is given by

$$\Gamma_\eta = \Gamma_R \, 0.50 \, \frac{k_\eta}{k_\eta^R} \, \Theta(k_\eta^2) , \tag{6.4.13}$$

so that the ratio

$$\frac{\Gamma_\eta}{k_\eta} = 0.50 \, \frac{\Gamma_R}{k_\eta^R} , \tag{6.4.14}$$

is constant.

According to eq. (6.4.10) the ηn elastic amplitude is

$$f_{\eta n \to \eta n} = \frac{1}{k_\eta} \, \frac{M_R \Gamma_\eta}{M_R^2 - W^2 - i\Gamma(W) M_R} . \tag{6.4.15}$$

The amplitudes in equations (6.4.9) and (6.4.15) must be equated, *i.e.*

$$f_{\eta n\to\eta n} = \frac{m_\eta}{2\pi}\,\frac{\lambda_\eta^2(v(k_\eta))^2}{1-\sum_l \lambda_l^2\Delta_{ll}} = \frac{1}{k_\eta}\,\frac{M_R\Gamma_\eta}{M_R^2 - W^2 - i\Gamma(W)M_R}\,. \tag{6.4.16}$$

At resonance $M_R = W$. Hence the real parts of both denominators vanish and our first of three equation to determine the coupling constants reads

$$\sum_l \lambda_l^2\ \mathrm{Re}\,(\Delta_{ll}) - 1 = 0\,. \tag{6.4.17}$$

More explicitly we have

$$\lambda_\eta^2\ \mathrm{Re}\,(\Delta_\eta) + \lambda_\pi^2\ \mathrm{Re}\,(\Delta_\pi) + \lambda_K^2\ \mathrm{Re}\,(\Delta_K) - 1 = 0\,. \tag{6.4.18}$$

As the $K\Lambda$ system is a virtual state, its centre-of-mass momentum is purely imaginary. Consequently, Δ_K is a real quantity and

$$\lambda_\eta^2\ \mathrm{Re}\,(\Delta_\eta) + \lambda_\pi^2\ \mathrm{Re}\,(\Delta_\pi) + \lambda_K^2\,\Delta_K - 1 = 0\,. \tag{6.4.19}$$

Further, the imaginary parts must also be equal. This results in our second equation, namely

$$\frac{m_\eta}{2\pi}\,\frac{\lambda_\eta^2\,(v(k_\eta))^2}{\sum_l \lambda_l^2\ \mathrm{Im}\,(\Delta_{ll})} = \frac{\Gamma_\eta}{k_\eta\,\Gamma(W)}\,. \tag{6.4.20}$$

In terms of the parameters of the individual channels we have

$$\frac{m_\eta}{2\pi}\,\frac{\lambda_\eta^2\,(v(k_\eta))^2}{\lambda_\eta^2\ \mathrm{Im}\,(\Delta_\eta) + \lambda_\pi^2\ \mathrm{Im}\,(\Delta_\pi)} = \frac{\Gamma_\eta}{k_\eta\,\Gamma(W)}\,. \tag{6.4.21}$$

Finally, our second equation takes the form

$$\frac{m_\eta}{2\pi}\,\frac{\lambda_\eta^2\,(v(k_\eta))^2}{\lambda_\eta^2\ \mathrm{Im}\,(\Delta_\eta) + \lambda_\pi^2\ \mathrm{Im}\,(\Delta_\pi)} - 0.5\frac{\Gamma_R}{k_\eta^R\,\Gamma(W)} = 0\,. \tag{6.4.22}$$

The third equation needed to determine our parameters can be obtained by fixing the relative size of the real and imaginary parts of the denominators on both sides of eq. (6.4.16) as follows

$$\frac{\frac{\partial}{\partial W^2}\,[\mathrm{Re}(1-\sum_l \lambda^2\Delta_{ll})]}{\mathrm{Im}(\sum_l \lambda_l^2\ \Delta_{ll})} = -\frac{1}{M_R\,\Gamma(W)}\,. \tag{6.4.23}$$

We have here divided by the imaginary parts to get rid of constants. Writing the above equation in terms of the individual Δ_{ll}, λ_{ll} and, remembering that Δ_K is purely real, we get

$$\frac{\frac{\partial}{\partial W^2}\left[\lambda_\eta^2 \,\mathrm{Re}(\Delta_\eta) + \lambda_\pi^2 \,\mathrm{Re}(\Delta_\pi) + \lambda_K^2 \Delta_K\right]}{\lambda_\eta^2 \,\mathrm{Im}(\Delta_\eta) + \lambda_\pi^2 \,\mathrm{Im}(\Delta_\pi)} = \frac{1}{M_R\,\Gamma(W)}\,. \tag{6.4.24}$$

To work out the partial differentiation with respect to W^2, we use the chain rule *viz.*

$$\frac{\partial \Delta}{\partial W} = \frac{\partial \Delta}{\partial k} \Big/ \frac{dW}{dk}\,. \tag{6.4.25}$$

Further

$$\frac{\partial \Delta}{\partial W^2} = \frac{1}{2W}\frac{\partial \Delta}{\partial W} = \frac{1}{2W}\frac{\partial \Delta}{\partial k} \Big/ \frac{dW}{dk}\,. \tag{6.4.26}$$

Therefore

$$\mathrm{Re}\left(\frac{\partial \Delta}{\partial W^2}\right) = \frac{1}{2W}\mathrm{Re}\left(\frac{\partial \Delta}{\partial k}\right) \Big/ \frac{dW}{dk}\,. \tag{6.4.27}$$

For a given value of β our three equations were solved to yield unique values for λ_η, λ_π and λ_K. But we still need a criterion to fix the value of β. This is the value at which the real parts of equations (6.4.9,6.4.15) best agree. This is obtained at $\beta = 1200$ MeV/c, which yields

$$\lambda_\eta^2 = 264.70\,\mathrm{fm}^{-2}/c, \quad \lambda_\pi^2 = 394.2\,\mathrm{fm}^{-2}/c \;\; \lambda_K^2 = 1795.3\,\mathrm{fm}^{-2}/c\,.$$

Since the amplitudes in eqs. (6.4.8,6.4.10) are factorisable, then by fitting the elastic scattering parameters one automatically fits the the inelastic ones.

6.4.3 Results of the Multi-Channel Resonance Model

In fig. (6.2), the broken line shows the variation of the real part of the inverse of our amplitude as a function of the centre-of-mass momentum k_η calculated using the above fit parameters. The solid line is the corresponding term using the

Breit-Wigner amplitude given in equation (6.4.15). The momentum $k_\eta \approx 1$ fm^{-1} corresponds to the resonance position where the amplitude was fitted. This is the point where $\mathrm{Re}[f(\eta n \to \eta n)]^{-1}$ vanishes as evident in the figure. The agreement between the solid and broken line is not quite exact, which may be due to the fact that the differential term in eq. (6.4.24) was calculated numerically. As we move away from the resonance point, the two curves begin to diverge slowly. We tried to improve the model by using a single β to describe the interactions in two channels with a different β value in the third one. This did not result in a significantly different results to those obtained above. Nevertheless, the overall characteristics of the amplitude variation with k_η is roughly reproduced. This is sufficient for our primary aim which is to investigate the effect of a finite life time on the production amplitude.

In ref. [15], a preprint which appeared after the completion of our work, the production of the $S_{11}(1535)$ resonance has been studied using a coupled channel model with four channels; πN, ηN, $K\Lambda$ and $K\Sigma$. They described the interactions between channels i and j using two different potentials, a local as well as a non-local S-wave separable potential, which were derived from the SU(3) chiral effective Lagrangian in next-to-leading order. A good fit for the πN S_{11} phase shift and inelasticity, as well as $\pi^- p \to \eta n$ cross section data was found using only two range parameters; one for the πN channel, and one common range for the other three. For the local potential they are

$$\beta_{\pi N} = 320\,\mathrm{MeV/c}, \quad \beta_{\eta N} = \beta_{K\Lambda} = \beta_{K\Sigma} = 530\,\mathrm{MeV/c}\,.$$

However, the ranges for the separable potential are

$$\beta_{\pi N} = 573\,\mathrm{MeV/c}, \quad \beta_{\eta N} = \beta_{K\Lambda} = \beta_{K\Sigma} = 776\,\mathrm{MeV/c}\,.$$

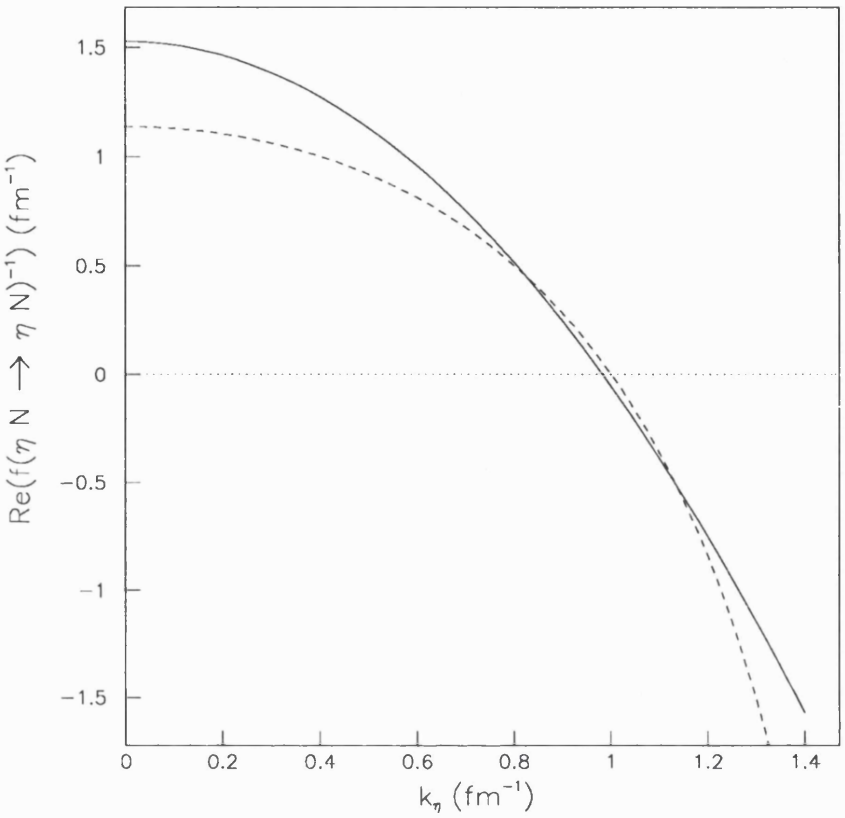

Figure 6.2: The solid line is the real part of the inverse of the amplitude given in eq. (6.4.15). The broken line, however, is the corresponding term of the amplitude given by eq. (6.4.9).

They concluded that the $S_{11}(1535)$ resonance is a quasi-bound $K\Sigma - K\Lambda$ state, whose mass and width are 1557 and 179 MeV/c^2 respectively.

6.5 Effect of the Finite Lifetime

The η has a small width compared to that of the ω. Therefore, it has a purely real momentum vector. If we assume a fictitious η particle which has a width equals to that of the ω, then the momentum vector becomes a complex quantity,

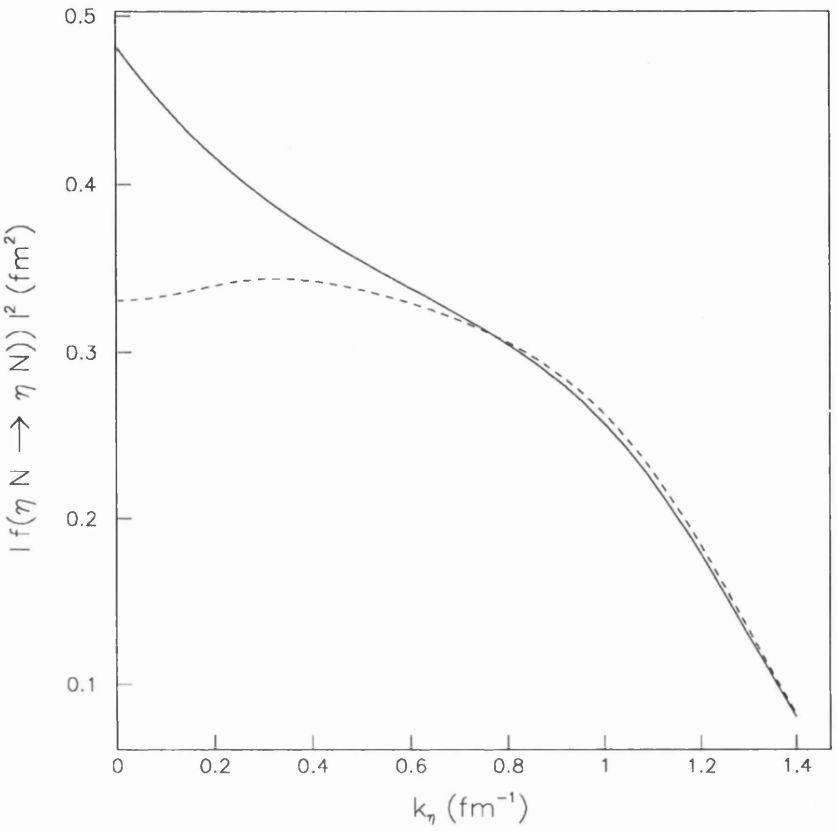

Figure 6.3: $\mid f(\eta n \rightarrow \eta n) \mid^2$, where the amplitude is given in eq. (6.4.9). The solid line corresponds to a real momentum vector, while the broken line relates to the case where the η is assumed to have a finite life time equal to that of the ω. The figure illustrates the effect of a finite width on the scattering amplitude.

which we shall denote by k_η^c. In terms of k_η this is given by

$$k_\eta^c = \sqrt{k_\eta^2 + i\Gamma_\omega M_r} \ , \tag{6.5.1}$$

where M_r is the reduced mass of the ωn system.

We calculated $\mid f(\eta n \rightarrow \eta n) \mid^2$ given in eq. (6.4.9) when the momentum vector is real and then complex, and the results are shown in fig. (6.3).

Clearly, the finite width has reduced the size of the modulus of the amplitude squared for $k_\eta < 0.6$ fm^{-1}. The effect is more noticeable for small k_η where the

imaginary part of k_η^c becomes dominant. As shown in appendix C, $f(\pi^- p \to \eta n)$ is related to the ηN elastic amplitude through a constant *i.e.*

$$f(\pi^- p \to \eta n) \approx 0.469\, f(\eta N \to \eta N)\ . \tag{6.5.2}$$

Hence a graph of $|f(\pi^- p \to \eta n)|^2$ as a function of k_η would only differ from the one above by an overall multiplicative constant.

The fact that the effect is most important at small k_η is in line with experiment. However the reduction obtained is not enough for this model on its own to account for the observed phenomenon.

Chapter 7

Multiple Scattering Enhancement Factor Near Threshold

7.1 Introduction

As has been stressed many times, the ω production amplitude in the $pd \rightarrow {}^3He\,\omega$ reaction is suppressed near threshold. This is in sharp contrast to the η production in a similar reaction ($pd \rightarrow {}^3He\,\eta$), where the amplitude seems to be enhanced. For the latter reaction, Fäldt and Wilkin [7] obtained an enhancement factor of 2.2 near threshold, which they ascribed to the multiple scattering of the produced η by the nucleons *via* strong-final state interactions.

One would be tempted to speculate that the ω production amplitude would be enhanced in analogy to the η case, but experimental results show a suppression rather than an enhancement. It is however possible that an enhancement might have been killed due to the ω short lifetime. For low p^*_ω, the ω decays before it has a chance to be multiply scattered by the nucleons.

In what follows we shall explain the FSI model of Fäldt and Wilkin [7]. We shall then modify their formalism to take account of the finite lifetime of the ω and hence examine its effect on the ω production amplitude. Since not much is known about the ω-nucleon scattering length we, regrettably, are forced once again to

use their parameterized η-nucleon scattering length, though some variation from this is also investigated.

7.2 Multiple Scattering Enhancement Model

Fäldt and Wilkin assumed the reaction $pd \rightarrow {}^3He\,\eta$ to proceeded *via* two intermediate steps. A pion beam, created in an $NN \rightarrow d\pi$ on one of the nucleons in the target deuteron, is converted into an η-meson on the second nucleon *via* a $\pi N \rightarrow \eta N$ reaction. We shall deal with this model in more detail in chapter 8.

They extended the two-step model to include strong final state interactions (FSI) between the produced η and the nucleons. The production amplitude was assumed to factorize into an S-wave nuclear reaction matrix element and an S-wave FSI. The FSI modifies the waves emerging from a nucleon, replacing them with *effective* waves [16] which they estimated. For simplicity, they considered the effective waves for the time-reversed reaction with an incident η-meson, a schematic diagram of which is presented in fig. (7.1)

The η-nucleon potential is taken to be of short range as compared to the size of ${}^3He$. Hence, the nucleons in this nucleus are viewed as three non-overlapping scattering centres. As a consequence, the overall scattering amplitude may be written in terms of the individual on-shell amplitudes [17]. This is also true for the wave function outside the range of interaction, *i.e.* the effective waves at one of the centres can be found in terms of the incident wave modified by the on-shell scattering from the other centres.

In the ${}^3He$ case, the effective waves may be evaluated by considering the scattering by three fixed centres at positions $\vec{x}_A$, $\vec{x}_B$ and $\vec{x}_C$. Outside the ranges of interaction, the wave function $\Psi(\vec{x})$ is the sum of the incident plane wave and

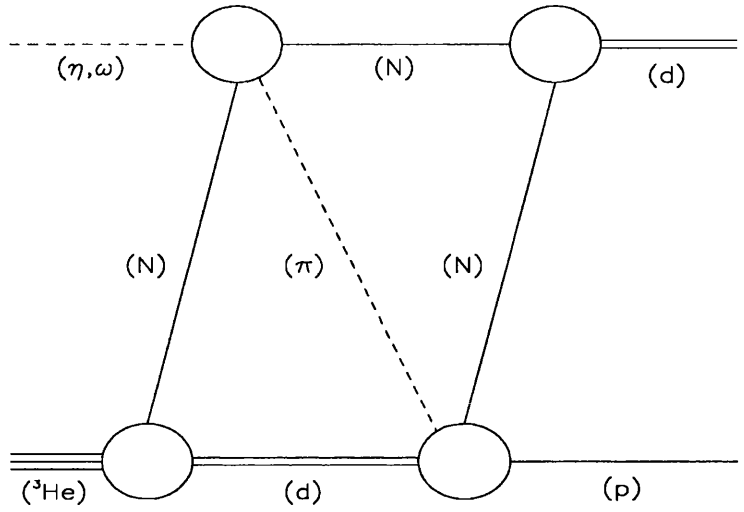

Figure 7.1: A schematic diagram for the reaction $\eta\,(\omega)\,^3He \rightarrow pd$ in the two-step model.

waves emerging from the three nucleon scattering centres [18]. Keeping only S-wave scattering from each centre, with amplitudes f_A, f_B and f_C,

$$\Psi(\vec{x}) = e^{i\vec{k}\cdot\vec{x}} + f_A\frac{e^{ikR_A}}{R_A}\Psi_A(\vec{x}) + f_B\frac{e^{ikR_B}}{R_B}\Psi_B(\vec{x}) + f_C\frac{e^{ikR_C}}{R_C}\Psi_C(\vec{x})\,, \qquad (7.2.1)$$

where Ψ_A, Ψ_B and Ψ_C are the effective waves incident on the scattering centres A, B and C respectively. Also

$$R_Q = \mid \vec{x} - \vec{x}_Q \mid, \quad Q = A, B \, or \, C. \qquad (7.2.2)$$

Similarly, an effective wave is the sum of the incident plane wave and the waves scattered from the two other centres

$$\Psi_A(\vec{x}) = e^{i\vec{k}\cdot\vec{x}_A} + f_B\frac{e^{ikR_{AB}}}{R_{AB}}\Psi_B(\vec{x}) + f_C\frac{e^{ikR_{AC}}}{R_{AC}}\Psi_C(\vec{x})\,, \qquad (7.2.3)$$

where the separations of the scattering centres are

$$R_{AB} = \mid \vec{x}_A - \vec{x}_B \mid \ .$$

The other waves may be obtained by cyclic permutation. Since the η and ω have isospin of zero, then $f_A = f_B = f_C = f$.

They simplified even further by taking the three nucleons to be placed at the corners of an equilateral triangle with side length l, *i.e.*

$$R_{AB} = R_{BC} = R_{AC} = l \ . \tag{7.2.4}$$

At $\vec{x} = \vec{x}_A$, eq. (7.2.3) has the solution,

$$\Psi_A(\vec{x}_A) = e^{i\vec{k}\cdot\vec{x}_A}\left[1 + f\frac{e^{ikl}}{l}(e^{i\vec{k}\cdot(\vec{x}_B-\vec{x}_A)} + e^{i\vec{k}\cdot(\vec{x}_C-\vec{x}_A)} - 1)\right] \Big/ D \ , \tag{7.2.5}$$

where

$$D = \left(1 + f\frac{e^{ikl}}{l}\right)\left(1 - 2f\frac{e^{ikl}}{l}\right) \ . \tag{7.2.6}$$

In this rigid equilateral triangle model, the ^3He charge form factor is given by,

$$F_{ch}(q) = \frac{j_0(ql/\sqrt{3})}{(1+q^2a^2)^2} \ . \tag{7.2.7}$$

A dipole form factor for the proton was introduced with $a = 0.234$ fm.

The ^3He charge form factor has a clear minimum at $q \approx 3.1$ fm^{-1}. When this is used to determine the free parameter l, it results in $< r^2 >^{1/2} \approx 1.28$ fm, where $< r^2 >^{1/2}$ is the RMS radius of the ^3He charge distribution. This is much less than the charge-weighted experimental value of 1.89 fm [19]. Consequently, they modified their model by considering a superposition of equilateral triangles, which gives a point-nucleon form factor

$$F(q) = \int dl\, G(l)\, j_0(ql/\sqrt{3}) \ ,$$

where the smearing function, $G(l)$, was taken to be

$$G(l) = N(l - l_{\min})\Theta(l - l_{\min})\exp(-\lambda^2(l - A)^2) \,. \qquad (7.2.8)$$

The step function $\Theta(l - l_{\min})$ restricts the value of l such that the separate scattering centres assumption is still valid. The RMS radius and the form factor zero can be reproduced for parameter values

$$l_{\min} = 0.52\,\mathrm{fm},\ A = 0.87\,\mathrm{fm},\ \lambda = 0.433\,\mathrm{fm}^{-1} \,.$$

Therefore, the S-wave enhancement factor becomes

$$F = \left\langle \frac{1}{D}\left[1 + f\frac{e^{ikl}}{l}(e^{i\vec{k}\cdot(\vec{x}_B - \vec{x}_A)} + e^{i\vec{k}\cdot(\vec{x}_C - \vec{x}_A)} - 1)\right]\right\rangle \,, \qquad (7.2.9)$$

where the averages are over the lengths of the sides and the orientation of the triangles, which projects out the S-wave.

Carrying out the angular average gives

$$F = \int_0^\infty dl\, G(l)\left[\frac{1}{D}\left(1 + f\frac{e^{ikl}}{l}\{\, 2j_0(kl) - 1\}\right)\right] \,. \qquad (7.2.10)$$

To apply the enhancement factor F, the S-wave part of the nuclear matrix element should in principle be projected out. However, since they were only interested in near threshold data and only the FSI contributes significantly to the energy variation, they used the threshold value for the nuclear amplitude, which they calculated in the two-step model.

In deriving eq. (7.2.9), the nucleon masses were taken to be infinite. However, in order to reproduce the single scattering term correctly, reduced mass factors had to be introduced;

$$f = \left(\frac{1 + M_\eta/M_N}{1 + M_\eta/M_h}\right)\, f_{\eta N}(k_{\eta N}) \,.$$

where $f_{\eta N}$ is the η-nucleon c.m. scattering amplitude evaluated at a c.m. momentum,

$$k_{\eta N} = \left(\frac{1 + M_\eta / M_h}{1 + M_\eta / M_N} \right) p_\eta \ ,$$

as shown in appendix D.

A low energy parameterization of the η-nucleon amplitudes is presented in appendix C.

At threshold $j_0(kl) \rightarrow 1$ and hence eq. (7.2.10) reduces to

$$F = \left\langle \left(1 - \frac{2f}{l} \right)^{-1} \right\rangle \ . \tag{7.2.11}$$

Substituting the parameterized form of f, they found that the attractive η-N interaction enhances the prediction by a factor $\mid F \mid^2 = 2.2$, as shown in fig. (7.2)

The effect of the FSI is clearer if one examines the inverse reaction, $\eta\, {}^3He \rightarrow pd$, where an η is incident on a Helium nucleus. The η is then attracted to the nucleons *via* strong attractive interactions. This leads to the formation of an almost resonating system, which results in the enhancement of the production amplitude.

7.3 Incorporation of a Finite Lifetime

In this section we shall investigate the effect of a finite lifetime on the FSI-related enhancement near threshold. A perfect candidate for this purpose is the ω-meson whose lifetime is considerably shorter than the η. For this purpose, we used the formalism derived by Fäldt and Wilkin in which we incorporate the ω lifetime. The reduced mass factors are also calculated using the ω mass. As the ω-nucleon scattering length is not known we used the η-nucleon one.

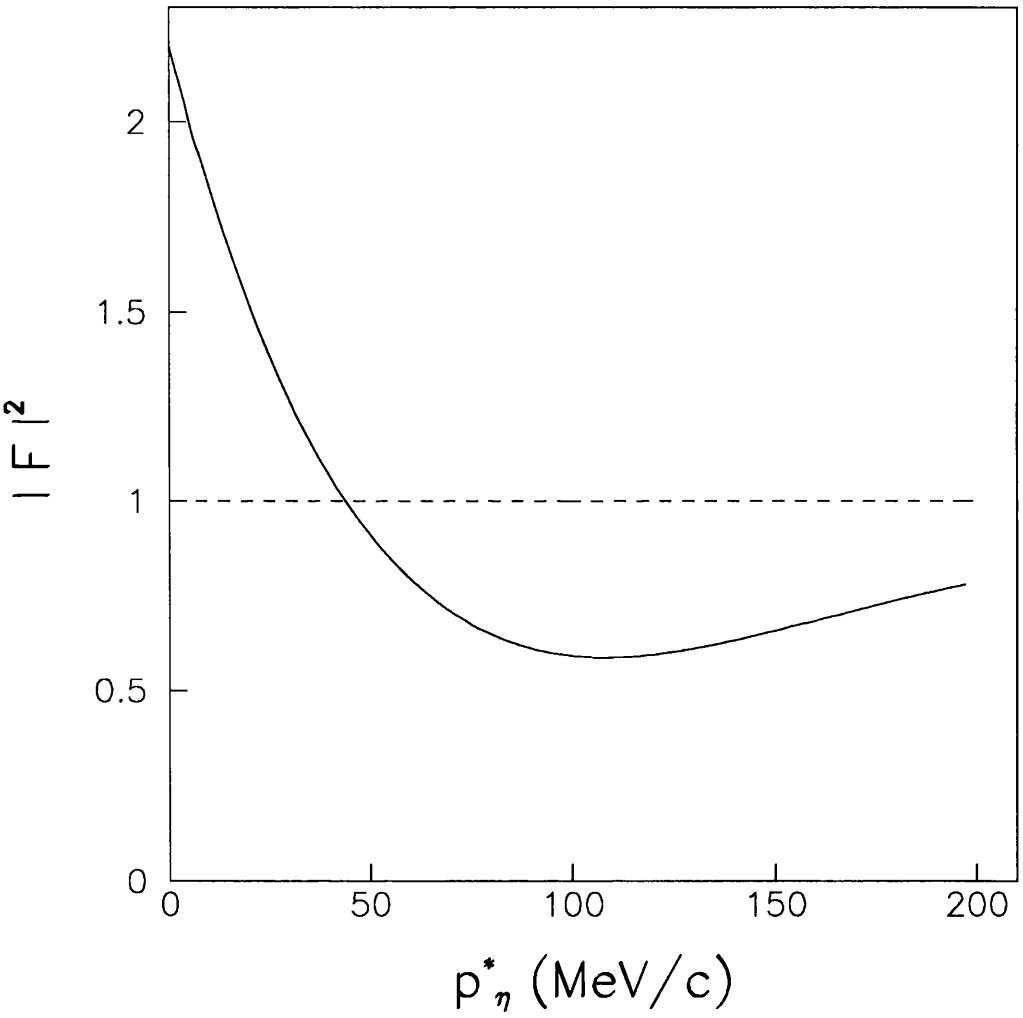

Figure 7.2: $pd \rightarrow He\eta$. Enhancement factor $\mid F \mid^2$ evaluated in the constant $\eta - N$ scattering length *versus* the c.m. momentum p^*_η

The inclusion of a finite lifetime turns the momentum vector k in eq. (7.2.10) into a complex quantity k', *i.e.*

$$k' \to \sqrt{k^2 + i\alpha}\,, \tag{7.3.1}$$

where $\alpha = M_r\Gamma_\omega$, with M_r being the reduced mass of the system. This is the same prescription as in the ω-nucleon resonance model of eq. (6.5.1).

In the limit $k^2 \gg \alpha$,

$$k' \approx k + \frac{i\alpha}{2k}\,,$$

so the exponential factor in eq. (7.2.10) becomes

$$\exp(ik'l) \to \exp(ikl)\exp\left(-\frac{\alpha l}{2k}\right) = \exp(ikl)\exp\left(-\frac{\Gamma_\omega M_r l}{2k}\right)\,. \tag{7.3.2}$$

Classically $k = M_r v$, where v is the relative speed in the c.m. system. Hence

$$\exp\left(-\frac{\alpha l}{2k}\right) = \exp\left(\frac{-\Gamma_\omega l}{2v}\right) = \exp\left(-\frac{\Gamma_\omega t}{2}\right)$$

where we have used the classical relation $l = vt$. Finally, eq. (7.3.2) reads

$$\exp(ik'l) \to \exp(ikl)\exp\left(-\frac{\Gamma_\omega t}{2}\right)\,. \tag{7.3.3}$$

So $\exp(-\Gamma_\omega t/2)$ is a damping factor which we could, *in this limit*, have obtained by the replacement $E \to E - i\Gamma_\omega/2$.

Clearly, if the ω were to have zero width then there would be no damping effect. Equation (7.3.3) also shows that the effect becomes greater as the width increases.

7.4 Results and Conclusion

The effect of the short ω lifetime on the enhancement factor $|F|^2$ is shown in fig. (7.3) below. The solid (broken) curves correspond to the absence (inclusion)

of the ω finite lifetime. The case where there is no FSI effects is represented by the horizontal straight line.

Although no significant threshold suppression has been obtained, the enhancement at low p^*_ω has been greatly reduced. According to the model of Fäldt and Wilkin, the produced particle must undergo many scatterings for the production amplitude to be enhanced near threshold. This crucial condition is satisfied by the η but not the ω as it decays before it has a chance to be multiply scattered. At $p^*_\omega = 20$ MeV/c the ω travels an average distance ≈ 0.6 fm before it decays. Assuming the nucleons to be placed at the corners of an equilateral triangle of an average side length $l = 2.72$ fm, then the ω will decay before it even reaches the second nucleon! For $k > 100$ MeV/c, the curves represented by the solid and broken line coincide, which means that the short lifetime effect decreases for large k as we predicted earlier. Using eq. (7.3.1), namely,

$$k' \rightarrow \sqrt{k^2 + i\alpha}\,,$$

one would expect the lifetime effect to start being significant when $k \leq \sqrt{\alpha} \approx 80$ MeV/c, which agrees with the results..

We investigated changes of the real part of the ω-nucleon scattering length to see the effect on the enhancement factor. On reversing the sign of the real part (keeping the imaginary part unchanged), a slight suppression was obtained as shown in fig. (7.4). However the sign reversal had roughly the same effect on both cases (with and without the inclusion of the finite lifetime).

Even though it has not been possible to obtain a *sharp* suppression near threshold, an 'enhancement' can be eliminated. Until the ω-nucleon scattering length is known, one cannot of course be sure about the actual behaviour of the enhance-

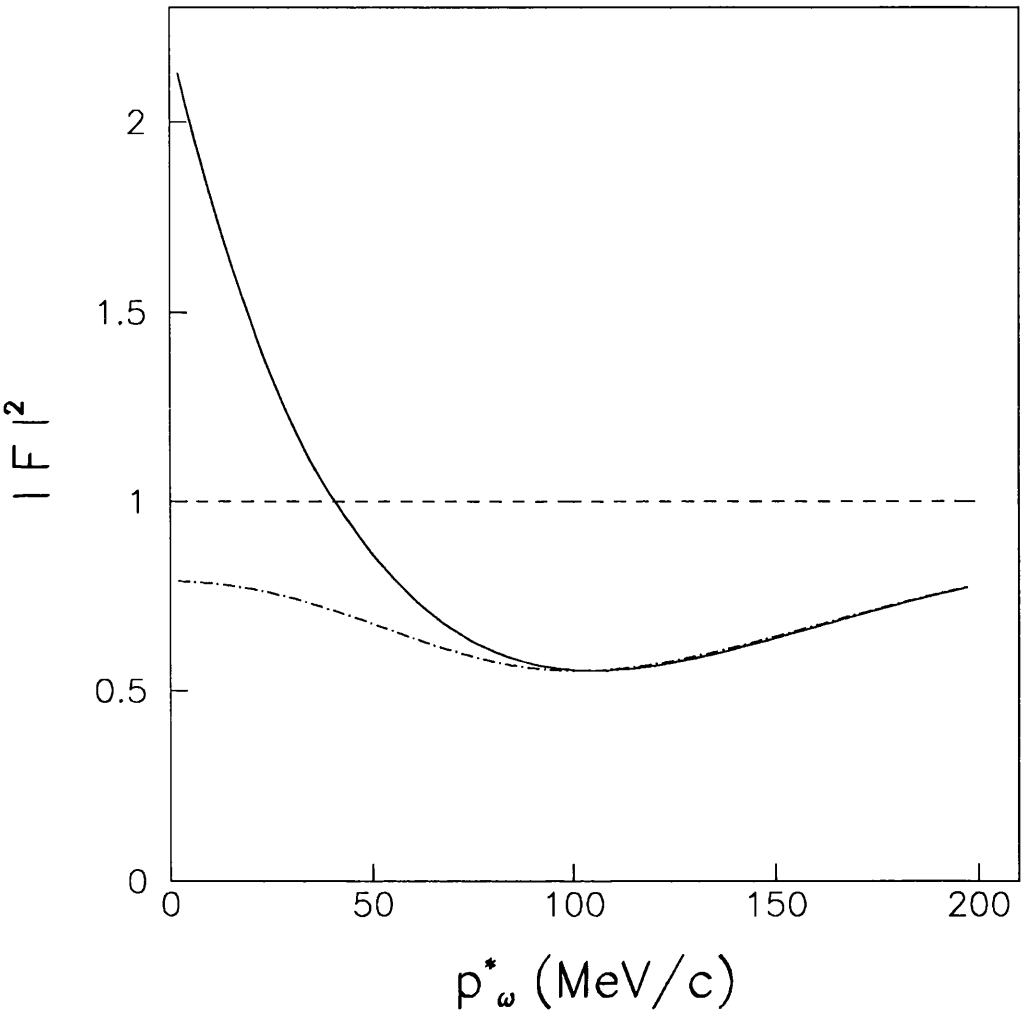

Figure 7.3: $pd \rightarrow {}^3He\,\omega$. The 'enhancement factor' $|F|^2$ *versus* the ω c.m. momentum. Solid curve: finite life time *not* included. Broken line: finite life time included. Straight line: no FSI effects are taken into account.

ment factor at threshold.

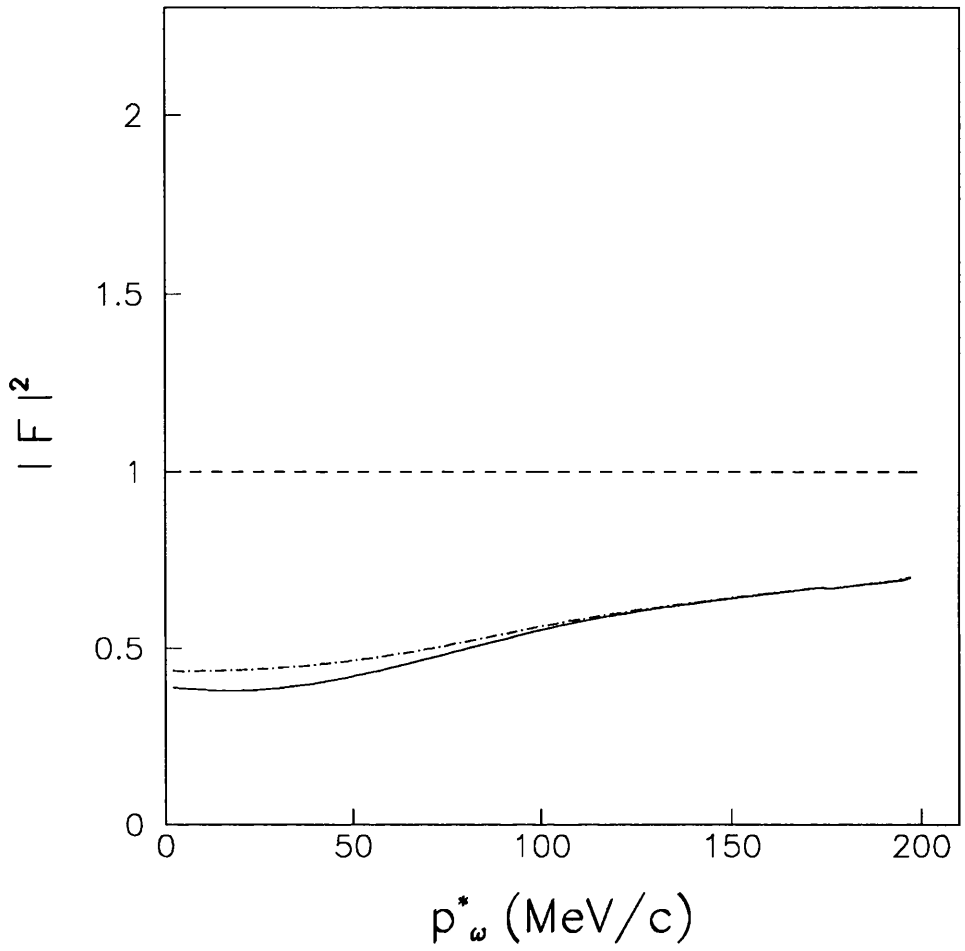

Figure 7.4: $pd \rightarrow {}^3He\,\omega$. The 'enhancement factor' $|F|^2$ *versus* the ω c.m. momentum. Solid curve: finite life time *not* included. Broken line: finite life time included. Straight line: no FSI effects are taken into account. The sign of the real part of the η-nucleon scattering length is reversed.

Chapter 8

The Reaction $pd \rightarrow {}^3He\,\omega$ Near Threshold

8.1 Introduction

As we pointed out in previous chapters, the ω production amplitude in $\pi^- p \rightarrow \omega n$ reaction is suppressed near threshold. Exactly the same type of behaviour is seen in the more complex $pd \rightarrow {}^3He\,\omega$ reaction, suggesting either a common cause or that the suppression effect is propagated through from the $\pi^- p$ to the pd case. In this chapter we shall study the later reaction in a two-step model similar to that used by Fäldt and Wilkin [7] to study the threshold enhancement in $pd \rightarrow {}^3He\,\eta$. This two-step process was also studied by Kilian and Nann [20] in a semi-classical model.

In section 8.2 we shall briefly describe the semi-classical model of Kilian and Nann, before moving on to the more realistic quantum model of Fäldt and Wilkin. Finally, we shall apply the formalism of the quantum model to the ω case in section 8.3.

8.2 The Two-Step Model

Unlike the ω case, the η production amplitude squared in $pd \rightarrow {}^3He\,\eta$ decreases by a factor of three over an η c.m. momentum of 70 MeV/c.

Kilian and Nann studied this reaction by considering double-scattering contributions, where a pion beam produced on one of the nucleons in the target deuteron is converted into the observed η-meson on the second of the target nucleons. They noticed that the kinematics of the $pd \rightarrow pd\eta$ reaction near threshold are almost exactly consistent with those of a physical $pp \rightarrow d\pi^+$ reaction followed by that of $\pi^+ n \rightarrow \eta p$. The large cross section near threshold was then ascribed to what they called a 'kinematic miracle'. Consequently, they estimated the cross section in a semi-classical model where two free interactions were simulated leading to real final protons and deuterons. An interaction to produce a ^3He was assumed if the final relative proton-deuteron momentum were small. This model assumed the dominance of physical intermediate pions which was confirmed in preliminary calculations [21, 22] for the η-meson, but this is less clear for the heavier mesons.

Fäldt and Wilkin studied the same reaction by considering double-scattering graphs in a more realistic quantum mechanical model. They expressed the threshold production amplitude for the whole reaction ($pd \rightarrow {}^3He\,\eta$) in terms of the amplitudes of the two intermediate steps. By extending this model to include strong final state interactions between the produced η and the helium nucleons, they obtained an enhancement factor of 2.2 in the production amplitude near threshold.

In this section, we shall briefly outline their two-step model, and extend it to the ω case. Our aim is to express the ω production amplitude in $pd \rightarrow {}^3He\,\omega$

in terms of the amplitudes of the intermediate reactions namely, $pp \rightarrow \pi^+ d$ and $\pi^+ n \rightarrow \omega p$. We shall also investigate the validity of such a model beyond the threshold region.

In this model, the $pd \rightarrow {}^3He\,\eta$ reaction is viewed as proceeding in two intermediate steps. A pion beam created on one of the target nucleons *via* $p\,p \rightarrow d\pi^+$, is then converted into an η-meson on the second nucleon *via* a $\pi^+ n \rightarrow \eta p$ reaction, as shown in fig. (8.1).

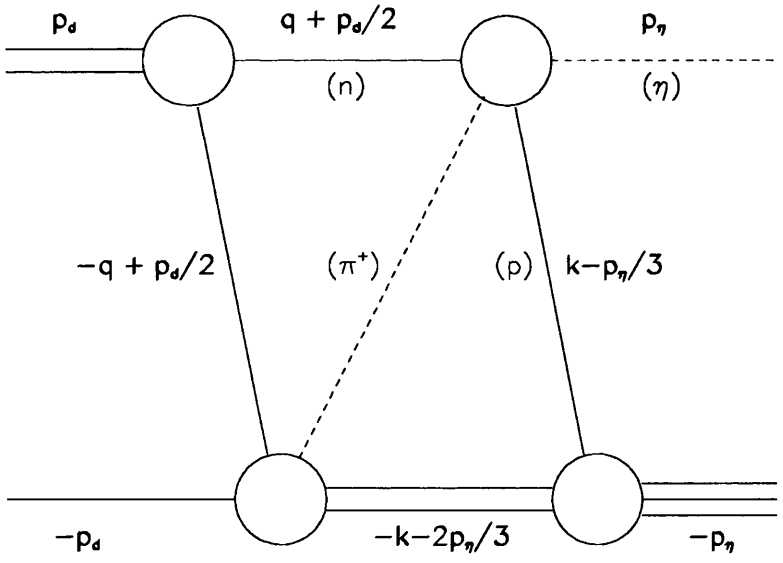

Figure 8.1: A schematic diagram for the reaction $pd \rightarrow {}^3He\,\eta$ in the two-step model.

The nuclear matrix element for the reaction can be written as

$$\mathcal{M} = \int \frac{m_d}{E_d} d^3k \int \frac{m_n}{E_n} d^3q \, \frac{1}{(2\pi)^3 \, 2E_\pi} \, \frac{i}{E_0 - E_{int} + i\epsilon} \, \mathcal{M}_K \,, \tag{8.2.1}$$

where the total energy of the initial (and final) state is denoted by $E_0 = E_\eta + E_h$. E_n and E_d are the energies of the neutron and deuteron in the intermediate state where the total energy is E_{int}.

$\mathcal{M}_K$ is the product of individual matrix elements;

$$\mathcal{M}_K = \sum_{\text{int}} \mathcal{M}(pd \to {}^3He_f)\mathcal{M}(\pi^+ n \to p\eta_f)\,\mathcal{M}(d_i \to p_c n)\,\mathcal{M}(p_i p_c \to \pi^+ d)\,, \tag{8.2.2}$$

where the sum is over the spin degrees of freedom of the intermediate particles.

In addition to the process described by eq. (8.2.2) there is a similar contribution from a neutral intermediate pion, *i.e.*

$$\tilde{\mathcal{M}}_K = \sum_{\text{int}} \mathcal{M}(pd \to {}^3He_f)\,\mathcal{M}(\pi^o p \to p\eta_f)\,\mathcal{M}(d_i \to n_c p)\,\mathcal{M}(p_i n_c \to \pi^o d)\,. \tag{8.2.3}$$

The normalization of the $\mathcal{M}$–matrices is that of Bjorken and Drell [23].

The nuclear matrix element given in eq. (8.2.1) essentially represents a second order perturbation theory type calculation. The amplitudes for the reactions $pp \to \pi^+ d$ and $\pi^+ n \to \eta p$ are sandwiched between the helium and the deuteron wave functions. In this language

$$\frac{i}{E_0 - E_{int} + i\epsilon}\,, \tag{8.2.4}$$

is viewed as the intermediate state propagator.

The so-called kinematic miracle suggests that the intermediate state, consisting of a pion, nucleon and deuteron, is almost on the energy shell where the denominator of eq. (8.2.1) vanishes. This lead Kilian and Nann to replace the

quantum mechanical propagator of eq. (8.2.4) by a purely on-shell propagation in their semi-classical calculation.

Fäldt and Wilkin improved on this by keeping the full propagator, while expanding the denominator around the point where the Fermi momenta $\vec{q}$ and $\vec{k}$ vanish, retaining only terms linear in $\vec{q}$ and $\vec{k}$. They neglected all dependence on the Fermi momenta in evaluating the nuclear matrix element $\mathcal{M}_k$ apart from those in the denominator and wave functions.

The linearization of the energy difference, $\Delta E = E_0 - E_{int}$, leads to

$$\Delta E = \Delta E_0 + \vec{k} \cdot \vec{W} + \vec{q} \cdot \vec{V} \,, \tag{8.2.5}$$

where

$$\Delta E_0 = E_\eta(\vec{p}_\eta) + E_h(-\vec{p}_\eta) - E_d(-\tfrac{2}{3}\vec{p}_\eta) - E_n(\tfrac{1}{2}\vec{p}_d) - E_\pi(\tfrac{2}{3}\vec{p}_\eta - \tfrac{1}{2}\vec{p}_d) \,. \tag{8.2.6}$$

Here, $\vec{V}$ and $\vec{W}$ are relativistic velocity vectors given by

$$\begin{aligned}
\vec{V} &= \vec{v}_\pi(\tfrac{2}{3}\vec{p}_\eta - \tfrac{1}{2}\vec{p}_d) - \vec{v}_n(\tfrac{1}{2}\vec{p}_d) \\
&= \frac{2}{3}\frac{1}{E_\pi(\frac{2}{3}\vec{p}_\eta - \frac{1}{2}\vec{p}_d)}\vec{p}_\eta - \frac{1}{2}\left[\frac{1}{E_\pi(\frac{2}{3}\vec{p}_\eta - \frac{1}{2}\vec{p}_d)} + \frac{1}{E_n(\frac{1}{2}\vec{p}_d)}\right]\vec{p}_d \,, \\
\vec{W} &= -\vec{v}_\pi(\tfrac{2}{3}\vec{p}_\eta - \tfrac{1}{2}\vec{p}_d) + \vec{v}_d(-\tfrac{2}{3}\vec{p}_\eta) \\
&= -\frac{2}{3}\left[\frac{1}{E_\pi(\frac{2}{3}\vec{p}_\eta - \frac{1}{2}\vec{p}_d)} + \frac{1}{E_d(-\frac{2}{3}\vec{p}_\eta)}\right]\vec{p}_\eta + \frac{1}{2}\frac{1}{E_\pi(\frac{2}{3}\vec{p}_\eta - \frac{1}{2}\vec{p}_d)}\vec{p}_d \,,
\end{aligned} \tag{8.2.7}$$

and depend on external kinematic variables only.

This simplifies the matrix element $\mathcal{M}$ of eq. (8.2.1) to

$$\begin{aligned}
\mathcal{M} = &\frac{1}{(2\pi)^3}\frac{1}{2E_\pi(\frac{2}{3}\vec{p}_\eta - \frac{1}{2}\vec{p}_d)}\frac{m_n}{E_n(\frac{1}{2}\vec{p}_d)}\frac{m_d}{E_d(-\frac{2}{3}\vec{p}_\eta)} \\
&\int d^3k \int d^3q \, \frac{i}{\Delta E_0 + \vec{k}\cdot\vec{W} + \vec{q}\cdot\vec{V} + i\epsilon}\,\mathcal{M}'_K \,,
\end{aligned} \tag{8.2.8}$$

where the prime on $\mathcal{M}'_K$ denotes the neglect of the Fermi momentum.

Near threshold, the internal deuteron is almost at rest so that the M_d/E_d factor in eq. (8.2.8) is essentially unity. On the other hand they took the Lorentz contraction of the deuteron wave function into account by letting

$$\vec{q}_\perp{}' = \vec{q}_\perp \,,$$

$$q_{||}{}' = m_d q_{||}/E_d = q_{||}/\gamma \,. \tag{8.2.9}$$

for the external deuteron momentum. This results in

$$\mathcal{M} = \frac{1}{(2\pi)^3}\frac{1}{2E_\pi(\frac{2}{3}\vec{p}_\eta - \frac{1}{2}\vec{p}_d)}\int d^3k \int d^3q' \, \frac{i}{\Delta E_0 + \vec{k}\cdot\vec{W} + \vec{q}'\cdot\vec{V}' + i\epsilon}\,\mathcal{M}'_K \,, \tag{8.2.10}$$

where

$$\begin{aligned} \vec{V}_\perp' &= \vec{V}_\perp \,, \\ V_{||}' &= \gamma V_{||} \,. \end{aligned} \tag{8.2.11}$$

After evaluating the matrix element $\mathcal{M}$, they arrived at a simple closed-form expression relating the η production cross section of $pd \to {}^3He\,\eta$ to the intermediate step amplitudes, *viz.*

$$\left[\frac{p_d}{p_\eta}\frac{d\sigma}{d\Omega}(pd \to {}^3He\,\eta)\right]_{cm} = \frac{3\,M_h\,(M_\eta + M_p)^2}{M_n\,(M_h + M_\eta)^2\,E_\pi^2(\frac{1}{2}\vec{p}_d)}\,\frac{1}{(2\pi)^4}\times$$

$$\left[|S_a(\vec{W},\vec{V}')|^2 + |S_b(\vec{W},\vec{V}')|^2\right]\left[\left(\frac{E_\pi + E_d}{m_d}\right)^2\frac{p_p}{p_\pi}\frac{d\sigma}{d\Omega}(pp \to \pi^+ d)\right]_{cm}\left[\frac{p_\pi}{p_\eta}\frac{d\sigma}{d\Omega}(\pi^+ n \to \eta p)\right]_{cm} \tag{8.2.12}$$

Here $S_a(\vec{W},\vec{V}')$ and $S_b(\vec{W},\vec{V}')$ are complex form factor combinations given by

$$\begin{aligned} S_a &= S_{00} - S_{20}\sqrt{2} \,, \\ S_b &= S_{02} - S_{22}\sqrt{2} \,, \end{aligned} \tag{8.2.13}$$

the indices a and b are either 0 (S-wave) or 2 (D-wave). The complex form factor

$$S_{ab}(\vec{W},\vec{V}') = (2\pi)^3 \int_0^\infty dt\, e^{it\Delta E_0} \psi_a^*(-t\vec{W})\varphi_b(t\vec{V}') \qquad (8.2.14)$$

involves integrals over *configuration–space* deuteron and ^3He wave functions.

In fig. (8.2), we compare the theoretical prediction of eq. (8.2.12), modified by the FSI effects and multiplied by a factor of 2.5, with experimental data. Clearly, apart from an overall constant of 2.5, the energy variation of the cross section is well reproduced.

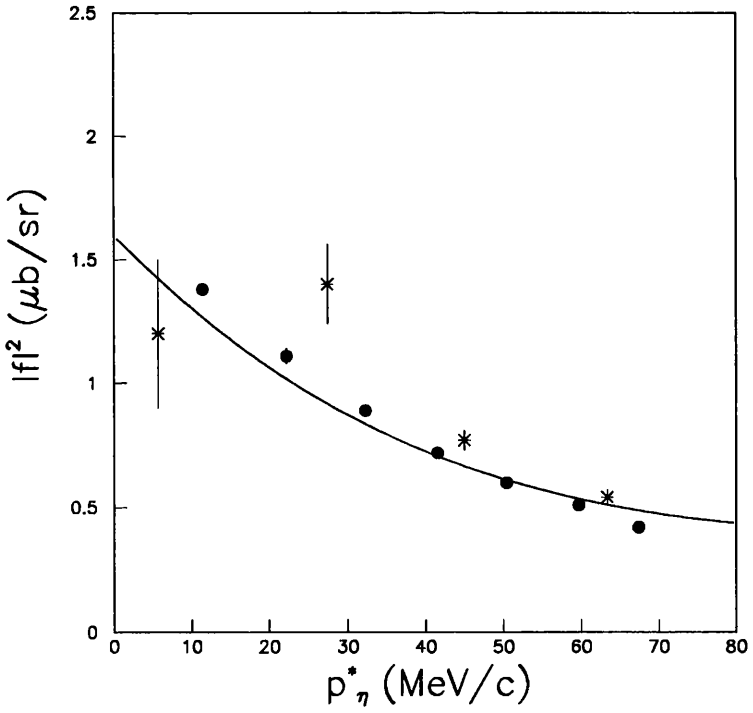

Figure 8.2: Spin-averaged amplitude squared for the reaction $pd \rightarrow {}^3He\,\eta$ as predicted by the two step-model, *versus* the η c.m. momentum. Solid line is the theoretical prediction of eq. (8.2.12) modified by the FSI effects and multiplied by a factor of 2.5. Experimental data from ref. [26] (crosses) and values quoted in ref. [27] (circles) are also shown.

8.3 Application to the ω-meson

We shall now apply eq. (8.2.12) to estimate ω production in the reaction $pd \rightarrow {}^3He\,\omega$. Here, the kinematics are less miraculous so that off-shell parts in the intermediate steps are important. This type of behaviour is shown in fig. (8.3), where the real (solid line) and imaginary (broken line) parts of the purely S-wave S_{00} complex form factor are plotted *versus* the ω c.m. momentum. Obviously, the off-shell part is dominant at low energies but its significance decreases as p^*_ω becomes larger.

A fit curve for

$$\left[\frac{p_\pi}{p_\omega}\frac{d\sigma}{d\Omega}(\pi^+ p \rightarrow \omega n)\right]_{cm} \tag{8.3.1}$$

was obtained using experimental data given in [2, 24]. The data and the fit curve are shown in fig. (8.4).

The other intermediate production amplitude in the two-step model namely,

$$\left[\frac{p_p}{p_\pi}\frac{d\sigma}{d\Omega}(pp \rightarrow \pi^+ d)\right]_{cm}$$

was calculated using the parameterization

$$\left[\frac{d\sigma}{d\Omega}(pp \rightarrow \pi^+ d)\right]^{cm}_{\theta=0} = \exp(2.514 - 0.011115T_\pi) + 0.000065(T_\pi - 500)\ , \tag{8.3.2}$$

given in [25].

The theoretical predictions of eq. (8.2.12) are compared to experimental data in fig. (8.5), with no arbitrary parameters except an overall normalization constant. It is worth noting that in the ω case there are no FSI contributions are expected due to the finite ω lifetime. As we saw chapter 7, the FSI-related enhancement was eliminated since the ω decays before it has a chance to form a resonance system with the nucleon.

Although the energy variation of the cross section is not well reproduced at high energies, the rapid rise from threshold is clearly obtained. This sharp rise proves that the suppression effect near threshold can propagate from the $\pi^- p \rightarrow \omega n$ to the $pd \rightarrow {}^3He\ \omega$ reactions.

The two-step model could be improved by taking the fermi momenta into account when evaluating the nuclear matrix element. Also the binding energy of the nucleons in the ^3He nucleus should not be neglected. But it is not expected that this would change significantly the momentum scale in fig. (8.5).

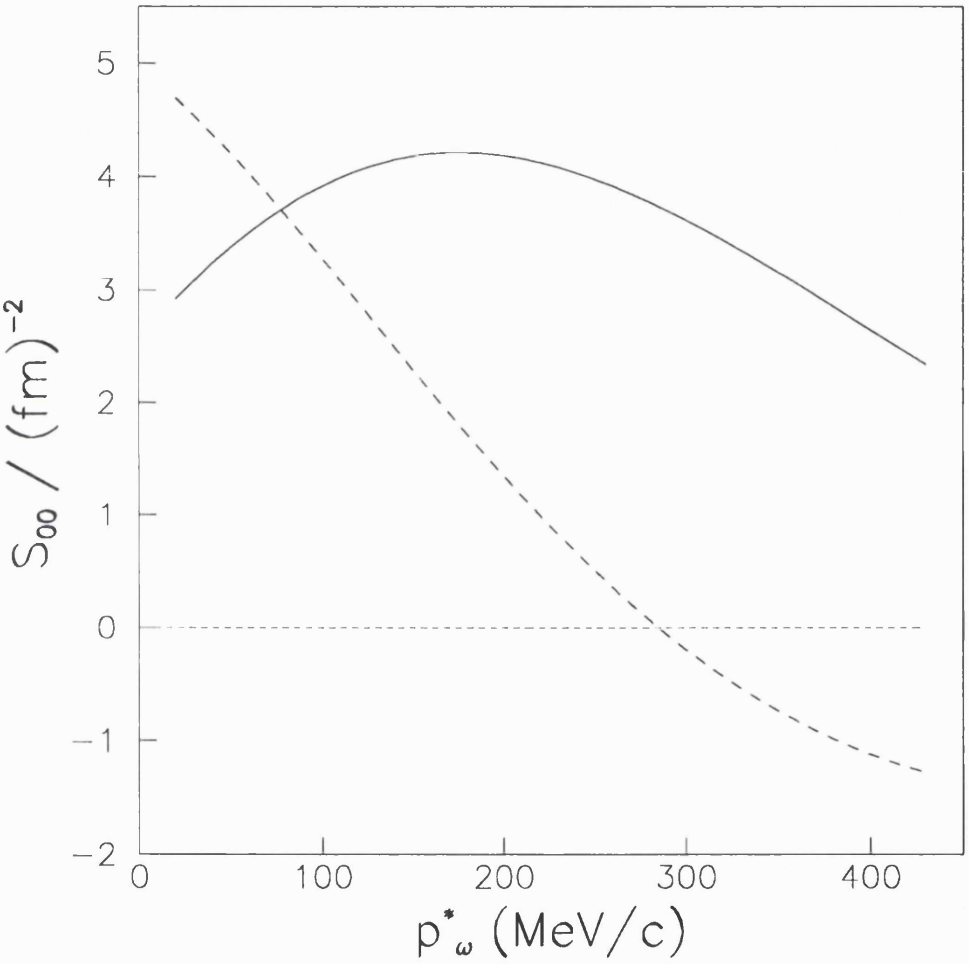

Figure 8.3: The real (solid line) and imaginary (broken line) of the purely S-wave complex form factor S_{00} *versus* the ω c.m. momentum p^*_ω.

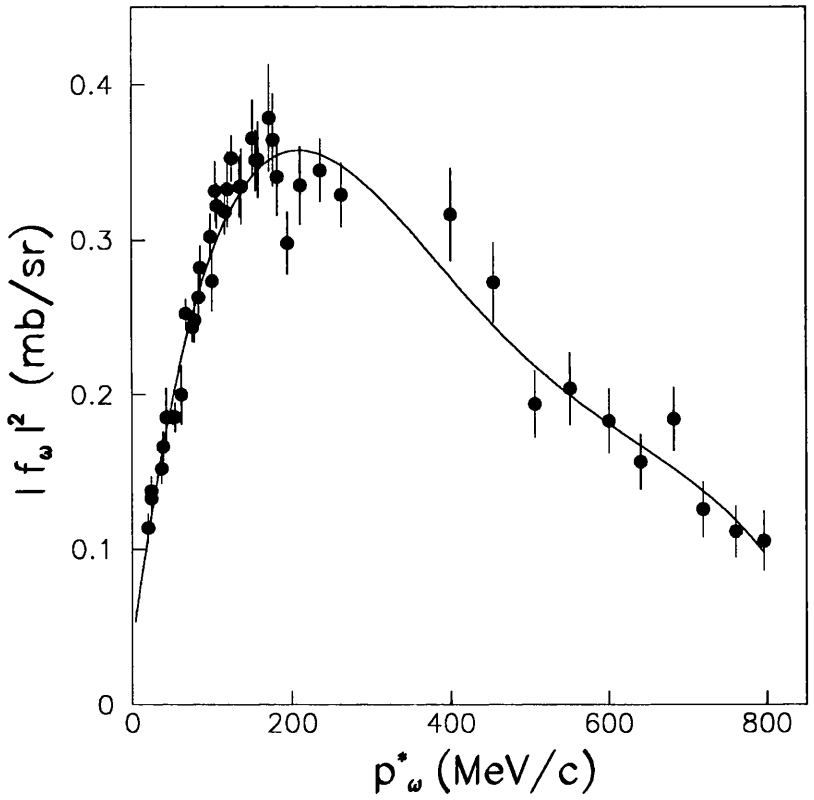

Figure 8.4: $\pi^- p \to \omega n$. Solid line is a fit for the experimental data taken from ref. [3,24]

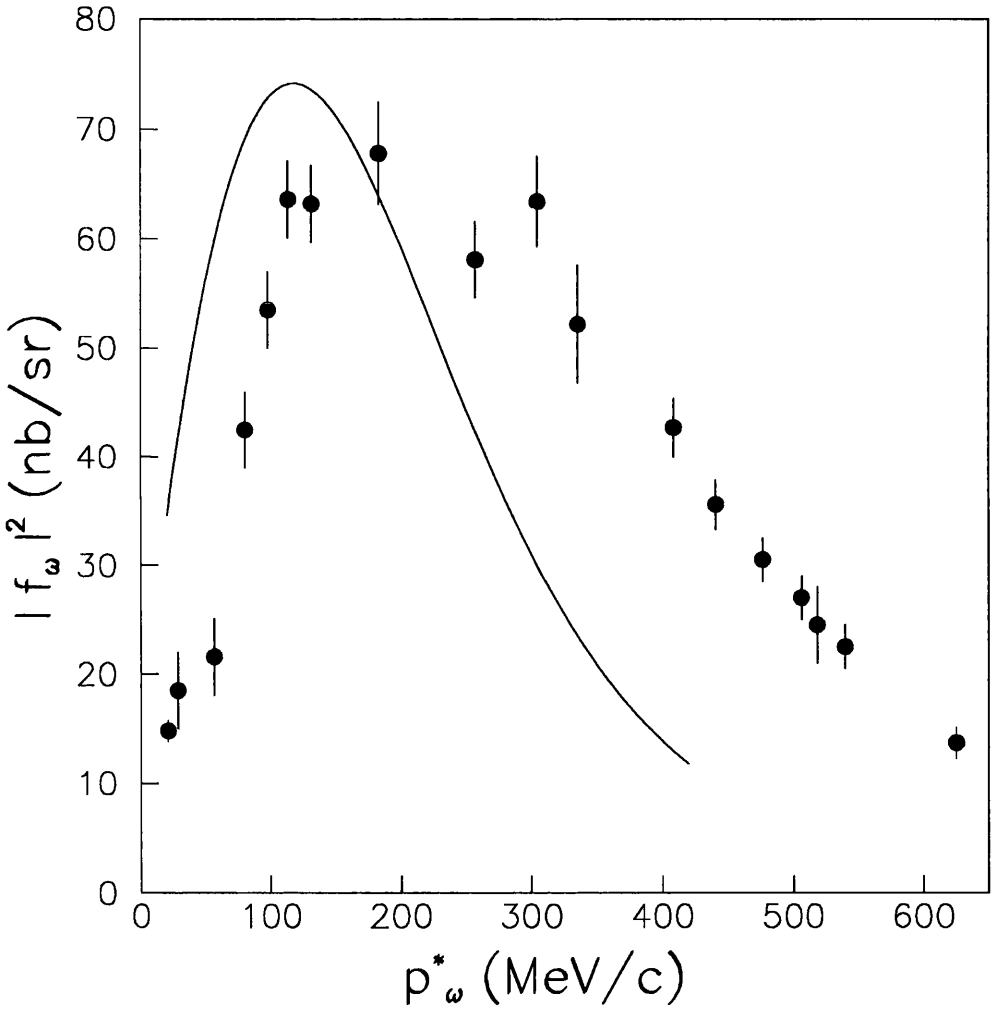

Figure 8.5: Spin-averaged amplitude squared for the reaction $pd \rightarrow {}^3He\,\omega$ as predicted by the two step-model, *versus* the ω c.m. momentum. Experimental data at $\theta_{p^*_\omega} = 180^0$ from ref. [5] are also shown.

Chapter 9

Conclusions

Final-state interactions between the ω-decay products and the recoil neutron (nucleus) do lead to a reduction in the observed ω production near threshold, in agreement with experimental results [3, 5]. In the semi-classical model considered in chapter 4, the rapid rise from threshold shown in figures (4.1,4.2), as well as the scale in p^*_ω of the phenomenon, is well reproduced. However, the size of the suppression is found to be greater in the three pion case than in the radiative one. This simple model therefore sheds no light as to why the branching ratio of $\omega \to \pi^-\pi^+\pi^0$ and $\omega \to \pi^0\gamma$ is constant in the pion-induced experiment [3]. On the other hand, considering only the radiative decay channel ($\omega \to \pi^0\gamma$), the quantum mechanical model of chapter 5 resulted in a 9% suppression near threshold, which is too small to explain the 70% reduction observed experimentally. Although we have not dealt with the three-pion decay mode in the quantum model, we feel that an upper bound of $\approx$ 27%, which is still much smaller than the observed 70% effect, can be placed on the threshold reduction corresponding to this channel for the following reasons

1. As the ω width is relatively narrow (8.43 MeV/c^2 [1]), the rescattering of one pion off the recoil neutron is most likely to throw the event out

of the ω peak. Consequently, more than one pion interacting with the nucleon will either push the event even further into the continuum, or knock it back into the ω peak. Therefore, double or triple scattering do not contribute to the reduction in the former case, but could *increase* the ω production in the latter one. Hence, the leading term contributing to the reduction near threshold is expected to come from single pion scattering. This has been estimated in the $\omega \to \pi^0\gamma$ decay channel, and resulted in a 9% reduction near threshold. Although the kinematics of the three pion and radiative decay channels are different, one would not expect the reduction effect due to the former to differ much from three times that due to the latter, where the factor of 3 arises because there are three pions rather than one.

2. According to ref. [3], the branching ratio of the dominant three-pion and radiative decay channels is constant independent of the ω momentum in the overall c.m. frame.

Since a large enough effect was not found, and final-state interactions are not expected to give a constant $\Gamma(\omega \to \pi^-\pi^+\pi^0)/\Gamma(\omega \to \pi^0\gamma)$ ratio, we decided to investigate other mechanisms in the hope of explaining the experimental observations.

In the reaction $\pi^- p \to \eta n$, an attractive ηn interaction results in the formation of the $N^*(1535)$ S-wave resonance, which enhances the η production near threshold. Similarly, the ω and the neutron from $\pi^- p \to \omega n$ are in an S-wave near threshold and an S-wave $\omega - n$ resonance system might be produced if the two particles interacted *via* an attractive potential. But, unlike the η, the ω has

a short lifetime which may destroy the resonance system. This is an alternative suppression mechanism, which is independent of the ω decay channel *i.e.* it would affect both decay modes equally. This hypothesis has been examined by deriving a dynamical ωn interaction amplitude, which was then fit using the parameters of the ηn scattering channel [7], as experimentally determined ωn ones are not known. This may be justified since our primary aim was to investigate the effect of short lifetime on resonance formation. This was done by assuming the η to have a finite width equals to that of the ω.

We adopted two different mechanisms that might lead to an S-wave resonance production. First, since a one-term attractive S-wave potential does not support resonances, a two-term S-wave non-local separable one was considered. Using such a potential the Schrödinger equation was solved and an ωn interaction amplitude extracted but no suitable fit could be obtained. This might be a reflection of the difficulty of producing S-wave resonances unless strong repulsive potentials are included. A better description is provided in a quantum multi-channel scattering model, where the resonance was taken to be trapped as a virtual state. Three channels were considered, ηn, $\pi^- p$ and $K\Lambda$ and, using multi-channel scattering formalism, an ηn amplitude was derived and used to investigate the effect of a finite width on the resonance formation. Fig. (6.3) shows that the short lifetime has 'killed' the enhancement near threshold, and its effect is most important at low energy.

In a two-step quantum model [7], the near threshold η production amplitude in the overall $pd \rightarrow {}^3He\eta$ was expressed in terms the $pp \rightarrow d\pi^+$ and $\pi^+ n \rightarrow \eta n$ intermediate steps amplitudes. By extending this model to include strong final-state interactions between the η and the ${}^3He$ nucleons a production enhancement

factor of 2.2 was obtained. We examined the effect of the ω short lifetime on the final-state interaction related enhancement. Unlike the η, the ω most probably decays before it has a chance to be multiply scattered by the nucleons. This greatly reduced the enhancement factor, as shown in fig. (7.3), especially at low p^*_ω.

Furthermore, using the formalism of the two-step model, we expressed the production amplitude of the ω in the $pd \rightarrow {}^3He\,\omega$ reaction in terms of $pp \rightarrow d\pi^+$ and $\pi^+ n \rightarrow \omega n$ intermediate steps amplitudes. We then investigated the ω production at low energies, and examined the validity of the model away from threshold. As fig. (8.5) shows, the rapid rise from threshold has been reproduced, but the agreement between the predicted amplitude and the experimental results becomes progressively poorer as the energy increases.

Clearly, no one single model has *solely* produced the 'magic' 70% reduction in the ω production near threshold. Nevertheless, it is possible that the reduction due to some of the different effects may be added together. On the other hand, there might be an effect due to the ω itself interacting with the recoil neutron. At low p^*_ω, the ω is produced within the range of the nucleon potential, which might enhance or suppress its decay rate. If the reduction effect due to final-state interactions were to be small as we found in chapter 5, then such a mechanism would affect both decay channels equally same, as the experimental results suggest. But the same results also show the ω width to be constant independent of p^*_ω, while one would expect it to vary if the ω decay rate were modified. Furthermore, there could be an interference between the amplitudes corresponding to graphs (a) and (b) in fig. (9.1), which is also true for the $\omega \rightarrow \pi^0\gamma$ decay channel. However, it would be difficult to estimate such an effect as the amplitude corresponding to

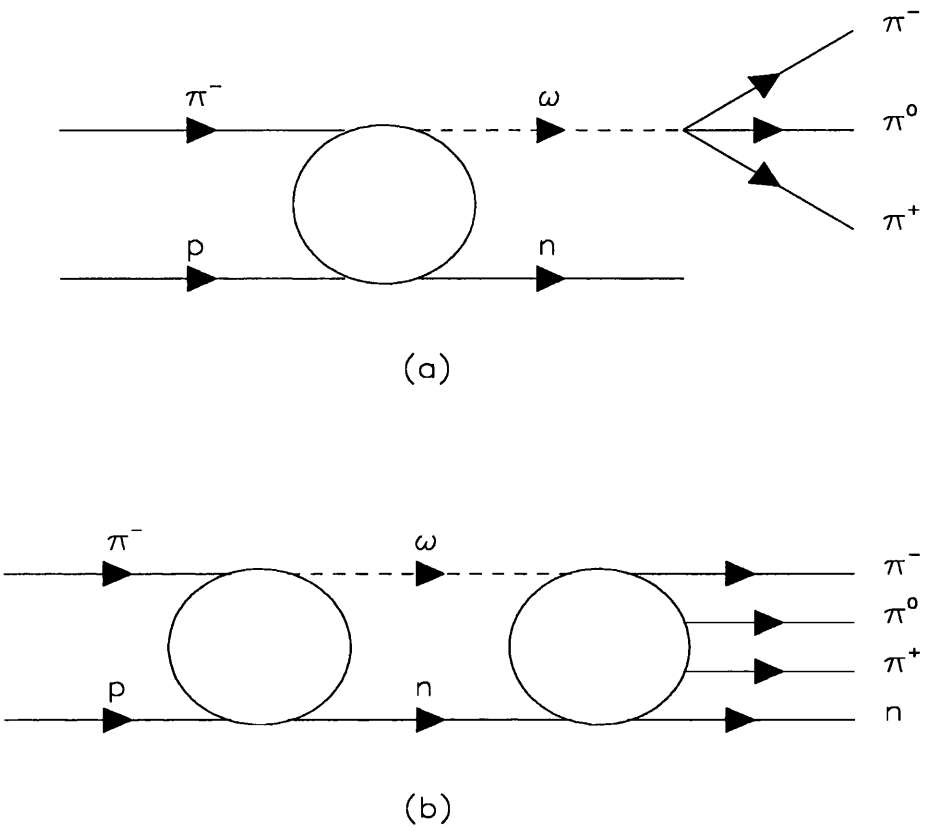

Figure 9.1: (a) a Feynman diagram describing the ω production, in $\pi p \rightarrow \omega n$, and its subsequent decay into three pions. (b) Feynman diagram representing the production of the ω which, before decaying, interacts with recoil neutron.

graph (b) is not known.

Appendix A

Determination of the ratios of the total $\pi^- n$, $\pi^0 n$ and $\pi^+ n$ cross sections

At low energies the total pion-nucleon cross sections are dominated by the processes of elastic scattering

$$\pi^{\pm} N \rightarrow \pi^{\pm} N \,, \tag{A.1.1}$$

and charge exchange scattering

$$\pi^{+} n \rightarrow \pi^{0} p \,. \tag{A.1.2}$$

Since the isospin of the pion is 1 and that of the nucleon is 1/2, the total isospin in pion-nucleon scattering can be 1/2 or 3/2. At low energies the total πN scattering cross sections are dominated by peaks at about 1232 MeV/c^2 corresponding to the formation of the $\Delta(1232)$ resonance. This has an isospin $I = 3/2$ and therefore exists in four charge states of roughly equal masses, Δ^{++}, Δ^{+}, Δ^{0} and Δ^{-}, corresponding to $I_3 = 3/2$, $1/2$, $-1/2$ and $-3/2$ respectively. In what follows, we shall seek to determine the relative ratios of the total cross sections of the $\pi^- n$, $\pi^0 n$ and $\pi^+ n$ reactions in the first resonance region. This can be achieved by defining a transition amplitude from an initial state ψ_i to a final ψ_f one as

$$M_{if} = < \psi_f(I^f)|H|\psi_i(I^i) > = M,\ I^i = I^f = 3/2$$
$$0,\ \text{otherwise}$$

where H is an isospin operator.

In the πn scattering, the possible processes are

$$\pi^- n \to \pi^- n\ , \tag{A.1.3}$$

$$\pi^0 n \to \pi^0 n\ , \tag{A.1.4}$$

$$\pi^0 n \to \pi^- p\ , \tag{A.1.5}$$

$$\pi^+ n \to \pi^+ n\ , \tag{A.1.6}$$

$$\pi^+ n \to \pi^0 p\ . \tag{A.1.7}$$

Obviously, one may write

$$\sigma_t(\pi^- n) = \sigma_t(\pi^- n \to \pi^- n)\ , \tag{A.1.8}$$

$$\sigma_t(\pi^0 n) = \sigma_t(\pi^0 n \to \pi^0 n) + \sigma_t(\pi^0 n \to \pi^- p)\ , \tag{A.1.9}$$

and

$$\sigma_t(\pi^+ n) = \sigma_t(\pi^+ n \to \pi^+ n) + \sigma_t(\pi^+ n \to \pi^0 p)\ , \tag{A.1.10}$$

The reaction (A.1.3) involves a pure state of $I = 3/2$, $I_3 = -3/2$ and therefore the total $\pi^- n$ cross section is given by

$$\sigma_t(\pi^- n) = A| < \psi_f|H|\psi_i > |^2 = A|M|^2\ , \tag{A.1.11}$$

where A is a scalar.

Similarly, for the reaction in (A.1.4) we have

$$|\psi_i >= |\psi_f >= \sqrt{\frac{2}{3}}|\chi(3/2, -1/2) > + \sqrt{\frac{1}{3}}|\chi(1/2, -1/2) >\ , \tag{A.1.12}$$

where the numerical factors are the Clebsch-Gordon coefficients. The total cross section is then given by

$$\sigma_t(\pi^0 n \to \pi^0 n) = \frac{4}{9} A|M|^2 \,. \tag{A.1.13}$$

For (A.1.5) we have

$$|\psi_i> = \sqrt{\frac{2}{3}}|\chi(3/2,-1/2)> + \sqrt{\frac{1}{3}}|\chi(1/2,-1/2)> \,, \tag{A.1.14}$$

$$|\psi_f> = \sqrt{\frac{1}{3}}|\chi(3/2,-1/2) - \sqrt{\frac{2}{3}}|\chi(1/2,-1/2) \,, \tag{A.1.15}$$

therefore

$$\sigma_t(\pi^0 n \to \pi^- p) = \frac{2}{9} A|M|^2 \tag{A.1.16}$$

Considering the reaction in (A.1.6) results in

$$|\psi_i> = |\psi_f> = \sqrt{\frac{1}{3}}|\chi(3/2,1/2)> + \sqrt{\frac{2}{3}}|\chi(1/2,1/2)> \,, \tag{A.1.17}$$

and

$$\sigma_t(\pi^+ n \to \pi^+ n) = \frac{1}{9} A|M|^2 \tag{A.1.18}$$

Finally in (A.1.7) we have

$$|\psi_i> = \sqrt{\frac{1}{3}}|\chi(3/2,1/2)> + \sqrt{\frac{2}{3}}|\chi(1/2,1/2)> \,, \tag{A.1.19}$$

$$|\psi_f> = \sqrt{\frac{2}{3}}|\chi(3/2,1/2)> - \sqrt{\frac{1}{3}}|\chi(1/2,1/2)> \,, \tag{A.1.20}$$

leading to

$$\sigma_t(\pi^+ n \to \pi^0 p) = \frac{2}{9} A|M|^2 \tag{A.1.21}$$

Hence, according to equations (A.1.8)-(A.1.10)

$$\sigma_t(\pi^- n) = A|M|^2 \,, \tag{A.1.22}$$

$$\sigma_t(\pi^0 n) = \left(\frac{4}{9} + \frac{2}{9}\right) A|M|^2 = \frac{2}{3} A|M|^2 \,, \qquad \text{(A.1.23)}$$

$$\sigma_t(\pi^+ n) = \left(\frac{1}{9} + \frac{2}{9}\right) A|M|^2 = \frac{1}{3} A|M|^2 \,. \qquad \text{(A.1.24)}$$

Therefore

$$\sigma_t(\pi^- n) : \sigma_t(\pi^0 n) : \sigma_t(\pi^+ n) = 3 : 2 : 1 \,. \qquad \text{(A.1.25)}$$

Appendix B

Fitting of the range parameter β in pion-nucleon scattering at low energies

The production of the $\Delta(1232)$ resonance in the $\pi N \rightarrow \pi N$ reaction is in a P-wave and spin dependent. Our aim is to determine the interaction range β using experimental data presented in ref. [3, 11]. To do so, we shall extract a scattering amplitude by solving the non-homogeneous Schrödinger equation

$$(\nabla^2 + k^2)\Psi(\vec{r}) = \int U(\vec{r},\vec{r}')\Psi(\vec{r}')d^3r' \,, \tag{B.1.1}$$

where

$$U(\vec{r},\vec{r}') = \lambda u(r)u(r')\vec{r}\cdot\vec{r}' = \lambda u(r)u(r')\sum_{m=-1}^{1} Y_1^m(\hat{r})Y_1^m(\hat{r}') \,, \tag{B.1.2}$$

is a reduced P-wave non-local separable potential. Furthermore, $u(r)$ and $u(r')$ are given by

$$u(r) = \sqrt{\frac{\pi}{2}}\frac{e^{-\beta r}}{r} \quad u(r') = \sqrt{\frac{\pi}{2}}\frac{e^{-\beta r'}}{r'} \,. \tag{B.1.3}$$

It should be stressed that our derived amplitude does not take account of spin effects. This simplification is justifiable since our quantum mechanical model produced only a 9% reduction effect which is much too small to account for 70%

suppression observed experimentally. Spin refinements are not expected to bring our results in line with experiment.

The general solution of eq. (B.1.1) may be written as

$$\Psi(\vec{r}) = e^{i\vec{k}\cdot\vec{r}} + \int G(\vec{r},\vec{r}\,')U(\vec{r}\,',\vec{r}\,'')\Psi(\vec{r}\,'')d^3r'd^3r'' \,, \qquad \text{(B.1.4)}$$

where $G(\vec{r},\vec{r}\,')$ is a Green's function given by

$$G(\vec{r},\vec{r}\,') = -\frac{1}{4\pi}\frac{e^{ik|\vec{r}-\vec{r}\,'|}}{|\,\vec{r}-\vec{r}\,'\,|} \,. \qquad \text{(B.1.5)}$$

Substituting for $G(\vec{r},\vec{r}\,')$ results in

$$\Psi(\vec{r}) = e^{i\vec{k}\cdot\vec{r}} - \frac{1}{4\pi}\int \frac{e^{ik|\vec{r}-\vec{r}\,'|}}{|\,\vec{r}-\vec{r}\,'\,|}U(\vec{r}\,',\vec{r}\,'')\Psi(\vec{r}\,'')d^3r'd^3r'' \,, \qquad \text{(B.1.6)}$$

Apart from the form of the potential given by eq. (B.1.2), $\Psi(\vec{r})$ has the same structure as eq. (6.2.10) in chapter 6 where we dealt with an S-wave potential. Therefore the integral may be evaluated in the same way as we did then with the following two points in mind

1. $U(\vec{r}\,',\vec{r}\,'')$ is a P-wave potential which only singles out the partial wave corresponding to $l = 1$.

2. The incident plane wave is assumed to be along the z direction *i.e.* the wave vector $\vec{k} = k\hat{z}$. Hence, there is no ϕ dependence in the initial state (where ϕ is the azimuthal angle) which implies that the final state does not depend on ϕ either. Consequently $m = 0$.

Carrying out the integral results in

$$\Psi(\vec{r}) = e^{i\vec{k}\cdot\vec{r}} - (3/2)\,k^2\,\hat{k}\cdot\hat{r}\left[\frac{(k^2+\beta^2)^4}{2\pi\lambda} - \frac{(\beta^2-k^2)(k^4+10k^2\beta^2+\beta^4)}{16\beta^3} - ik^3\right]^{-1} \times$$

$$[i(k^2+\beta^2)e^{-\beta r} + 2\beta^2 h_1^{(1)}(i\beta r) + 2k^2 h_1^{(1)}(kr)] \,. \qquad \text{(B.1.7)}$$

Here

$$h_1^{(1)}(x) = -\left(\frac{1}{x} + \frac{i}{x^2}\right) e^{ix} , \tag{B.1.8}$$

is a spherical Hankel function, whose asymptotic behaviour as $x \to \infty$ is

$$h_1^{(1)}(x) \approx -\frac{e^{ix}}{x} . \tag{B.1.9}$$

Hence

$$\lim_{r\to\infty} \Psi(\vec{r}) = e^{i\vec{k}\cdot\vec{r}} - 3k^2 \hat{k}\cdot\hat{r} \left[\frac{(k^2+\beta^2)^4}{2\pi\lambda} - \frac{(\beta^2-k^2)(k^4+10k^2\beta^2+\beta^4)}{16\beta^3} - ik^3\right]^{-1} \frac{e^{ikr}}{r} , \tag{B.1.10}$$

and the scattering amplitude reads

$$f(\theta) = 3k^2 \cos\theta \left[\frac{(k^2+\beta^2)^4}{2\pi\lambda} - \frac{(\beta^2-k^2)(k^4+10k^2\beta^2+\beta^4)}{16\beta^3} - ik^3\right]^{-1} . \tag{B.1.11}$$

Therefore

$$k^3 \cot\delta = \frac{(k^2+\beta^2)^4}{2\pi\lambda} - \frac{(\beta^2-k^2)(k^4+10k^2\beta^2+\beta^4)}{16\beta^3} . \tag{B.1.12}$$

Our aim is to fit $k^3 \cot\delta$ in order to obtain a value for β. To this end we turn to ref.[11], where the authors fitted $\pi^+ p$ total cross section scattering data, after correcting for Coulomb distortion, to a Breit-Wigner form

$$\sigma_{tot}(W) = \frac{8\pi}{k^2} \frac{W_0^2\Gamma^2}{(W_0^2-W^2)^2 + W_0^2\Gamma^2} , \tag{B.1.13}$$

with an energy dependent width

$$\Gamma = \Gamma_0 \left(\frac{k}{k_0}\right)^3 \frac{1+k_0^2a^2}{1+k^2a^2} . \tag{B.1.14}$$

The k and W stand for the pion momentum and the total πN energy in the centre-of-mass frame. The fit parameters (W_0, Γ_0, a) the resonance energy, its width and the πN interaction radius were determined to be

$$W_0 = 1233.8 \pm 0.2\,\text{MeV} , \quad \Gamma_0 = 117.9 \pm 0.9\,\text{MeV} , \quad a = 1.15 \pm 0.02\,\text{fm} .$$

The c.m. momentum k_0 is determined from W_0 and has a value of ≈ 230 MeV/c.

In their energy range all partial waves other than the resonating $I = J = 3/2$ were considered as a background and therefore removed using amplitudes reconstructed from phase shifts.

When a spin-0 particle scatters off one of a spin-1/2, as is the case here, we have a scattering amplitude of the form [28]

$$f(k,\theta) = \frac{1}{k}\sum_{l=0}^{\infty}[(l+1)e^{i\delta_{l+}}\sin\delta_{l+} + le^{i\delta_{l-}}\sin\delta_{l-}]P_l(\cos\theta)\,, \qquad \text{(B.1.15)}$$

where

$$\delta_{l\pm} \equiv \delta_{l,j=l\pm 1/2}\,. \qquad \text{(B.1.16)}$$

For the $\Delta(1232)$, $l = 1, j = 3/2$, and so we shall only consider that part of $f(k,\theta)$ that couples to the P-wave corresponding to $j = 3/2$. Thus

$$f(\theta,k) \approx 2\frac{e^{i\delta_{1+}}\sin\delta_{1+}}{k}P_1(\cos\theta)\,. \qquad \text{(B.1.17)}$$

As the experimental data were taken in the forward direction the spin-flip terms vanish. Further, using the optical theorem we get

$$\sigma_{tot} = 8\pi\frac{\sin^2\delta}{k^2}\,, \qquad \text{(B.1.18)}$$

where the label 1+ is understood. Comparing equations (B.1.13) and (B.1.18) it can be easily seen that

$$\sin^2\delta = \frac{W_0^2\Gamma^2}{(W_0^2 - W^2)^2 + W_0^2\Gamma^2}\,, \qquad \text{(B.1.19)}$$

which leads to

$$\cot\delta = \frac{W_0^2 - W^2}{W_0\Gamma}\,. \qquad \text{(B.1.20)}$$

Multiplying both sides by k^3 results in

$$k^3\cot\delta = k^3\frac{W_0^2 - W^2}{W_0\Gamma}\,. \qquad \text{(B.1.21)}$$

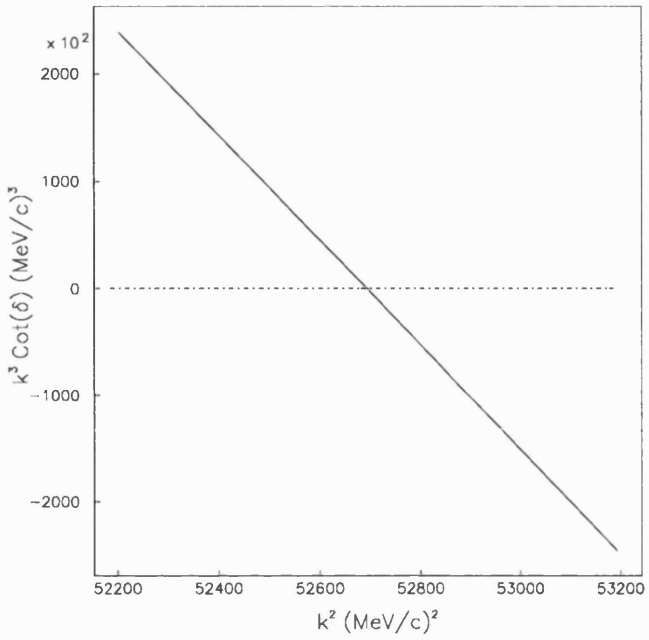

Figure B.1: A graph of $k^3 \cot\delta$ as a function of k^2 in the vicinity of the $\Delta(1232)$ resonance. The straight line is perfectly fit by the first order polynomial in k^2, $y(k^2) = 0.25781 \times 10^8 - 489.27\, k^2$.

Fig. (B.1) is a graph of $k^3 \cot\delta$ as a function of k^2 in the vicinity of the $\Delta(1232)$ resonance. In this energy region the function is evidently a straight line which is perfectly fit by the first order polynomial in k^2, namely

$$y(k^2) = 0.25781 \times 10^8 - 489.27\, k^2 \ . \qquad \text{(B.1.22)}$$

Now we return to our derived expression of $k^3 \cot\delta$ in eq. (B.1.12). According to the effective range expansion theory this is an even function in k which we shall expand as

$$k^3 \cot\delta = \left(\frac{\beta^8}{2\pi\lambda} - \frac{\beta^3}{16}\right) + \left(\frac{2\beta^6}{\pi\lambda} - \frac{9\beta}{16}\right) k^2 + \left(\frac{3\beta^4}{\pi\lambda} + \frac{9}{16\beta}\right) k^4$$
$$+ \left(\frac{1}{16\beta^3} + \frac{2\beta^2}{\pi\lambda}\right) k^6 + \frac{k^8}{2\pi\lambda} \,. \qquad \text{(B.1.23)}$$

As we saw in fig. (B.1), only terms up to and including k^2 are important around $W = W_0$. Hence

$$k^3 \cot\delta \approx \left(\frac{\beta^8}{2\pi\lambda} - \frac{\beta^3}{16}\right) + \left(\frac{2\beta^6}{\pi\lambda} - \frac{9\beta}{16}\right) k^2 \,, \qquad \text{(B.1.24)}$$

is a very good approximation. Comparing the coefficients of the same powers of k in equations (B.1.22) and (B.1.24) leads to

$$0.25781 \times 10^8 = \frac{\beta^8}{2\pi\lambda} - \frac{\beta^3}{16} \,, \qquad \text{(B.1.25)}$$

and

$$-489.27 = \frac{2\beta^6}{\pi\lambda} - \frac{9\beta}{16} \qquad \text{(B.1.26)}$$

Solving the two simultaneous equations results in

$$\beta = 1682 \text{MeV/c} \,.$$

It must be stressed that our manner of estimating β did not take account of relativistic effects. In ref. [29] such effects were included and resulted in $\beta = 1100$ MeV/c. Using this value, instead of our above estimate for β, would lead to the the reduction effect increasing by only about 2%.

Appendix C

Extraction of the ηn elastic scattering amplitude using the $\pi^- p \rightarrow \eta n$ scattering data

Assuming a Breit-Wigner form of the amplitude describing the transition from channel i to channel j, Fäldt and Wilkin [7] took the ratio

$$\frac{f(\pi^- p \rightarrow \eta n)}{f(\eta n \rightarrow \eta n)} ,$$

to be constant with

$$f(\pi^- p \rightarrow \eta n) \approx 0.469 f(\eta n \rightarrow \eta n) . \qquad \text{(C.1.1)}$$

The channels

$$\gamma p \rightarrow \eta p ,$$

$$\pi^- p \rightarrow \eta n ,$$

and the elastic channel

$$\eta p \rightarrow \eta p ,$$

were all taken to proceed *via* a single partial wave, for which

$$f_{ij}^2 = f_{ii} f_{jj} , \qquad \text{(C.1.2)}$$

where f_{ij} are simple multi-channel Breit-Wigner amplitudes describing the transition from channels i to channels j. The f_{ii} and f_{jj} are the corresponding amplitudes describing elastic scatterings. Imposing unitarity, f_{ij} takes the simple form

$$f_{ij} = \frac{1}{\sqrt{k_i\, k_j}} \frac{M_R \sqrt{\Gamma_i\, \Gamma_j}}{M_R^2 - W^2 - i\Gamma(W)\, M_R} \,. \tag{C.1.3}$$

Here $\Gamma(W)$ is the total $N^*(1535)$ resonance width which has three contributions, *viz.*

$$\Gamma(W) = \Gamma_R \left(0.50 \frac{k_\eta}{k_\eta^R} \Theta(k_\eta^2) + 0.40 \frac{k_\pi}{k_\pi^R} \Theta(k_\pi^2) + 0.10 \right) \,, \tag{C.1.4}$$

where k_η and k_π are the centre-of-mass momenta of the η and π particles at a total c.m. energy W. k_η^R and k_π^R are the corresponding momenta evaluated at the resonance position $W = M_R$, where the branching ratios to the ηN, πN and $\pi\pi N$ channels were imposed to be 0.50, 0.40, and 0.10 respectively. $M_R = 1540.1 \pm 1.1$ MeV/c^2 is the resonance mass, and $\Gamma_R = 134.6 \pm 5.6$ MeV/c^2 is the resonance width. The step functions are included to ensure that only open channels contribute to the total width. The partial width corresponding to the ηN channel is

$$\Gamma_\eta = 0.50\, \Gamma_R \frac{k_\eta}{k_\eta^R} \Theta(k_\eta^2) \,, \tag{C.1.5}$$

and hence the ratio

$$\frac{\Gamma_\eta}{k_\eta} = 0.50 \frac{\Gamma_R}{k_\eta^R} \,, \tag{C.1.6}$$

is a constant. Similarly

$$\frac{\Gamma_\pi}{k_\pi} = 0.40 \frac{\Gamma_R}{k_\pi^R} \,, \tag{C.1.7}$$

Using eq. (C.1.3) the amplitudes for the elastic ηN and πN channels may be written respectively as

$$f(\eta N \to \eta N) = \frac{\Gamma_\eta}{k_\eta} \frac{M_R}{M_R^2 - W^2 - i\Gamma(W)\, M_R} \,, \tag{C.1.8}$$

and

$$f(\pi N \to \pi N) = \frac{\Gamma_\pi}{k_\pi} \frac{M_R}{M_R^2 - W^2 - i\Gamma(W)\, M_R} \,. \qquad \text{(C.1.9)}$$

In terms of the ηn elastic amplitude, $f(\pi N \to \pi N)$ is given by

$$\begin{aligned} f(\pi N \to \pi N) &= \frac{\Gamma_\pi}{k_\pi} \frac{k_\eta}{\Gamma_\eta} f(\eta N \to \eta N) \,, \\ &= \frac{0.4}{0.5} \frac{k_\eta^R}{k_\pi^R} f(\eta N \to \eta N) \,, \qquad \text{(C.1.10)} \end{aligned}$$

where to arrive at our last expression we used equations (C.1.6) and (C.1.7).

Remembering that the $I = 1/2$ pion-nucleon channel is 2/3 in $\pi^- p$ and 1/3 in $\pi^0 n$, and using eq. (C.1.2), we get

$$\begin{aligned} f(\pi^- p \to \eta n) &= \sqrt{\frac{2}{3}} f(\pi N \to \eta N) \\ &= \sqrt{\frac{2}{3}} \sqrt{f(\pi N \to \pi N)\, f(\eta N \to \eta N)} \,. \qquad \text{(C.1.11)} \end{aligned}$$

Substituting for $f(\pi N \to \pi N)$ using eq. (C.1.10) we finally obtain

$$f(\pi^- p \to \eta n) = \sqrt{\frac{1.6}{3} \frac{k_\eta^R}{k_\pi^R}} f(\eta N \to \eta N) \qquad \text{(C.1.12)}$$

At resonance $W = M_R$, $k_\eta^R = 190.4$ and $k_\pi^R = 471$ MeV/c. Hence,

$$f(\pi^- p \to \eta n) \approx 0.469\, f(\eta N \to \eta N) \,, \qquad \text{(C.1.13)}$$

which is our first equation in this appendix.

Using eq. (C.1.3), they numerically calculated the inverse of the ηp elastic amplitude and parameterized the result in terms of a scattering length a_0 and and effective range r_0. Hence

$$[f(\eta n \to \eta n)]^{-1} = \frac{1}{a_0} + \frac{1}{2} r_0 k_\eta^2 \,, \qquad \text{(C.1.14)}$$

with an ηp scattering length and effective range given by

$$a_0 = (0.476, 0.279)\,\mathrm{fm} \qquad r_0 = (-3.16, -0.13)\,\mathrm{fm}$$

The ηn scattering length is slightly changed, $a_0 = (0.481, 0.289)$ fm, due to the different masses but the effective range is little modified.

Appendix D

Centre of Mass Momentum of the ω-meson in $pd \rightarrow {}^3He\,\omega$

According to the model of Fäldt and Wilkin, the reaction $\eta\,{}^3He \rightarrow pd$ can be studied in terms of intermediate steps, the first being $\eta p \rightarrow \pi N$ on one of the nucleons in the helium nucleus, followed by $\pi d \rightarrow NN$. A schematic diagram of this two step model is shown in fig. (D.1) below.

For zero Fermi momentum, we assume the laboratory kinetic energy of the η in the overall reaction ($\eta\,{}^3He \rightarrow pd$) to be the same as that for $\eta p \rightarrow \pi N$. We shall also define p_η to be the η c.m. momentum in the overall reaction, and p'_η the corresponding one in the $\eta - N$ reaction. Hence

$$s_a = M_\eta^2 + M_h^2 + 2M_h E_l \,, \tag{D.1.1}$$

$$s_b = M_\eta^2 + M_p^2 + 2M_p E_l \,, \tag{D.1.2}$$

where M is the mass and the subscripts h, p refer to ${}^3He$ and the proton respectively. E_l is the η laboratory kinetic energy.

Multiplying the first equation by M_p and the second by M_h and then subtracting gives

$$M_p s_a - M_h s_b = (M_p - M_h)(M_\eta^2 - M_p M_h) \,. \tag{D.1.3}$$

In the overall c.m. system, s_a is given by

$$s_a = \left(\sqrt{M_\eta^2 + p_\eta^2} + \sqrt{M_h^2 + p_\eta^2}\right)^2 ,$$

which, non-relativistically, is approximated by

$$s_a \approx (M_h + M_\eta)^2 \left(1 + \frac{p_\eta^2}{M_\eta M_h}\right) . \qquad \text{(D.1.4)}$$

Similarly

$$s_b \approx (M_p + M_\eta)^2 \left(1 + \frac{p_\eta'^2}{M_\eta M_p}\right) . \qquad \text{(D.1.5)}$$

Substituting eq. (D.1.4) and eq. (D.1.5) into eq. (D.1.3) and rearranging yields

$$p_\eta' = \left(\frac{1 + M_\eta/M_h}{1 + M_\eta/M_p}\right) p_\eta \qquad \text{(D.1.6)}$$

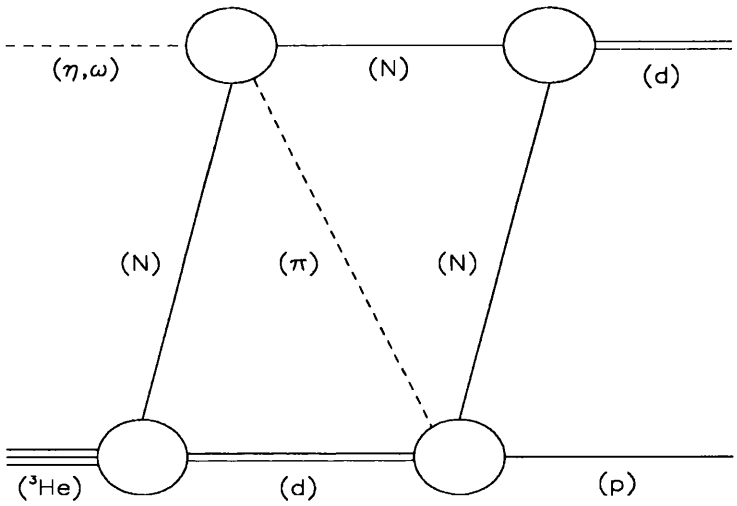

Figure D.1: Schematic diagram of the two-step model for $(\omega\,\eta)^3He \rightarrow pd$

Bibliography

[1] Particle Data Group, Phys. Rev. **D50** (1994) 1459.

[2] D.M. Binnie *et al.,* Phys. Rev. **D8** (1973) 2789.

[3] J. Keyne *et al.,* Phys. Rev. **D14** (1979) 28.

[4] R. Wurzinger, Phys. Rev. **C51** (1995) R443.

[5] R. Wurzinger, PhD. thesis, University of Bonn, (1992).

[6] H. Karami *et al.,* Nucl. Phys. **B154** (1979) 503.

[7] G. Fäldt and C. Wilkin, Nuclear Physics, **A 587** (1995) p 769.

[8] D.H. Perkins, *Introduction to High Energy Physics.* 3rd edn, (Addison-Wesley, 1987).

[9] E. Byckling and K. Kajantie, *Particle Kinematics*, (Wiley, 1973).

[10] H. Pilkuhn, *The Interactions of Hadrons*, (North-Holland Publishing Company–Amsterdam, 1967).

[11] E. Pedroni *et al.,* Nucl. Phys. **A300** (1978) 321.

[12] S. Rodberg and R.M. Thaler, *Introduction to the Quantum Theory of Scattering,* (New York, Academic Press, 1967).

[13] R.J. Glauber, in *Lectures in Theoretical. Phys.*, **Vol. 1**. edited by W.Britten (Interscience, New York, 1959) p. 315.

[14] B. Schwesinger, in *Baryon Spectroscopy and the Structure of the Nucleon.* Proceedings of an International Workshop held at Saclay, France, from 23 to 25 September 1991, p112. Edited by H. Morsch and M. Soyeur.

[15] N. Kaiser, P. Siegel and W. Weise, (preprint 1995).

[16] M. Goldberger and K.M. Watson, *Collision Theory,* (New York, Wiley, 1964)

[17] M.A. Bég, Ann. Phys. **13** (1961) 110.

[18] G. Fäldt, Nucl. Phys. **A333** (1980) 357.

[19] D.R. Tilley *et al.,* Nucl. Phys. **A474** (1987) 1.

[20] K. Kilian and H. Nann in *Meson Production near Threshold*, edited by H. Nann and E. J. Stephenson, AIP Conf. Proc. No. 221 (AIP, New York, 1990), p. 185.

[21] C. Wilkin, Proceedings *Sixièmes Journées d'Études Saturne*, edited by M.Bordry (LNS, Saclay, 1992) p. 121.

[22] S. Persson, Uppsala dissertation *A Relativistic Multiple Scattering Model for the Reaction* $\eta\,{}^3He \rightarrow pd$. UPTEC–93–041E, 1993.

[23] J.D. Bjorken and S.D. Drell, *Relativistic Quantum Mechanics.* (McGraw–Hill, New York, 1964)

[24] J.S. Danburg *et al.,* Phys. Rev. **D2** (1970) 2564.

[25] G. Fäldt and C. Wilkin, Physics Letters **B 354** (1995) p 20.

[26] J. Berger *et al.,* Phys. Rev. Lett. **61**, (1988) 919

[27] M. Garçon *et al.*, in *Spin and Symmetry in the Standard Model*, Lake Louise, 1992, edited by B. A. Cambell (World Scientific, Singapore) p 337; R Kessler, Ph.D. thesis (UCLA) 1992 *and* private communication (1993).

[28] C.J. Joachain, *Quantum Collision Theory*, (North-Holland Publishing Company, 1975.)

[29] C. Schmit, Physics Letters **52B** (1974) p 381.